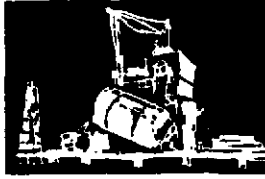
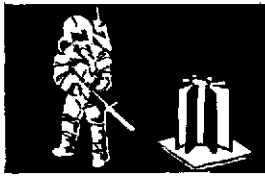
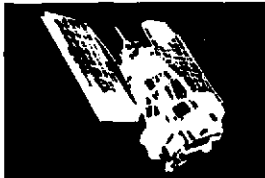
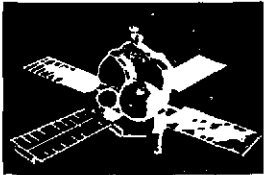
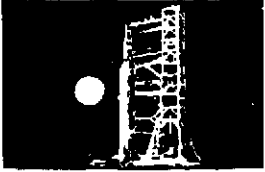
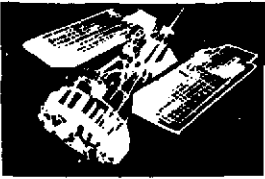


**SPACE
DIVISION**

NASA CR-132566
GE DOCUMENT NO. 74SD4264
5 NOVEMBER 1974



FINAL REPORT PASSIVE STABILIZATION OF THE LONG DURATION EXPOSURE FACILITY (LDEF)

(NASA-CR-132566) PASSIVE STABILIZATION OF
THE LONG DURATION EXPOSURE FACILITY (LDEF)
Final Report (General Electric Co.) 164 p
HC \$6.25

CSCL 22B

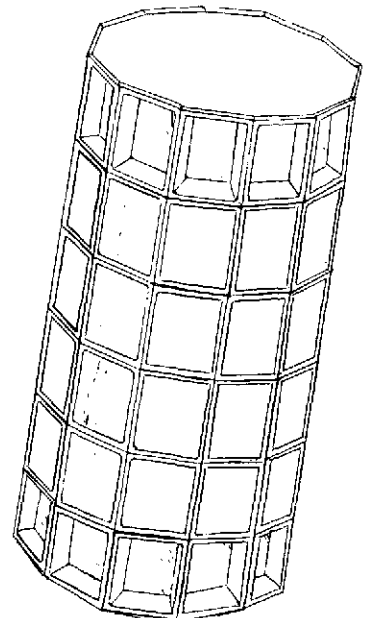
N75-17397

G3/15

Unclas
G9930

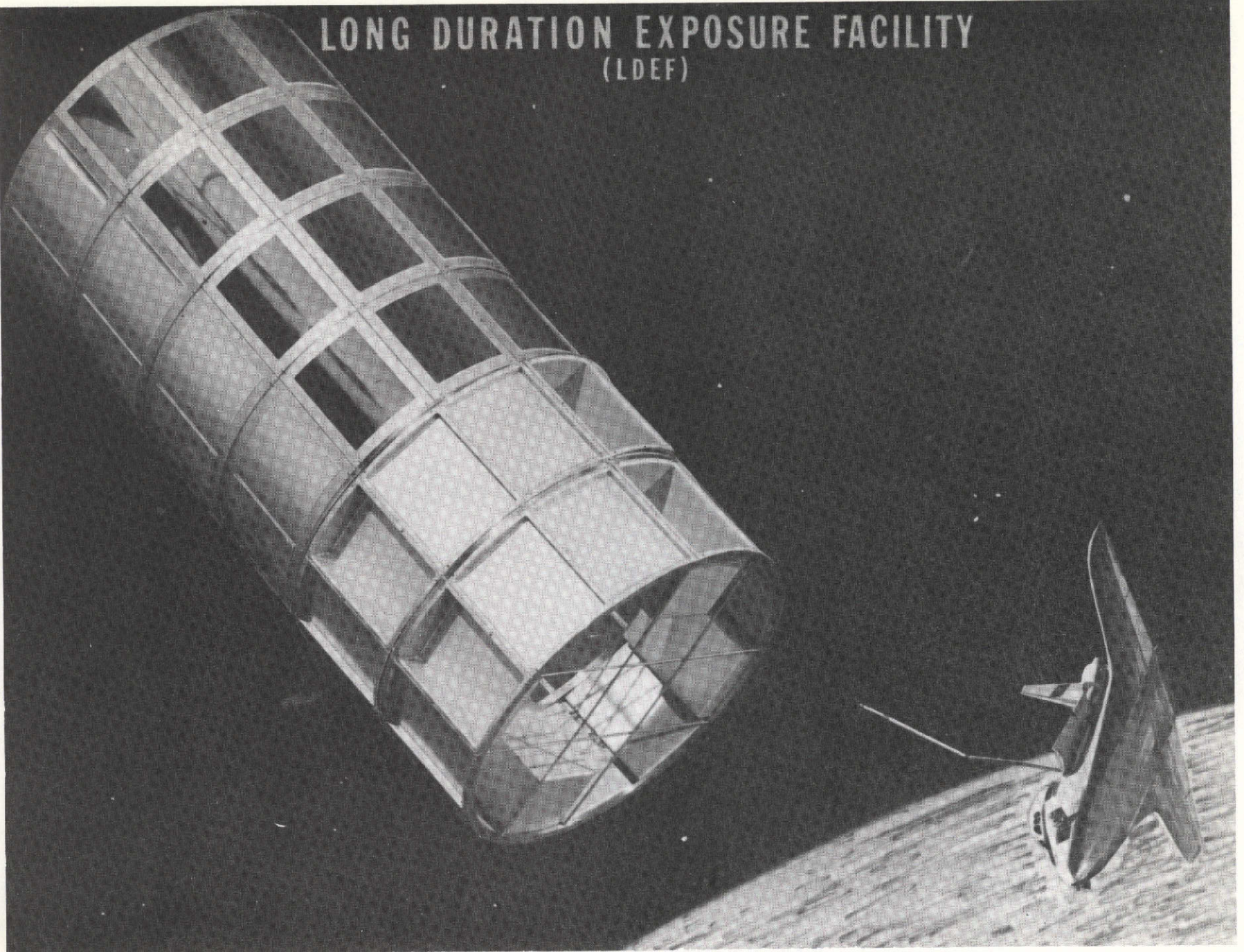
Prepared for:
LANGLEY RESEARCH CENTER
Hampton, Va.

Under
Contract NAS 1-13440



GENERAL  ELECTRIC

LONG DURATION EXPOSURE FACILITY (LDEF)



ORIGINAL PAGE IS
OF POOR QUALITY

TABLE OF CONTENTS

	Page
Table of Contents	i
List of Illustrations	iii
1.0 Introduction	1
2.0 Summary and Conclusions	2
2.1 Summary	2
2.2 Conclusions	4
3.0 Linearized Analysis - Two Axis Configuration	10
3.1 Steady State Performance Analyses	10
3.1.1 Magnetically Anchored Rate Damper	10
3.1.2 Solar Torque	13
3.1.3 Magnetic Torque	16
3.1.4 Orbit Eccentricity Torques	19
3.1.5 Aerodynamic Torques	20
3.1.5.1 Spacecraft Configuration	22
3.1.5.2 Orbit Eccentricity	33
3.1.5.3 Argument of Perigee/Ascending Node	45
3.2 Garber Instability	45
3.3 Transient and Capture Performance	49
3.3.1 Transient Performance	49
3.3.2 Capture Performance	53
3.4 Configuration Optimization	56
4.0 Linearized Analysis - Three Axis Configuration	60
4.1 Steady State Performance Analyses	60
4.2 Garber Instability	71
4.3 Transient and Capture Performance	73
4.3.1 Transient Performance	73
4.3.2 Capture Performance	73
4.4 Configuration Optimization	73
5.0 Performance Prediction	84
5.1 Two Axis Configuration	84
5.1.1 Steady State Performance	84
5.1.2 Transient and Capture Performance	90

TABLE OF CONTENTS (cont'd)

5.2	Three Axis Configuration	92
	5.2.1 Steady State Performance	92
	5.2.2 Transient and Capture Performance	101
	References	109

LIST OF ILLUSTRATIONS

<u>Figure</u>		<u>Page</u>
3.1	Magnetically Anchored Rate Damper	11
3.2	Definition of Coordinates and Angles	14
3.3	Effect of Damper Coefficient on the Pitch, Roll and Yaw Error - Two Axis	15
3.4	Magnetic and Solar Errors versus CM Offset - Two Axis	17
3.5	Orbit Eccentricity Errors - Two Axis	21
3.6	Effect of Shift of the CM on the Pitch Error Due to Pitch Torque (Constant Component)	23
3.7	Effect of Shift of the CM on the Pitch Error Due to Pitch Torque (Orbital Frequency Component)	24
3.8	Effect of Shift of the CM on the Pitch Error Due to Pitch Torque (Twice Orbital Frequency Component)	25
3.9	Effect of Shift of the CM on the Roll Error Due to Roll Torque (Constant Component)	27
3.10	Effect of Shift of the CM on the Roll Error Due to Roll Torque (Orbital Frequency Component)	28
3.11	Effect of Shift of the CM on the Roll Error Due to Roll Torque (Twice Orbital Frequency Component)	29
3.12	Effect of Shift of the CM on the Roll Error Due to Yaw Torque (Orbital Frequency Component)	30
3.13	Effect of Shift of the CM on the Roll Error Due to Yaw Torque (Twice Orbital Frequency Component)	31
3.14	Effect of a Shift Normal to the Cylinder Axis on the Pitch and Roll Errors	32
3.15	Aerodynamic Attitude Error Due to Center of Mass/Center of Pressure Uncertainty	34
3.16	Effect of Orbit Eccentricity, Pitch Error Due to Pitch Torque (Constant Component)	35
3.17	Effect of Orbit Eccentricity, Pitch Error Due to Pitch Torque (Orbital Frequency Component)	36
3.18	Effect of Orbit Eccentricity, Pitch Error Due to Pitch Torque (Twice Orbital Frequency Component)	37

LIST OF ILLUSTRATIONS (cont'd)

<u>Figure</u>		<u>Page</u>
3.19	Effect of Orbit Eccentricity, Roll Error Due to Roll Torque (Constant Component)	38
3.20	Effect of Orbit Eccentricity, Roll Error Due to Roll Torque (Orbital Frequency Component)	39
3.21	Effect of Orbit Eccentricity, Roll Error Due to Roll Torque (Twice Orbital Frequency Component)	40
3.22	Effect of Orbit Eccentricity, Roll Error Due to Yaw Torque (Orbital Frequency Component)	41
3.23	Effect of Orbit Eccentricity, Roll Error Due to Yaw Torque (Twice Orbital Frequency Component)	42
3.24	Effect of a Shift of the CM Normal to the Cylinder Axis on the Pitch and Roll Errors	43
3.25	Aerodynamic Attitude Error Due to Orbit Eccentricity	44
3.26	Effect of the Ascending Node Position on the Aerodynamic Pitch Error Due to Pitch Torque, Eccentricity = 0	46
3.27	Effect of the Ascending Node Position on the Aerodynamic Pitch Error Due to Pitch Torque, Eccentricity = 0.01	47
3.28	Effect of the Ascending Node Position on the Aerodynamic Pitch Error Due to Pitch Torque, Eccentricity = 0.02	48
3.29	Two-Axis Pitch Time Constant versus Damping Coefficient	52
3.30	Capture Performance for the Damper	54
3.31	Effect of the Distance the Damper is Offset from the Center on the Centrifugal Force on the Damper Per Pound of its Weight	55
4.1	The LDEF: 3 - Axis Configuration	61
4.2	Spacecraft Moments of Inertia	62
4.3	Three Axis Pitch Errors versus Added Mass	64
4.4	Three Axis Roll Errors versus Added Mass	65
4.5	Three Axis Yaw Errors versus Added Mass	66
4.6	Attitude Errors versus Radial CM Offset - 400 lbs	67
4.7	Attitude Errors versus Radial CM Offset - 800 lbs	68

LIST OF ILLUSTRATIONS (cont'd)

<u>Figure</u>		<u>Page</u>
4.8	Attitude Errors versus Radial CM Offset - 1600 lbs	69
4.9	Attitude Errors versus Radial CM Offset - 2000 lbs	70
4.10	Effect of Mass Addition on the Attitude Errors	74
4.11	Effect of Mass Addition & Damping Coefficient on the Pitch Damping Time Constant - 225,00 pole-cm	75
4.12	Effect of Mass Addition & Damping Coefficient on the Pitch Damping Time Constant - 450,000 pole-cm	76
4.13	Effect of Mass Addition & Damping Coefficient on the Pitch Damping Time Constant - 900,000 pole-cm	77
4.14	Effect of a Shift of the CM Normal to the Cylinder Axis on the Attitude Error	79
5.1	Steady-State Performance; Two Axis Configuration - Damper Only	85
5.2	Steady-State Performance; Two Axis Configuration - All Disturbances	88
5.3	Steady-State Performance; Two Axis Configuration - 1.0 lb-ft-sec Damping Coefficient	89
5.4	Capture Run; Two Axis Configuration, 0.04 deg/sec	91
5.5	Capture Run; Two Axis Configuration, 0.25 deg/sec - .51 lb-ft-sec Damping Coefficient	93
5.6	Capture Run; Two Axis Configuration, 0.25 deg/sec - 1.0 lb-ft-sec Damping Coefficient	95
5.7	Steady-State Performance; Three Axis Configuration - Damper Only	98
5.8	Steady-State Performance; Three Axis Configuration - All Disturbances	99
5.9	Steady-State Performance; Three Axis Configuration - 1.0 lb-ft-sec Damping Coefficient	100
5.10	Capture Run; Three Axis Configuration, 0.04 deg/sec	103
5.11	Capture Run; Three Axis Configuration, 0.04 deg/sec - No Disturbances	105

LIST OF ILLUSTRATIONS (cont'd)

<u>Figure</u>		<u>Page</u>
5.12	Capture Run; Three Axis Configuration, 0.04 deg/sec - 1.0 lb-ft-sec Damping Coefficient	106
5.13	Capture Run; Three Axis Configuration, 0.25 deg/sec	107

PASSIVE STABILIZATION OF THE
LONG DURATION EXPOSURE FACILITY (LDEF)

By Aniruddha Das
Howard F. Foulke
Sherman H. Siegel

Prepared under Contract No. NAS 1-13440 by
GENERAL ELECTRIC COMPANY
Valley Forge, Pennsylvania

for

NATIONAL AERONAUTICS AND SPACE ADMINISTRATION

SECTION 1.0

INTRODUCTION

This report, entitled "Passive Stabilization of the Long Duration Exposure Facility" has been prepared for Langley Research Center under contract number NAS 1-13440. It presents the results of a seventeen week study on the application of the Magnetically Anchored Rate Damper to gravity gradient stabilization of the Long Duration Exposure Facility (LDEF). The study objectives were to perform the analyses and simulations required to investigate the use of an existing viscous magnetic rate damper for rate stabilizing the LDEF spacecraft. The study itself was broken into three main tasks; Linear Performance Estimates, Capture and Damper Requirements, and Performance Prediction. Each of these tasks was performed for two gravity gradient stabilization configurations; an axisymmetric configuration for two-axis (pitch and roll) stability; and a non-axisymmetric configuration for three-axis stability. The report presents the results by stabilization configuration.

SECTION 2.0

SUMMARY AND CONCLUSIONS

2.1 SUMMARY

The nominal LDEF configuration and the anticipated orbit parameters are shown in Table 2.1. Using these parameters, two linear steady state analyses were performed; one for two axis (pitch and roll) stabilization, and one for three axis (pitch, roll and yaw) stabilization. In each of these analyses, the effects of orbit eccentricity, solar pressure, aerodynamic pressure, magnetic dipole, and the magnetically anchored rate damper were evaluated to determine the configuration sensitivity to variations in these parameters. The worst case conditions for steady state were identified, and the performance capability calculated.

Garber instability bounds (a linear instability associated with gravity gradient stabilized spacecraft) were evaluated for the range of configurations and damping coefficients under consideration.

The transient damping capabilities of the damper were evaluated for both the two and three axis configurations, and the time constant as a function of damping coefficient, magnet strength, and spacecraft moment of inertia determined. The capture capabilities of the damper were calculated, and the results combined with the steady state, transient, and Garber instability analyses to select a damper design.

After completion of the linearized analyses, the selected configurations and damper design were simulated on a large three axis digital computer program.

Table 2.1

Nominal Configuration and Orbit Parameters

Spacecraft weight	4180 kg	9200 lbs
Configuration	Cylindrical	Cylindrical
Diameter	4.27 m	14.0 ft.
Length	9.15 m	30.0 ft.
Moments of Inertia		
Yaw	19200 kg-m ²	14200.0 slug-ft ²
Roll	39300 kg-m ²	29000.0 slug-ft ²
Pitch	39300 kg-m ²	29000.0 slug-ft ²
Products of Inertia	0	0.0
Spacecraft Magnetic Dipole	1000 pole-cm/ axis	1000.0 pole-cms/ axis
Orbit Altitude	500 km	270.0 n.miles
Orbit Inclination	28.8 degrees	28.8 degrees

The performance of the spacecraft in steady state was simulated for both configurations, as was the transient performance. Capture from an initial rate of 0.25 deg/sec was also simulated for both configurations.

2.2 CONCLUSIONS

The LDEF spacecraft can be gravity gradient to and three axis stabilized within the range of parameters considered.

Table 2.2 shows the linearized performance estimates for the two axis configuration, with associated error breakdown; and the results of the three axis digital simulations. The largest sources of attitude error are the magnetically anchored rate damper, which is controllable by design; and aerodynamics. Solar pressure is small, and as discussed in Section 3.1.2, can never be large. The magnetic errors are based upon a 1000 pole-cm magnetic dipole, which was the value estimated for the spacecraft. Magnetic errors will, of course, increase if the dipole is increased beyond 1000 pole-cm. The effect of larger dipoles can be estimated from the errors provided, since magnetic errors are linear with magnetic moment up to a value of 30,000 pole-cm (for LDEF).

The errors caused by aerodynamics depend upon center of pressure/center of mass offset, orbit eccentricity, argument of perigee, right ascension, and time period with respect to the solar cycle. The errors shown in Table 2.2 were calculated for a 1978 time period with the worst position of perigee and right ascension (section 3.1.5). The effect of center of pressure/center of mass offset and orbit eccentricity is considered in the text, and the change in performance associated with changes in these parameters can be estimated from

Table 2.2

Two Axis Stabilization Performance

Linear Error Estimates

<u>Error Source</u>	<u>Attitude Errors</u>	
	<u>Pitch (deg)</u>	<u>Roll (deg)</u>
Magnetic Rate Damper	.48	.65
Solar Torque	.02	.03
Magnetic Torque	.06	.07
Orbit Eccentricity	.43	-
Aerodynamic Torque	1.90	.28
Total Error (RSS)	2.03	.79

Simulation - Steady State Results *

Peak Pitch Error	1.50 deg
Peak Roll Error	.88 deg
Peak Pitch Rate **	.002 deg/sec
Peak Roll Rate **	.002 deg/sec
Peak Yaw Rate	.001 deg/sec

Simulation - Transient Results

Time to Stop Tumbling	150 hours
Transient Decay Time Constant	43.8 orbits

* Magnetic dipole not included in simulation because its effects are insignificant relative to other disturbances.

** Relative to orbital

Figure 3.15 and Figure 3.25, respectively.

The capture ability and transient performance values are shown in Table 2.2, and the time histories of the spacecraft motion are shown in Figures 5.4 and 5.5, respectively. For rates below 0.04 deg/sec, the spacecraft will capture rightside up (if initially rightside up within ± 15 deg per axis). For 0.25 deg/sec, the spacecraft will tumble. As indicated in Table 2.2 and Figure 5.5, the two axis configuration did not stop tumbling even after 150 hours. The analysis of the performance (Section 5.1.2) indicates that the spacecraft will not stop tumbling because its pitch natural frequency (at large amplitudes) is orbital, and the damper torque, as well as other disturbance torques, excite the spacecraft and prevent stabilization. This condition can be eliminated only by changing the moments of inertia of the spacecraft to change its natural frequency.

Table 2.3 contains the same information as Table 2.2 for the three axis configuration, which was obtained from the two axis configuration by adding 182 kg (400 lb) of mass in specific locations. Again, solar torque is small and magnetic errors can be scaled linearly with magnetic dipole. The errors resulting from an axial offset of the center of pressure/center of mass are the same or less than those for the two axis configuration, but the effect on yaw of a radial offset is pronounced. A two inch offset has been assumed for the error determination. Figure 4.14 can be used to estimate the effect on performance of a larger offset.

The three axis configuration did capture successfully after 76 hours of tumbling, with the same damper as the one selected for the two axis configuration. Its moments of inertia, which were altered by adding mass, prevented the pitch resonance condition from occurring. Since the amount of added mass is small,

and the difference between the pitch and roll moments of inertia is small (less than 826 kg-m^2 - 609 slug-ft^2), a three axis configuration is likely to be the nominal configuration because of packaging limitations.

The damper design selected for both the two and three axis configuration is shown in Table 2.4. The design is consistent with existing damper designs.

The choice of damping coefficient was based upon previous experience, and can be increased or decreased if required.

Table 2.3

Three Axis Stabilization Performance

Linear Error Estimates

<u>Error Source</u>	Attitude Errors		
	Pitch (deg)	Roll (deg)	Yaw (deg)
Magnetic Rate Damper	.42	.55	.89
Solar Torque	.01	.02	.22
Magnetic Torque	.05	.06	.43
Orbit Eccentricity	.40	-	-
Aerodynamic Torque	1.61	.52	8.67
Total Error (RSS)	1.75	.68	9.06

Simulation - Steady State Results *

Peak Pitch Error	1.38 deg
Peak Roll Error	.62 deg
Peak Yaw Error	9.30 deg
Peak Pitch Rate **	.002 deg/sec
Peak Roll Rate **	.002 deg/sec
Peak Yaw Rate	.002 deg/sec

Simulation - Transient Results

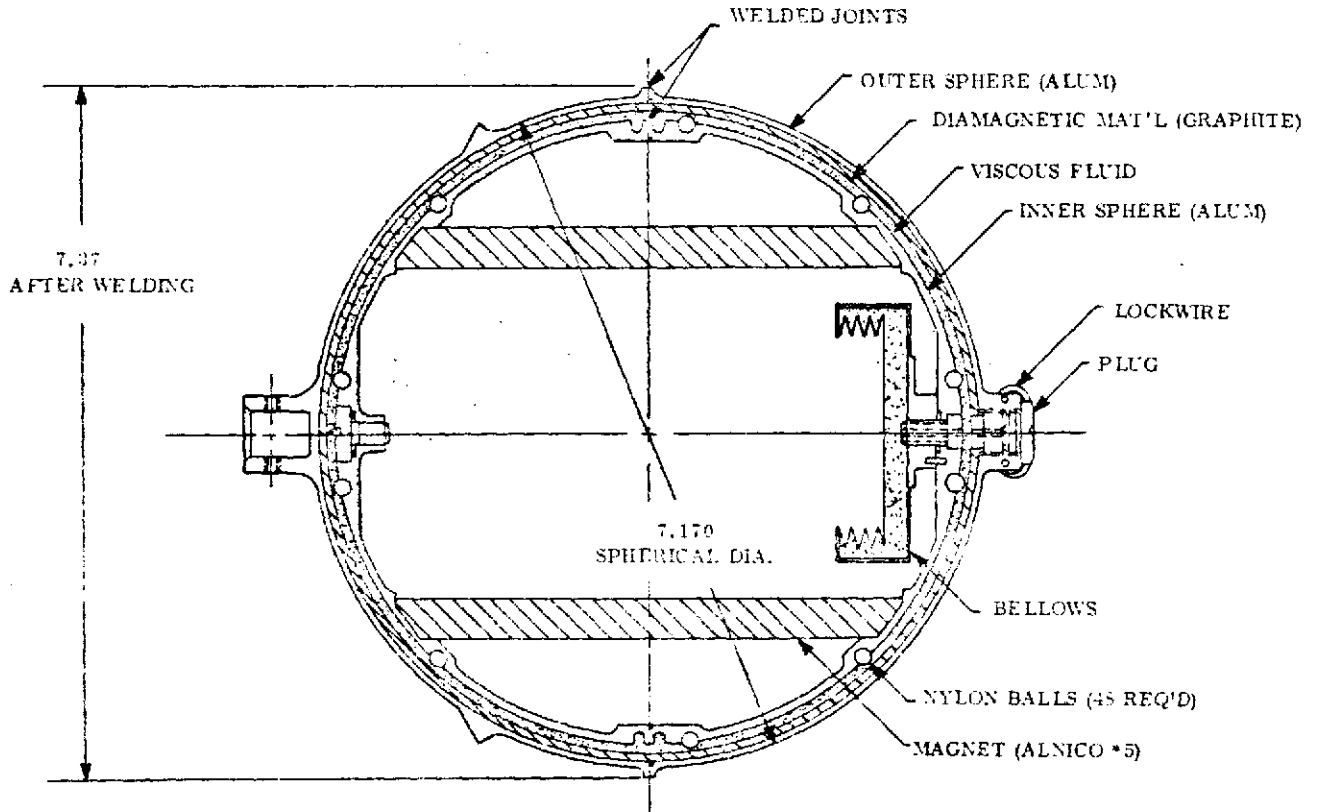
Time to Stop Tumbling	76 hours
Transient Decay Time Constant	46.6 orbits

* Magnetic dipole not included in simulation because its effects are insignificant relative to other disturbances.

** Relative to orbital

Table 2.4

Damper Design



Damping Coefficient (Total)	.692 n.m.sec (.51 lb-ft-sec)
Magnet Strength	225,000 pole-cm
Suspension	35.2 dynes/kg (16 dynes/lb)

SECTION 3.0

LINEARIZED ANALYSIS - TWO AXIS CONFIGURATION

The linearized analysis was divided into four parts; Steady State Performance, Garber Instability, Transient and Capture Performance, and Configuration Optimization.

3.1 STEADY STATE PERFORMANCE ANALYSIS

There are five major sources of attitude error for the LDEF gravity gradient stabilized spacecraft; the magnetically anchored rate damper, solar torque, magnetic torque, orbit eccentricity, and aerodynamic torque. The magnitude and nature of the torques, in conjunction with the spacecraft parameters, determines the pointing accuracy and capture capability of the spacecraft. The following sections describe each of these torques, and their effect upon the spacecraft performance.

3.1.1 MAGNETICALLY ANCHORED RATE DAMPER

The magnetically anchored rate damper is a GE developed component designed to damp large amplitude oscillations of gravity gradient stabilized spacecraft. The viscous fluid version of the damper is shown in Figure 3.1. It consists of an inner sphere, which contains a permanent magnet and bellows; and an outer sphere, constructed of pyrolitic graphite (for diamagnetic centering) and aluminum. The space between the spheres, and inside the bellows, is filled with Silicone oil, with a viscosity selected to provide the required damping coefficient.

The mechanism of damping depends upon the relative rate of rotation of the inner sphere of the damper, and the outer sphere; which is rigidly attached to the spacecraft. During spacecraft acquisition and capture, the relative

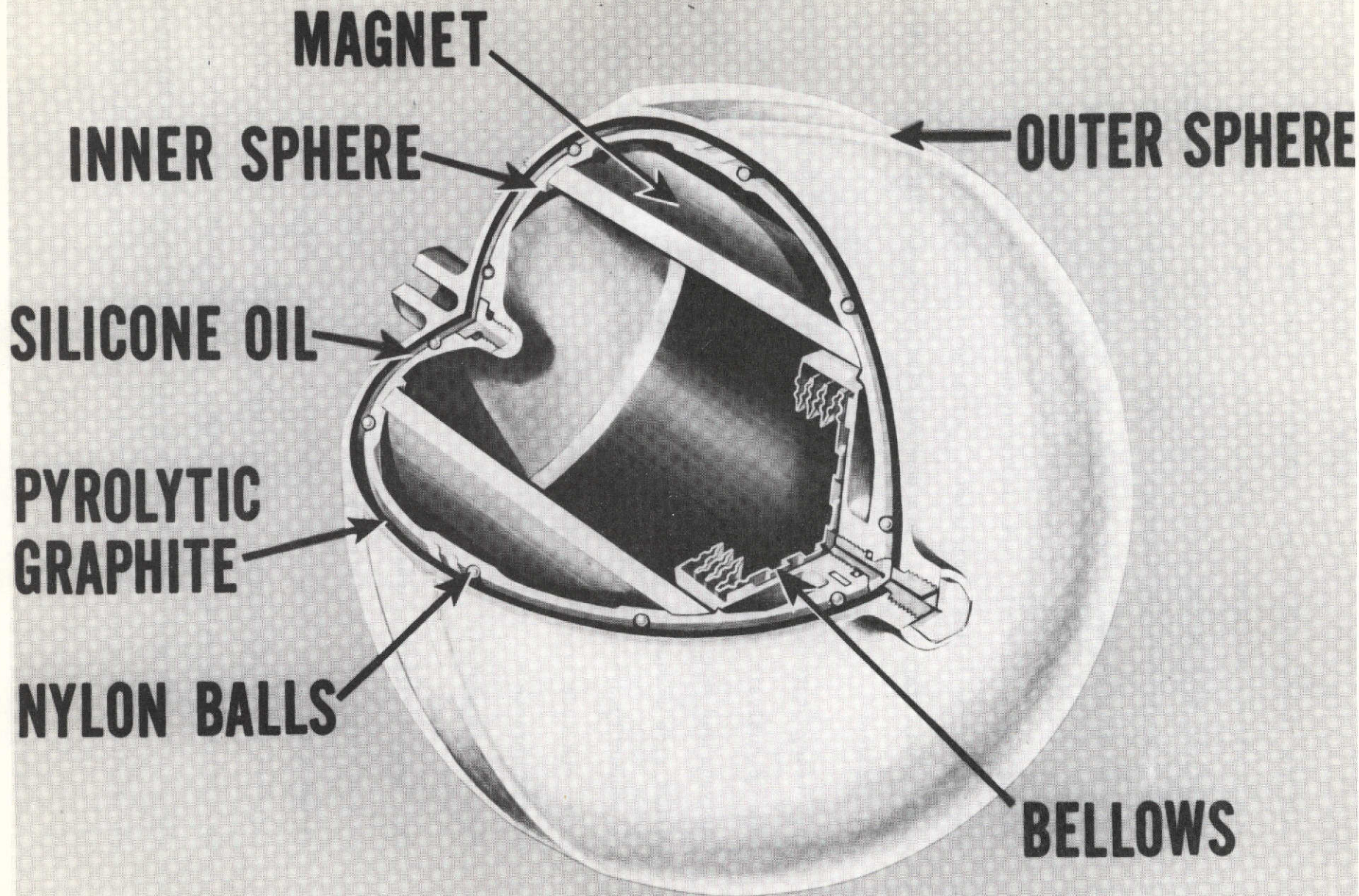


FIGURE 3.1

motion is largely the result of motions of the spacecraft. After the spacecraft has stabilized, however, relative motion continues to exist because the magnet follows the Earth's magnetic field, not the local vertical. The damping torques then become disturbance torques to the spacecraft and contribute to the overall pointing inaccuracy. The amplitude of this error is a linear function of the damping coefficient, and decreasing the damping level will decrease the contribution to steady state error. However, decreasing the damping coefficient will also increase the time to decay to the steady-state condition from initial conditions. As a consequence, a tradeoff exists between steady state accuracy and damping time constant. Section 3.4 discusses this tradeoff.

The steady state performance for the LDEF was determined both from a linear dynamic analysis, and a non-linear torque analysis. It is known from these analyses and many simulations, that the damper produces sinusoidal torques with a wide frequency spectrum, including high harmonics of orbital frequency. Consequently dynamic oscillations at several frequencies appear on the spacecraft attitude from the damper alone. To determine accurately the steady state characteristics, the torques at the frequencies of highest importance must be calculated.

The steady state disturbance torques induced by the magnetically anchored rate damper were calculated by an analysis of the earth's magnetic field, assuming the spacecraft was perfectly oriented. For simplicity, the earth's magnetic field was assumed to be a simple dipole field oriented along the spin axis of the earth, with the damper magnet following the field exactly. The rate of change of the magnetic field vector with respect to the orbiting coordinate system was determined, and instantaneous torque calculated. The

torques were then calculated at equal increments around the orbit, and frequency components (i.e., orbital frequency and the harmonics) computed by a Fourier Series analysis. Three torque coefficients were calculated for each axis; static, orbital, and twice orbital. Higher harmonics were not calculated since they produce negligible attitude errors.

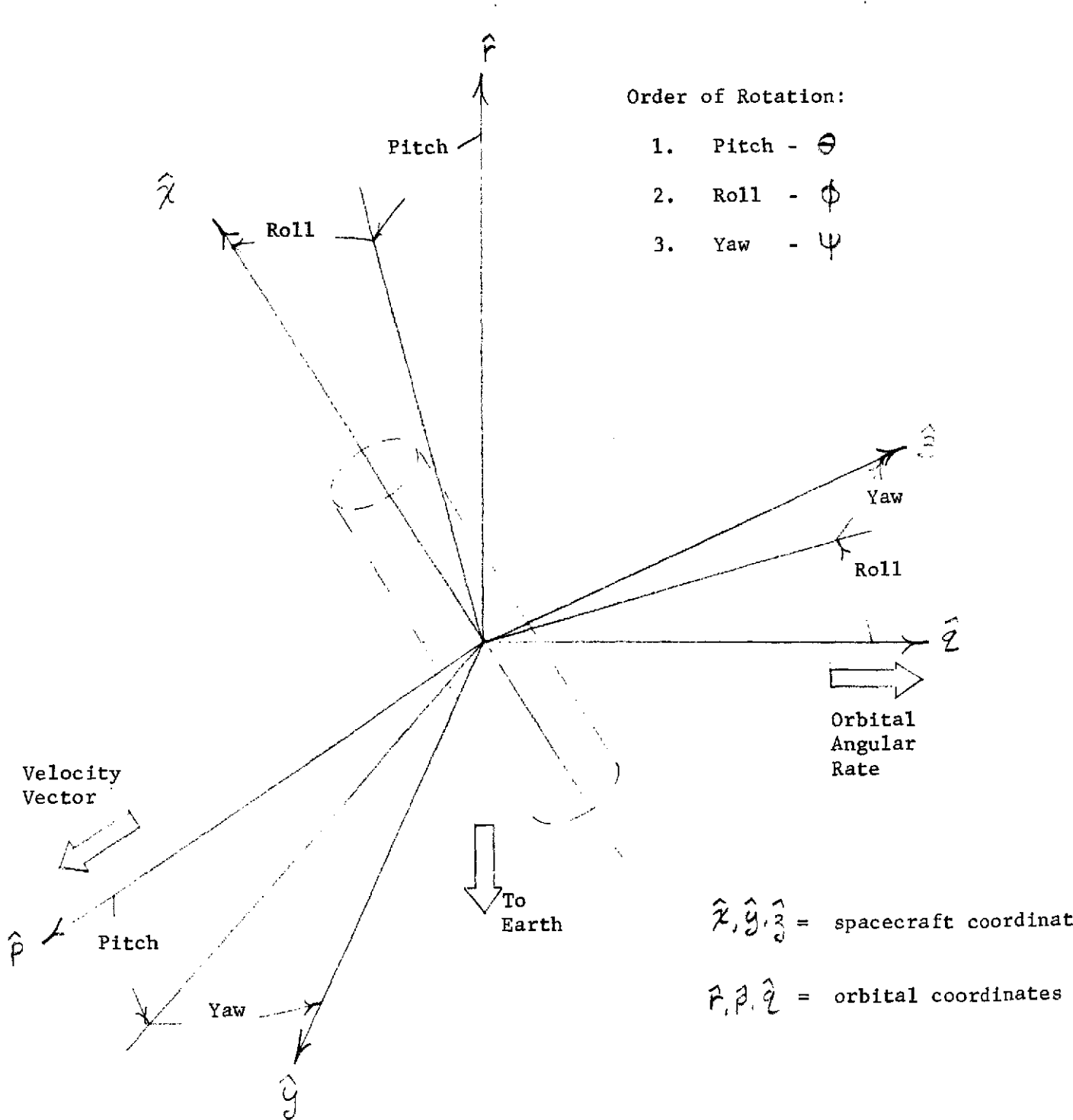
For a two axis stabilization performance analysis, only the pitch and roll coefficients are of importance. The yaw axis has no preferred orientation and simply "drifts" under the influence of the damper. The attitude errors resulting from the damper pitch and roll torques depend upon the damping coefficient, the orbit inclination, and the sensitivity of the roll and yaw axes to the disturbance frequencies. The pitch axis is disturbed most with torque components at all frequencies. Roll, however, has only orbital and twice orbital frequency coefficients, and yaw has only orbital frequency torques. The axes and Euler angles are shown in Figure 3.2.

The relationship between the steady-state damper induced error and damping coefficient is shown in Figure 3.3 for the LDEF two axis configuration. The steady-state errors, especially the pitch errors, are quite low. The worst roll error is slightly over one degree for the highest damping coefficient considered. Similarly the highest pitch error is 0.5 degrees. This is well below the 3-deg pitch bias error at which Garber instability can occur for the range of damping coefficients considered, (see Section 3.2). Note that the damper does not develop constant yaw torque and hence does not produce "infinite" yaw error (or continuous motion).

3.1.2 SOLAR TORQUE

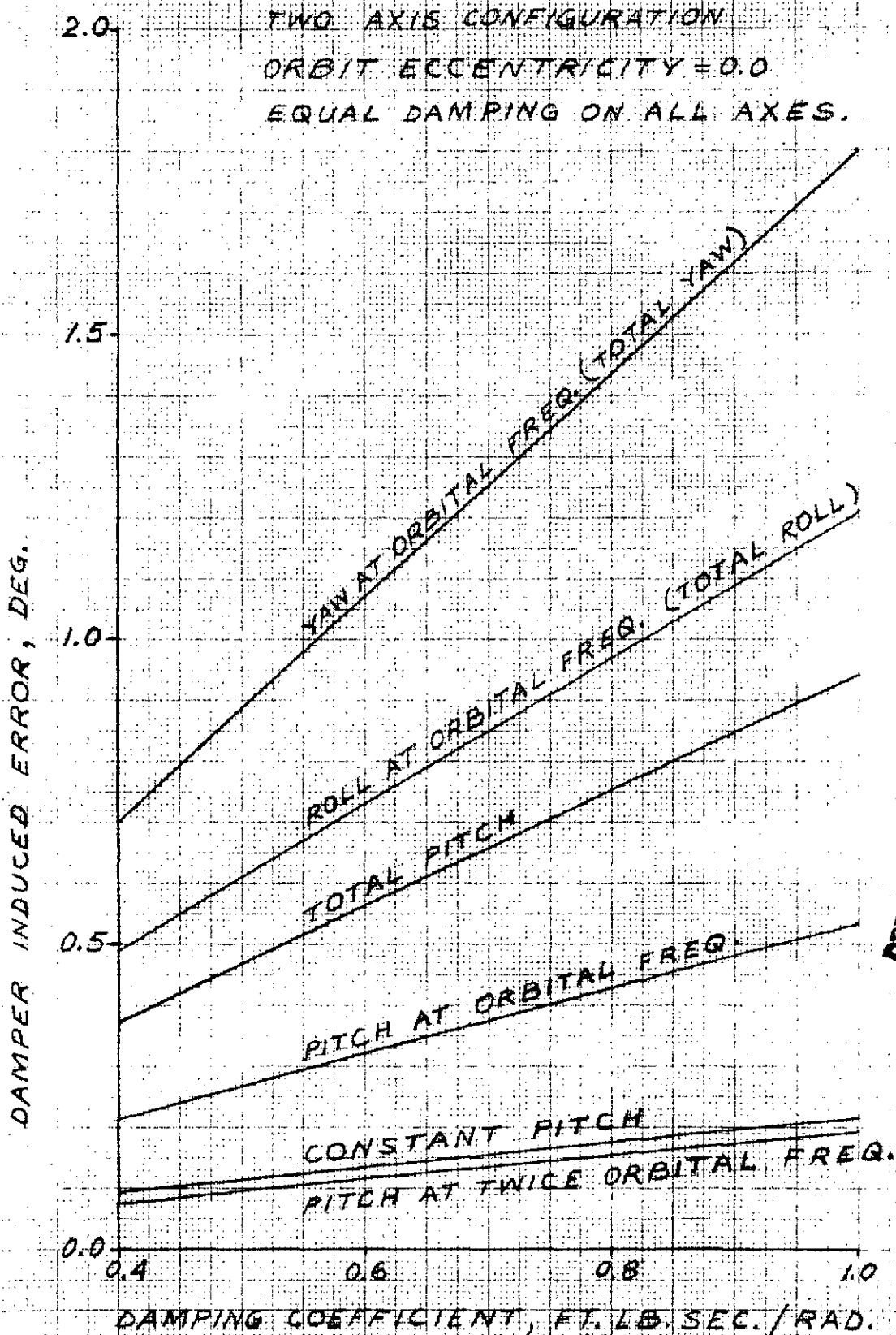
Solar torque is the result of the solar force vector, caused by the pressure of the sunlight (approximately $47.8 \times 10^{-7} \text{ n/m}^2 = 10^{-7} \text{ lb/ft}^2$), not passing through the spacecraft center of mass. The location of the center of mass

Figure 3.2 Definition of Coordinate and Angles



ORIGINAL PAGE IS
OF POOR QUALITY

EFFECT OF DAMPING COEFFICIENT ON THE PITCH, ROLL & YAW ERRORS.



ORIGINAL PAGE IS OF POOR QUALITY

FIGURE 3.3

is well defined, but the effective point of application of the solar force (i.e., the center of pressure) is not invariant, but moves as a function of sun angle. For a spacecraft as large as the LDEF, solar torque will be a strong function of sun angle, since the solar force vector is close to the surface of the spacecraft and the center of mass is on or near the axis of symmetry.

To generalize the study, solar torque was calculated for center of mass/center of geometry differences between 0 and .762 m (2.5 feet) along the axis of symmetry. This range more than encompasses the range of parameters likely to be encountered. For example, if the top half of the spacecraft were purely reflective (specular), and the lower half were purely absorptive, the effective center of pressure/center of mass misalignment would be .366 m (1.2 feet), less than half the maximum value considered.

The results of the solar torque analysis are shown in Figure 3.4. For this evaluation, the sun was assumed to be in the orbit plane, which places the torque primarily on the pitch axis. This is the worst sun orientation since "out of plane" torque will affect the roll axis, which is stronger than the pitch axis, and would produce less local vertical pointing error. It is evident from Figure 3.4 that the largest solar torque error is an orbital frequency error on pitch, and that it is negligible (.24 degrees worst case considered). Solar torque does not produce any significant pitch constant torque.

3.1.3 MAGNETIC DIPOLE TORQUE

In addition to indirectly causing a spacecraft torque through the magnetically anchored rate damper, the earth's magnetic field can produce a direct magnetic

MAGNETIC AND SOLAR ERRORS VS. C.M. OFFSET
TWO AXIS CONFIGURATION
ORBIT ECCENTRICITY = 0.0

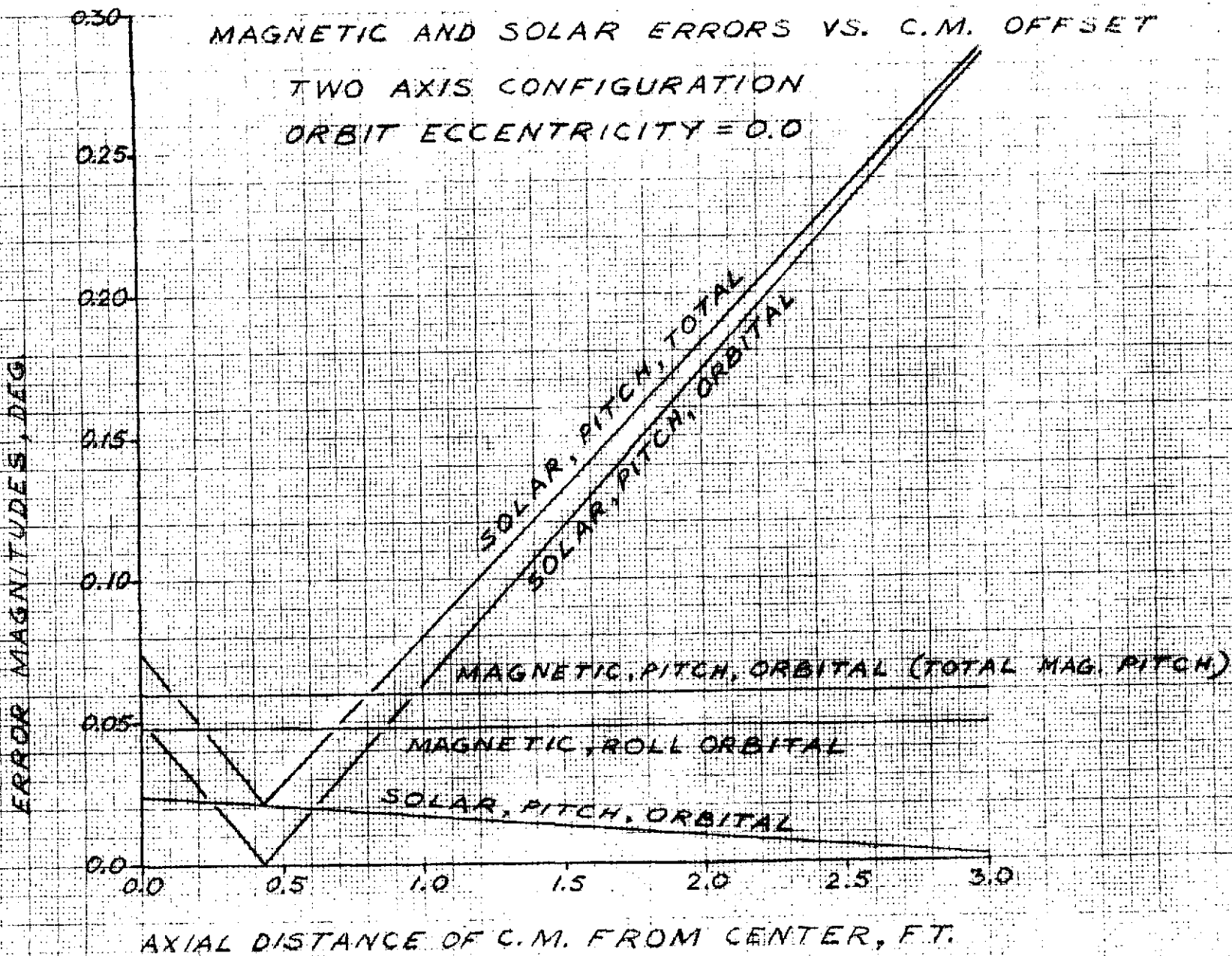


FIGURE 3.4

torque. Any magnetic dipole, caused by magnetic materials mounted on the spacecraft, will attempt to align itself to the earth's magnetic field and will torque the spacecraft. The magnitude of the torque is proportional to the strength of the magnetic dipole moment, the orientation of the dipole within the spacecraft, and the location of the spacecraft with respect to the earth. The magnetic field strength decreases with the cube of the orbit radius (exactly the same as gravity gradient), and is twice as strong at the poles (north and south) as at the equator. Hence, a spacecraft in a high inclination orbit has more magnetic torque on it than a spacecraft in a low inclination orbit, and similarly a spacecraft at a high altitude has less torque on it than a spacecraft at low altitude.

To quantitatively determine the magnitude of the attitude errors, the frequency of the magnetic disturbance torques must be known. At low altitudes, the local magnetic field changes as the spacecraft moves in orbit, and the magnetic torque changes as a function of time. For orbit periods short compared to earth's rotational period, the torques (pitch, roll and yaw) are largely constant (zero frequency) and/or sinusoidal at orbital frequency.

A magnetic analysis was performed with the same magnetic field assumptions as those of Section 3.1.1 except direct magnetic torques were considered. Torques appear on all axes, being exclusively sinusoidal at orbital frequency on pitch, and constant plus sinusoidal at orbital frequency on roll and yaw. In low inclinations the roll and yaw magnetic dipoles are the most effective, producing static torques on yaw and roll (respectively), with the pitch axis dipole producing only small sinusoidal roll and yaw torques. For a two axis gravity gradient spacecraft, a constant yaw magnetic torque implies a pre-

ferred yaw orientation, since the dipole will align itself to the magnetic field about the yaw axis. The torques on pitch reduce with orbit inclination, but in fact never go to zero since the earth's magnetic equator is not coincident with the earth's geographic equator.

The magnitude of the magnetic torques are directly proportional to the size of the spacecraft magnetic moment. In general, this dipole is not known in advance of the spacecraft construction, and varies with payload. The magnetic dipole of the LDEF spacecraft is not expected to be large because of the nature of its payload. Hence, only a single dipole magnitude, 1000 pole-cm per axis, was evaluated. The results of the evaluation are shown in Figure 3.4. Since magnetic torques are pure torque, not force, the error is independent of center of mass position.

3.1.4 ORBIT ECCENTRICITY TORQUES

One of the characteristics of a circular orbit is the constant rate of rotation of the radius vector (a vector from the center of the earth to the orbiting body). For a spherical earth the radius vector is parallel to the local vertical, and a gravity gradient spacecraft will align itself with the local vertical and acquire the average rate of rotation.

The rate of rotation of the radius vector is not uniform for an eccentric orbit, however, but varies from a minimum at apogee to a maximum at perigee. The spacecraft will acquire the average rate of rotation of the eccentric orbit, but cannot respond to the variations in rate. Consequently errors will develop between the axis of minimum moment of inertia and the local vertical. The spacecraft will therefore be torqued sinusoidally by gravity gradient, with peak torque at apogee and perigee. Since the disturbance torque is a gravity

gradient torque, absolute moments of inertia are irrelevant, and the attitude error is dependent only upon moment of inertia relationships, and orbit eccentricity

The attitude error resulting from orbit eccentricity is only a pitch error. Figure 3.5 shows the attitude error as a function of orbit eccentricity for the LDEF. Neither the orbit altitude, nor the orbit inclination, affect eccentricity errors.

3.1.5 AERODYNAMICS

At altitudes of 500 km (270 nm) the earth's atmosphere is a major source of disturbance to the LDEF. The dynamic pressure (the familiar $1/2 \rho v^2$) caused by the spacecraft's passage through the rarified atmosphere can exceed solar pressure by a factor of ten or more. Aerodynamic pressure is directly proportional to the aerodynamic density, and to estimate the density, a model of the earth's atmosphere is required. There are several atmospheric models in existence, the most widely used being that of JACCHIA⁽¹⁾. This model defines the atmospheric density as a function of altitude, solar sun spot cycle (F 10.7 cm solar flux) and diurnal bulge. The diurnal bulge is a "thickening" of the earth's atmosphere due to the earth temperature increase associated with solar heating. Typically, the greatest density occurs at 2 p.m. local time, where the density may be a factor of three higher than on the opposite side of the earth (at this altitude). The density difference is greater at higher altitudes.

Aerodynamic torques, like solar torques, are dependent upon the spacecraft configuration, but are particularly sensitive to orbit altitude, sun spot cycle, orbit eccentricity, argument of perigee, and position of the orbit with respect to the diurnal bulge.

ORIGINAL PAGE IS
OF POOR QUALITY

MAXIMUM PITCH ERROR VS. ECCENTRICITY
TWO AXIS CONFIGURATION

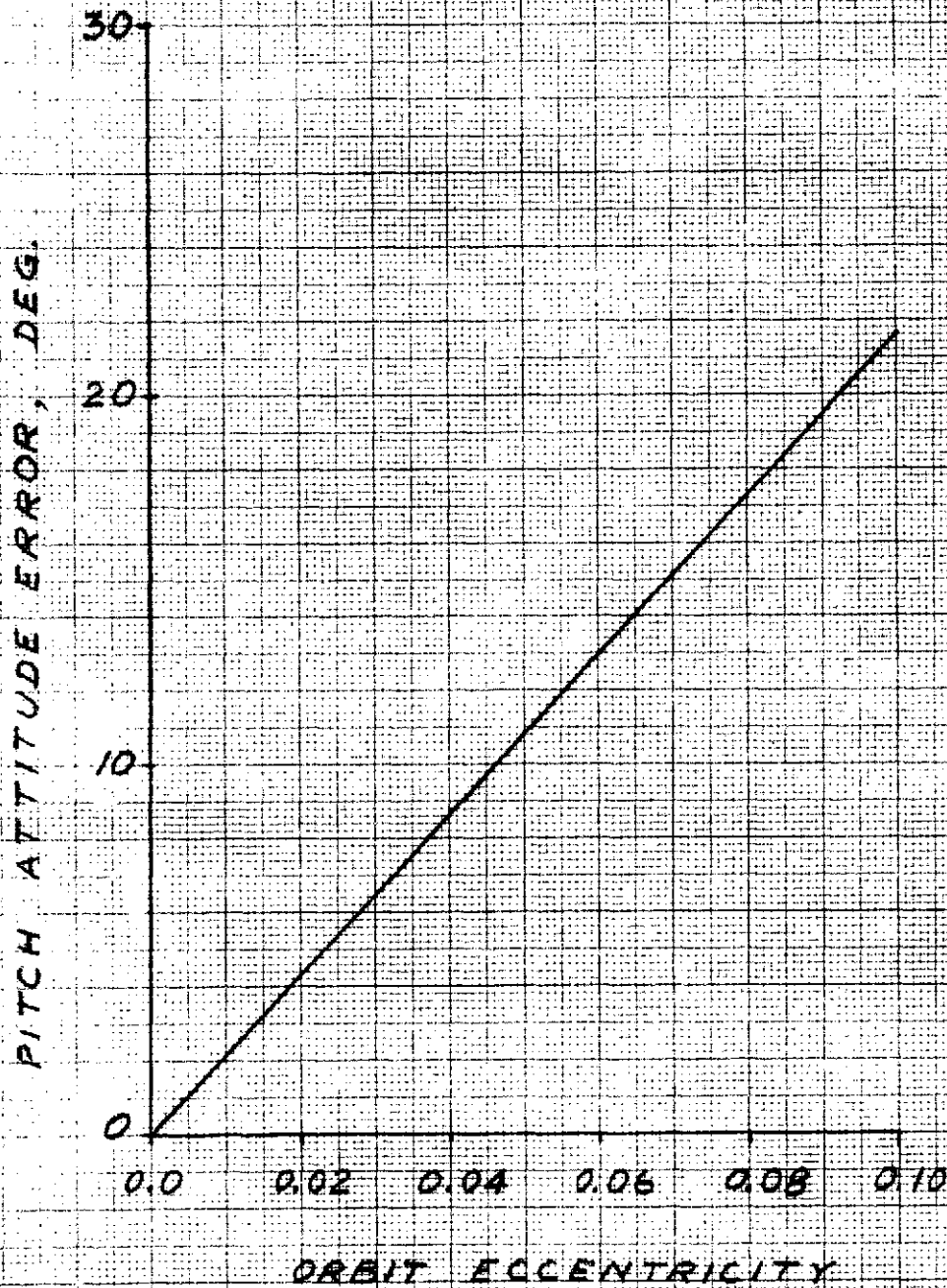


FIGURE 3.5

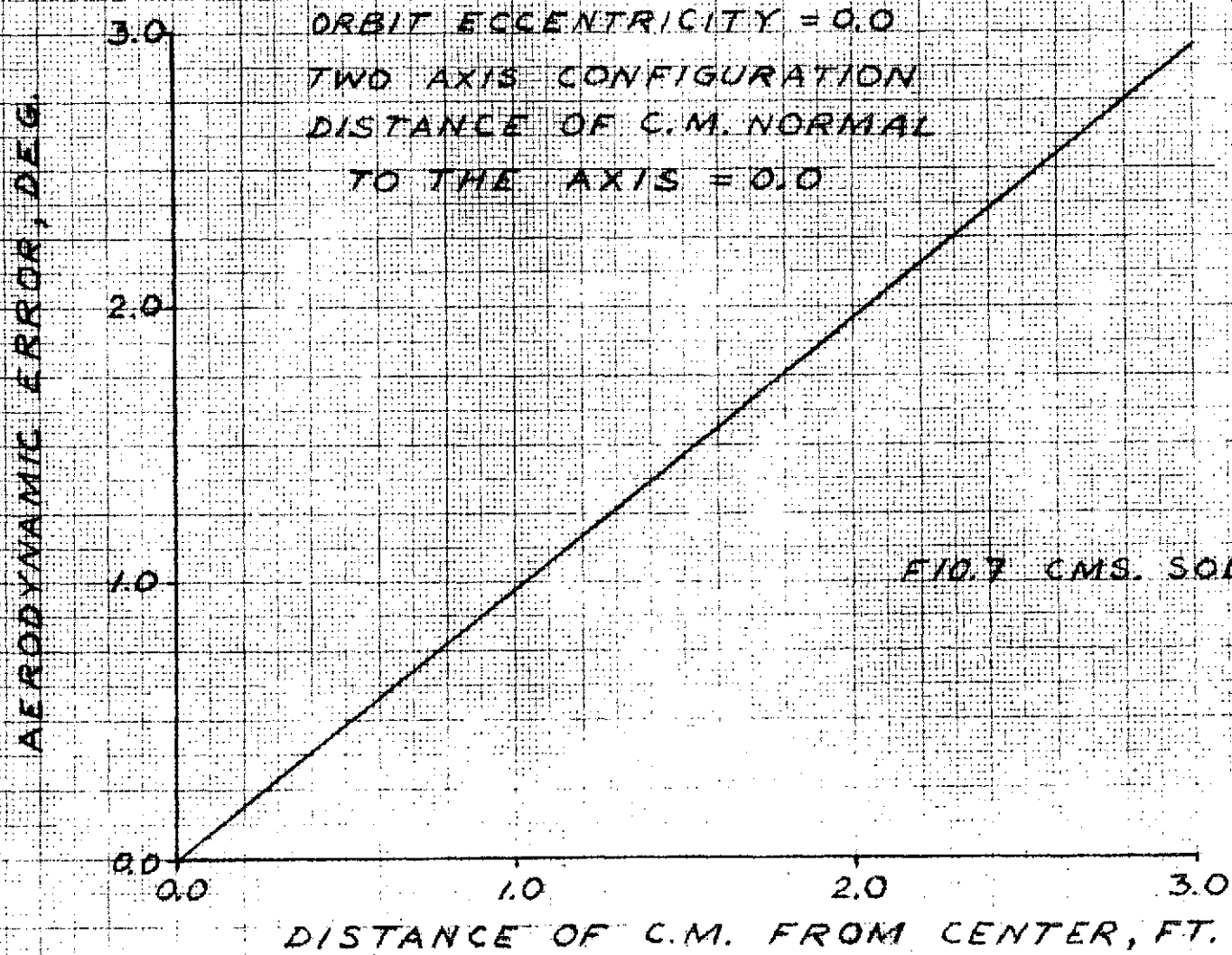
A general aerodynamic study was performed for LDEF, since it was anticipated that aerodynamic effects would be the largest source of disturbance torque. Four factors considered in the analysis were spacecraft configuration, orbit eccentricity, argument of perigee, and ascending node. The F10.7 centimeter solar flux index was selected to be 150, which is approximately 95 percentile for the 1978 time period⁽²⁾, and the nominal altitude was 500 km (270 n. miles). A drag coefficient of 2.0 was assumed.

3.1.5.1 Spacecraft Configuration

The LDEF spacecraft is symmetrical, and the aerodynamic torques would be negligible if the center of aerodynamic pressure coincided with the center of mass. The effect of angle of attack between the aerodynamic stream and the spacecraft, is insignificant because the angle of attack is relatively constant. Any shift in the center of mass from the center of geometry will, however, produce an aerodynamic torque, and hence an attitude error.

The effects on pitch and roll errors of the aerodynamic torques caused by an axial offset of the center of mass/center of pressure are shown in Figures 3.6 through 3.13. Axial offsets were considered the most important for the two axis configuration. The torques were calculated for a circular orbit with an ascending node position of zero degrees (at autumnal equinox). Figures 3.6, 3.7 and 3.8 show the constant, orbital frequency, and twice orbital frequency pitch errors resulting from aerodynamic torques on the pitch axis. The largest errors are those due to the orbital frequency component of the torque, reaching a peak of approximately 5 degrees at a center of mass offset of .762 m (2.5 feet). The constant torque error reaches a peak

EFFECT OF A SHIFT OF THE C.M. ON
PITCH ERROR DUE TO PITCH TORQUE
(CONSTANT COMPONENT)



DISTANCE OF C.M. FROM CENTER, FT.
FIGURE 3.6

EFFECT OF A SHIFT OF THE C.M.
ON PITCH ERROR DUE TO PITCH TORQUE
(ORBITAL FREQUENCY COMPONENT)

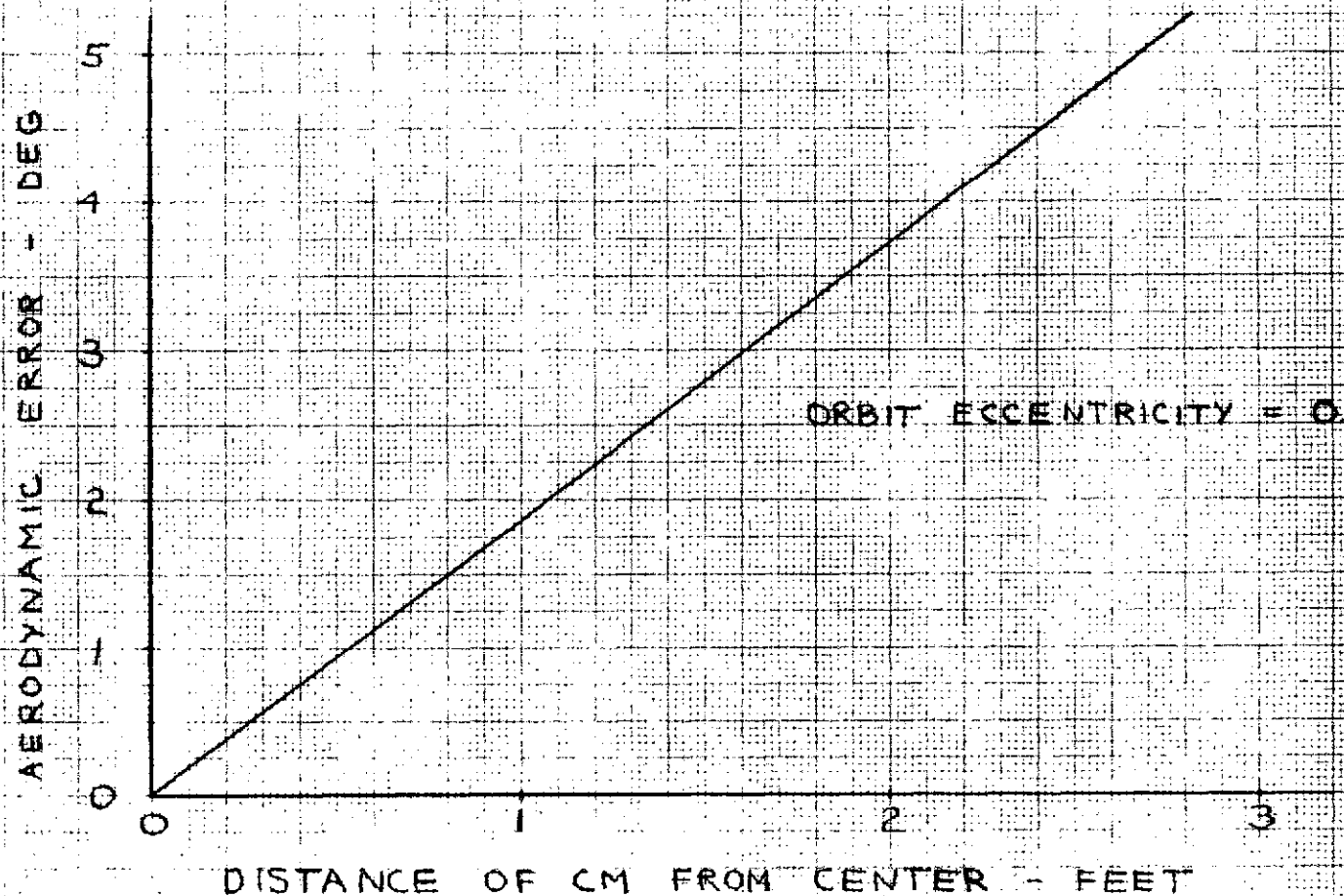


FIGURE 3.7

EFFECT OF SHIFT OF THE C.M. ON
PITCH ERROR DUE TO PITCH TORQUE
(TWICE ORBITAL FREQUENCY COMPONENT)

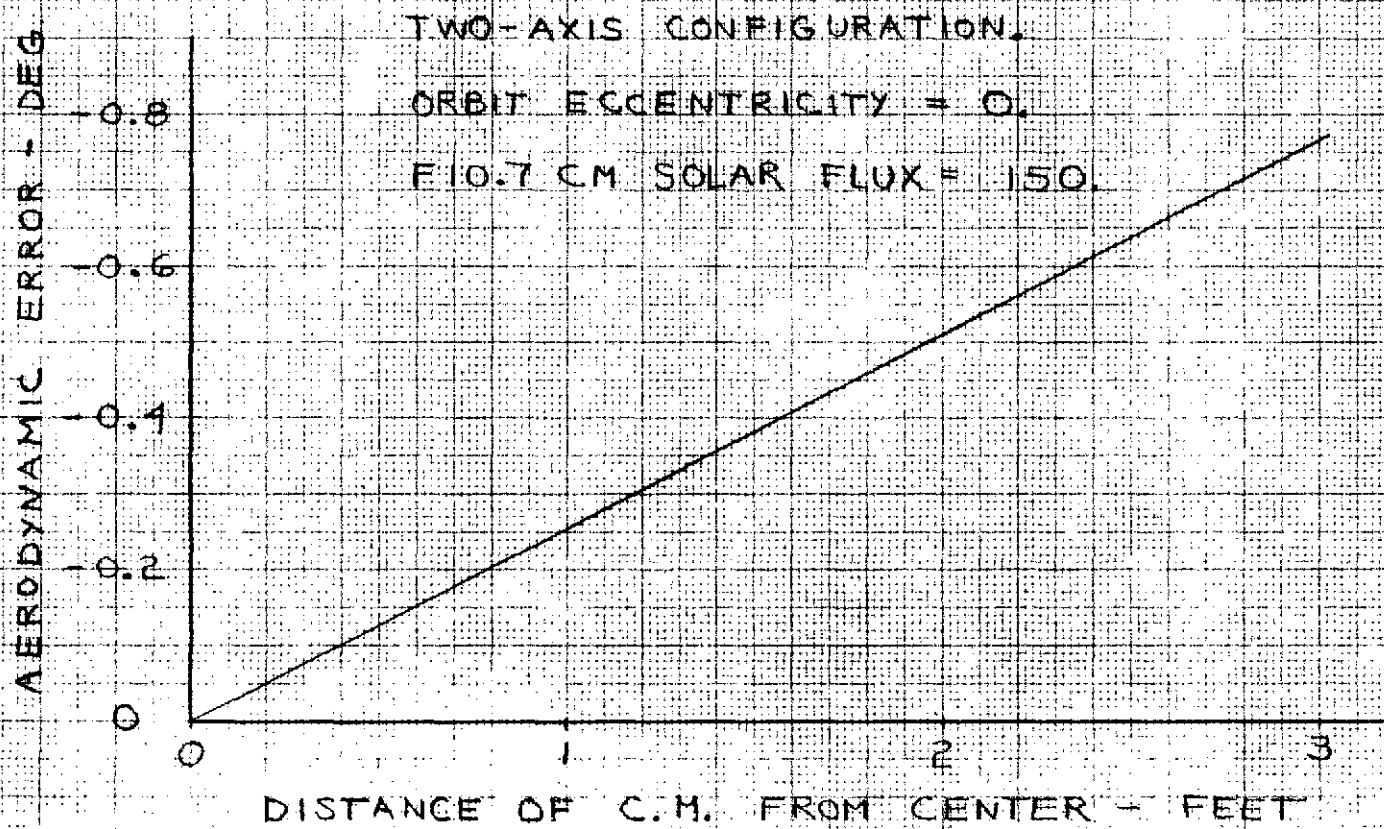


FIGURE 3.8

of approximately 2.5 degrees at the same center of mass offset. The value of the constant torque error is particularly important with regard to Garber Instability (Section 3.2). The pitch error due to the twice orbital component of the aerodynamic torque is small (.65 deg. at .762 m).

The motions of the roll and yaw axes are coupled, even in the linear model, and hence roll errors are obtained from both roll and yaw disturbance torques. Figure 3.9, 3.10 and 3.11 show the effects of the axial shift of the center mass on the constant, orbital frequency and the twice orbital frequency components, respectively, of the roll error caused by the roll torque. The primary cause of the roll torque is the rotational rate of the earth, which causes the atmosphere at an altitude of 500 km to have a velocity in inertial space; a component of which is along the pitch axis. The resulting torque is therefore along the roll axis. All of the roll errors are small.

Figure 3.12 and 3.13 demonstrate the influence on the orbital and the twice orbital frequency components of the roll error caused by the yaw torques. The constant components are zero because the roll yaw coupling is zero. All these errors are negligible.

For completeness, center of mass/center of pressure shifts along the cylinder radius (normal to the axis) were considered. For the two axis configuration, such a shift would cause the spacecraft to weathervane about yaw, and assume a preferred orientation. Pitch and roll torques would be reduced in this manner, but some pitch and roll errors will still result. Figure 3.14 shows the results of the analysis, and indicates no significant pitch or roll error increase (an axial offset of 0.152 m - six inches - is included in the figure).

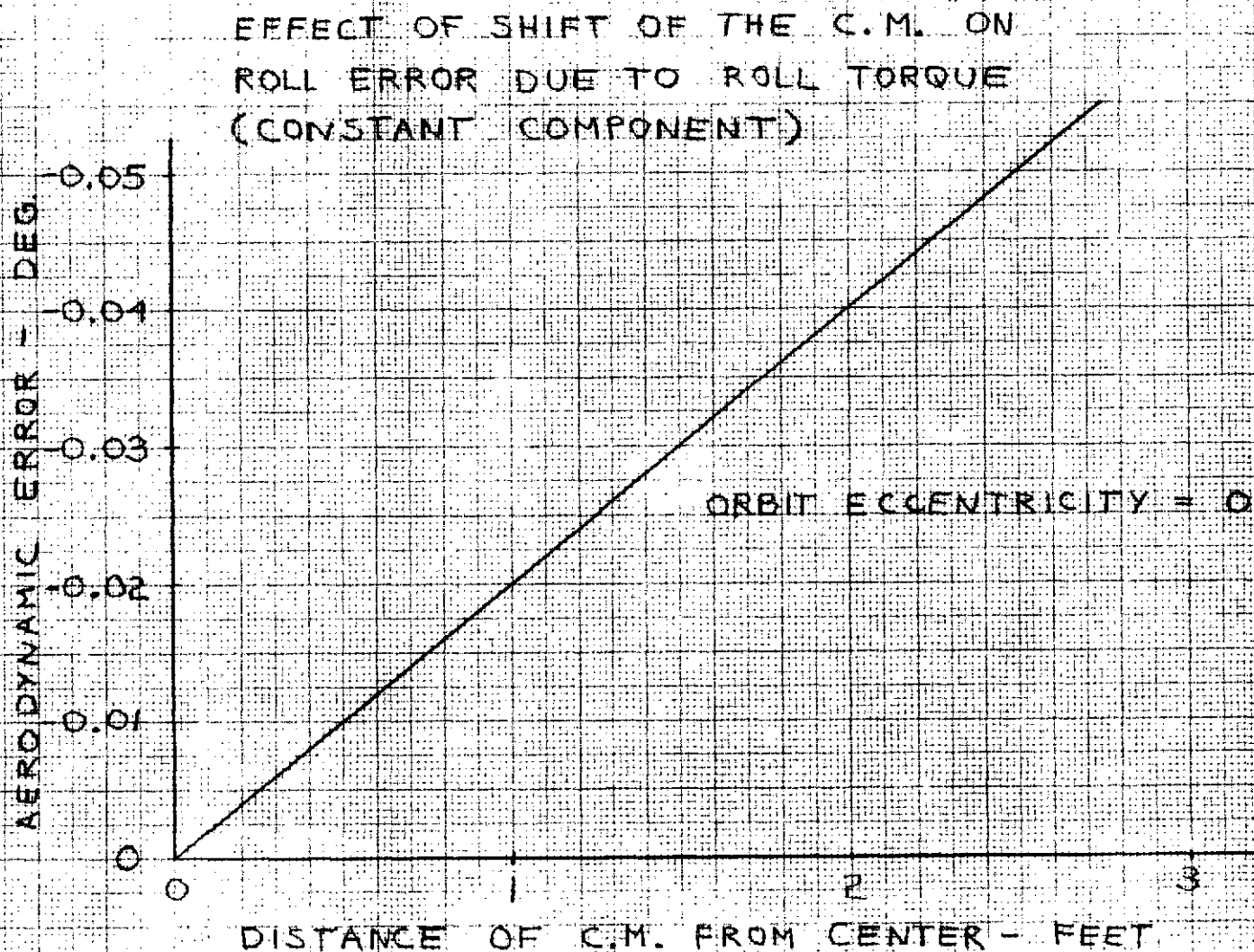


FIGURE 3.9

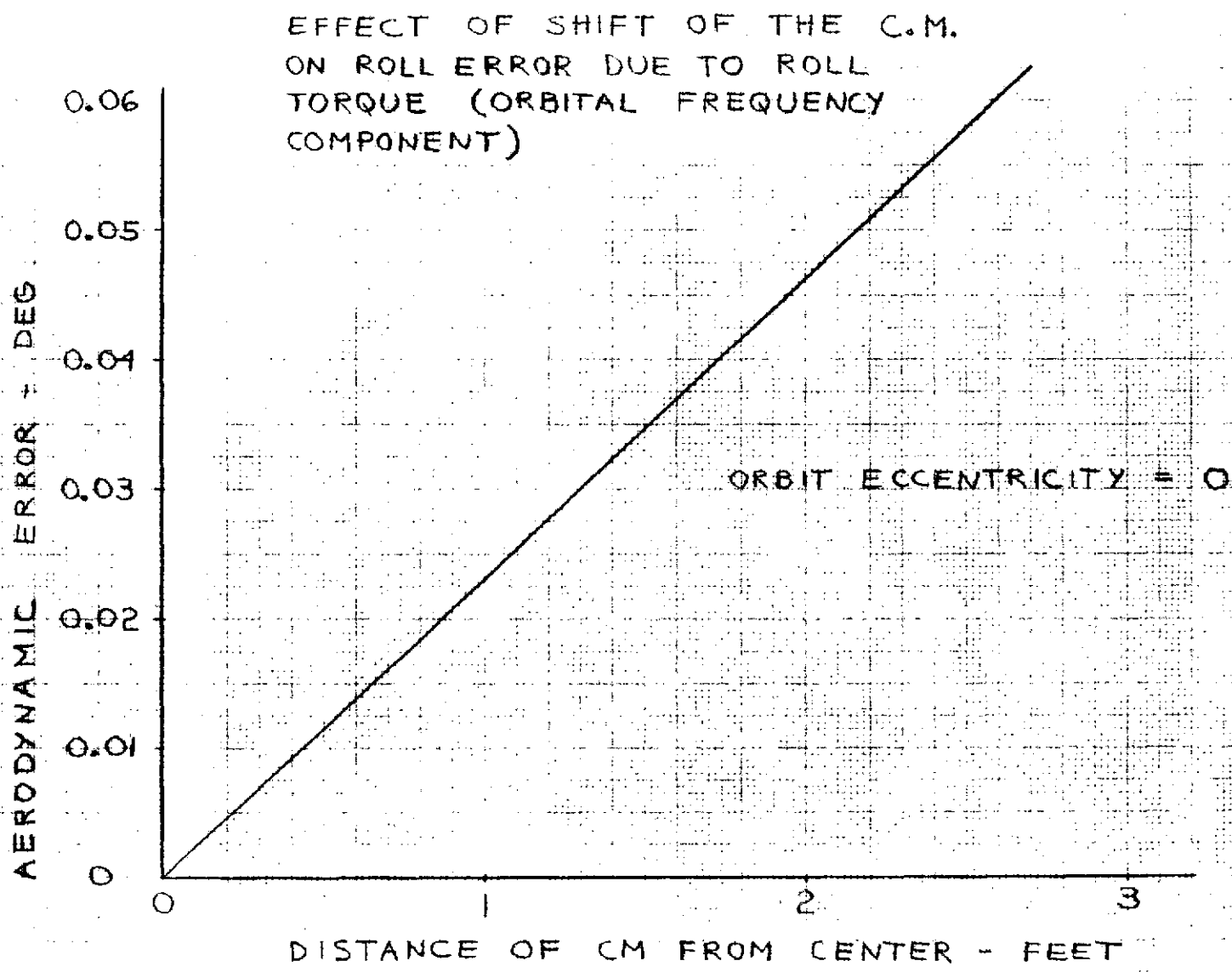


FIGURE 3.10

EFFECT OF SHIFT OF THE C.M. ON
ROLL ERROR DUE TO ROLL TORQUE
(TWICE ORBITAL FREQUENCY COMPONENT)

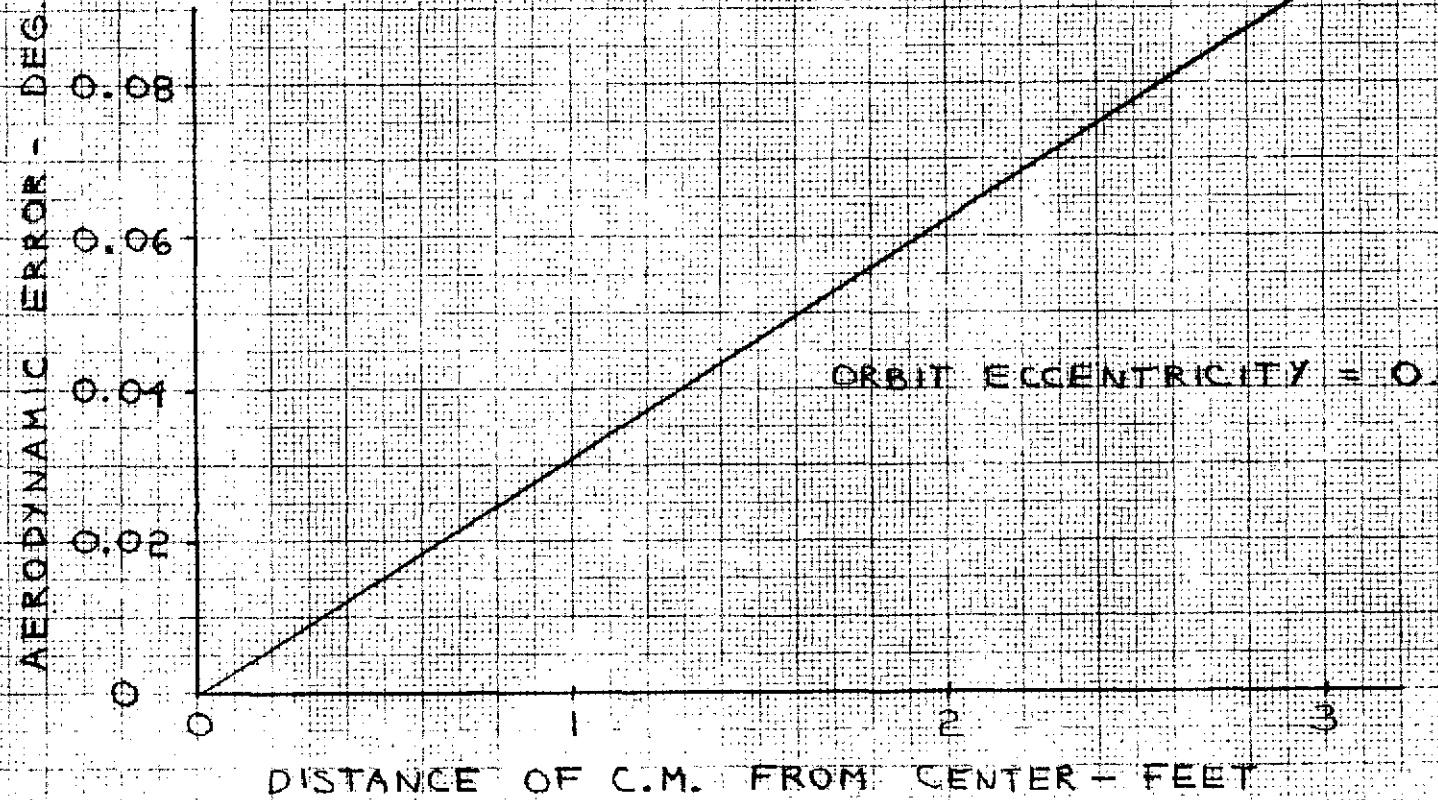


FIGURE 3.11

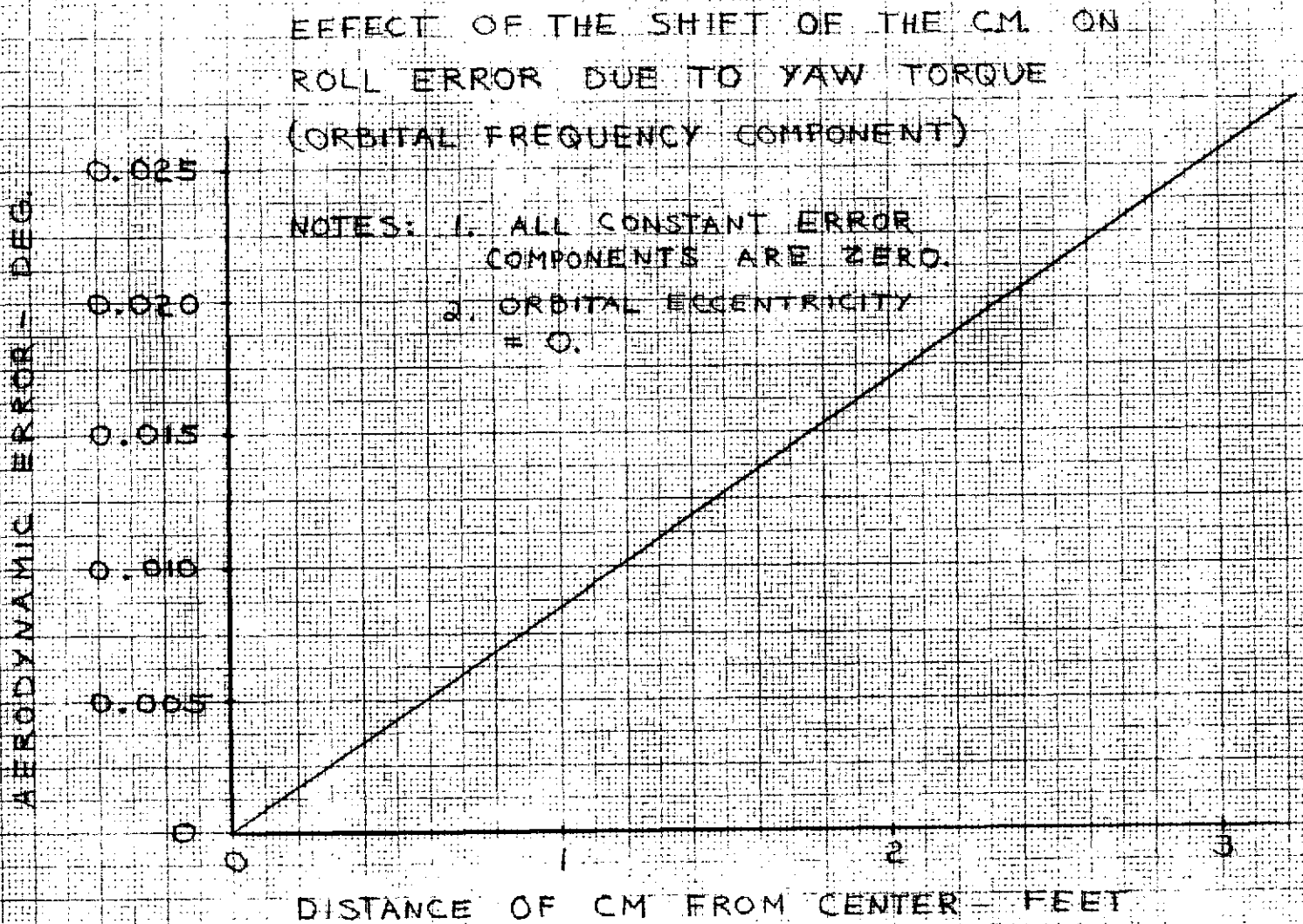


FIGURE 3.12

EFFECT OF A SHIFT OF THE C.M. ON
ROLL ERROR DUE TO YAW TORQUE
(TWICE ORBITAL FREQ. COMPONENT)

ORBIT ECCENTRICITY = 0.0

AERODYNAMIC ERROR, DEG.

0.04

0.03

0.02

0.01

0.0

0.0

0.5

1.0

1.5

2.0

2.5

3.0

AXIAL DISTANCE OF C.M. FROM CENTER, FT.

FIGURE 3.13

TWO AXIS ERRORS VS. RADIAL C.M. OFFSET

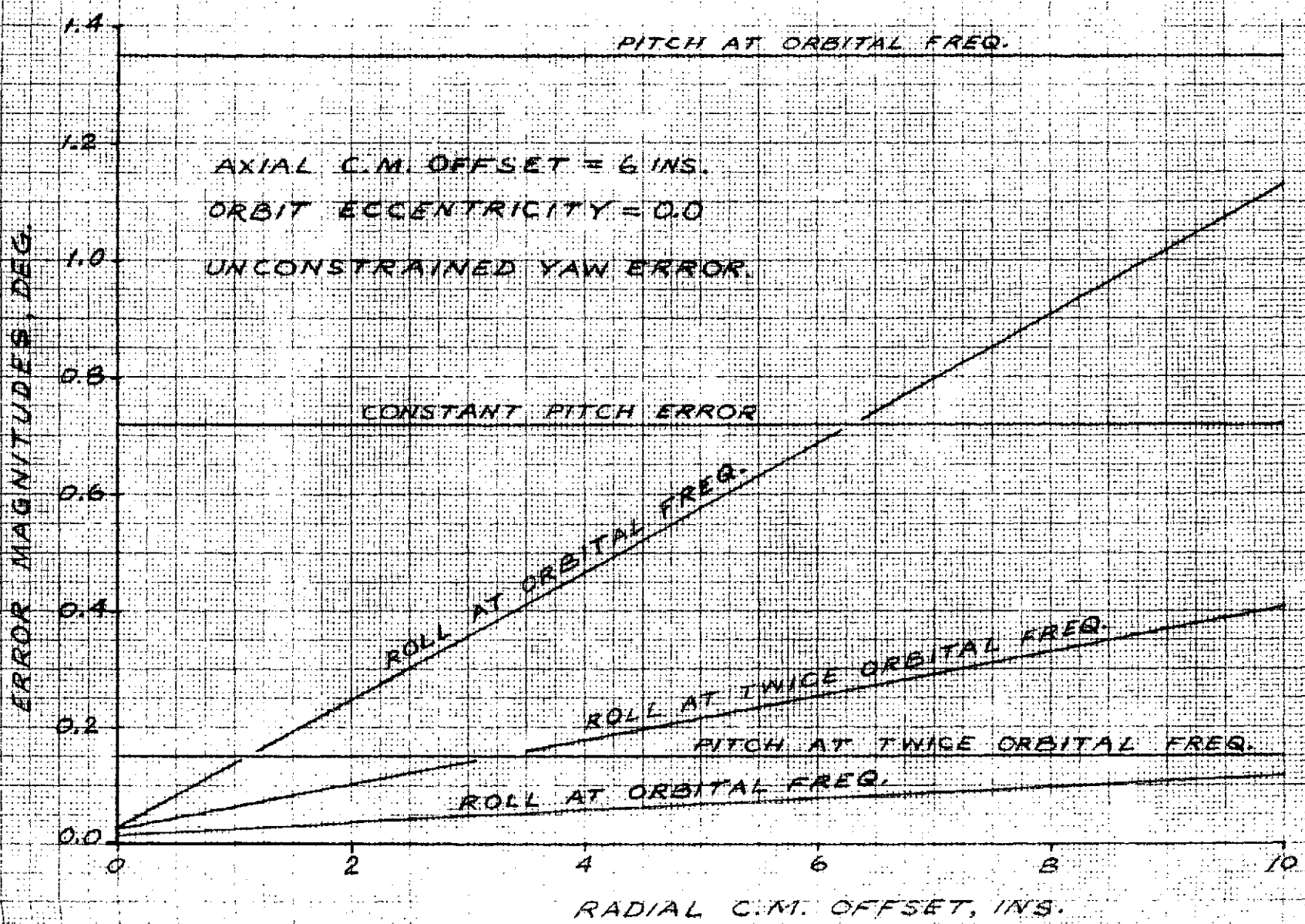


FIGURE 3.14

Figure 3.15 shows the total aerodynamic error in each axis as a function of axial offset.

3.1.5.2 Orbit Eccentricity

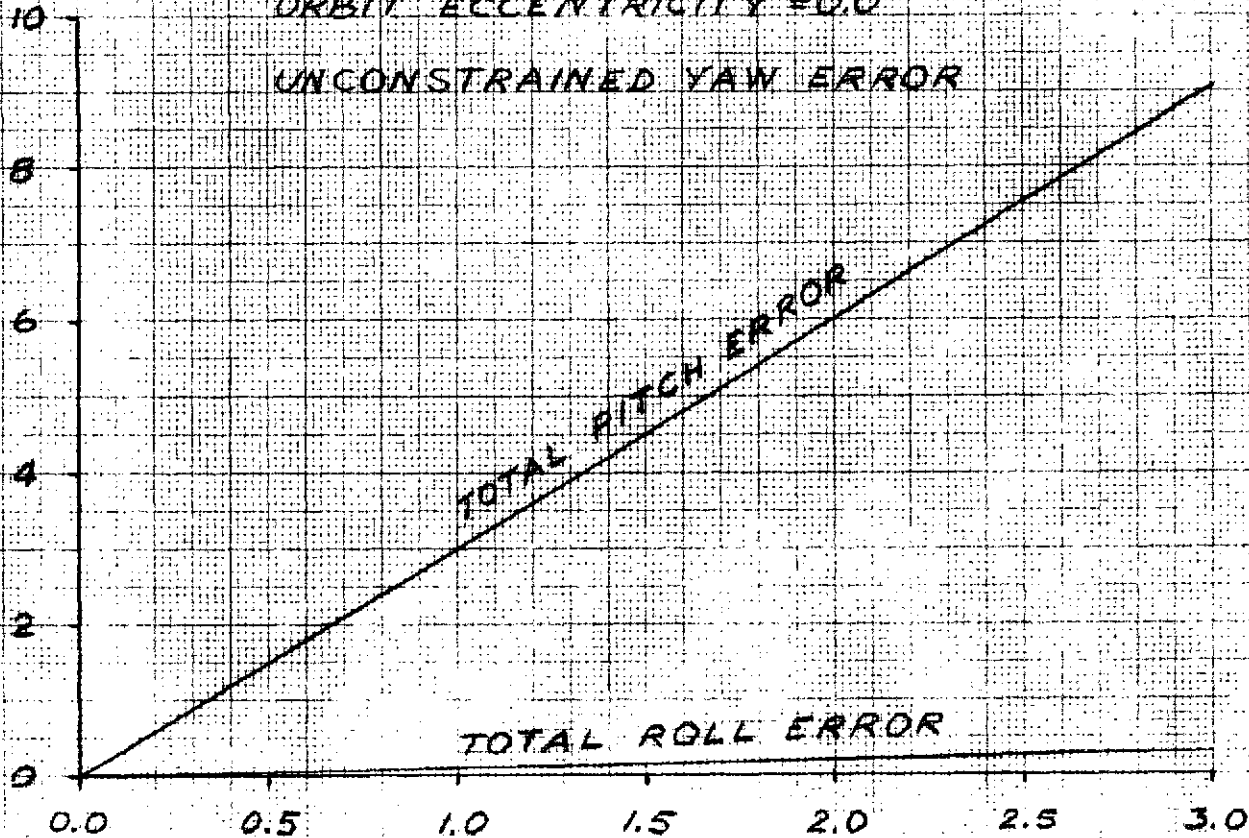
Figure 3.16, 3.17 and 3.18 show the effect of the orbit eccentricity on the constant, orbital, and twice orbital frequency components of the aerodynamic pitch error. The center of pressure/center of mass offset was selected as .152 m (six inches) for this evaluation. This would require a difference in drag coefficient of approximately 13 percent between the top half of the cylinder and the bottom half of the cylinder, or a center of mass shift of .152 m (six inches), or a combination of both. For a cylinder, a 13 percent change in drag coefficient is virtually impossible, hence a center of mass shift is assumed. It is evident from the figures that the effect of orbit eccentricity is severe at large (0.02) eccentricities. It must be recognized, however, that at an eccentricity of 0.0729, perigee is at the surface of the earth, well below any reasonable perigee.

The roll errors caused by aerodynamics in an eccentric orbit are shown in Figures 3.19, 3.20 and 3.21; and the roll errors due to yaw torques at orbital and twice orbital frequency are shown in Figure 3.22 and Figure 3.23. These errors are negligible.

The effect of a radial center of mass shift was evaluated for an orbit with a 0.01 eccentricity. Figure 3.24 shows the pitch and roll errors assuming a .152 m (six inch) axial offset. As in Figure 3.14, there is no pitch error increase, but the roll error is much larger than in Figure 3.19 through Figure 3.23. Figure 3.25 shows the total effect of orbit eccentricity on each axis. As indicated on the previous Figures, other error sources are negligibly affected by orbit eccentricity.

TWO AXIS AERODYNAMIC ERRORS
 VS.
 AXIAL C.M. OFFSET

TOTAL AERODYNAMIC ERROR, DEG.

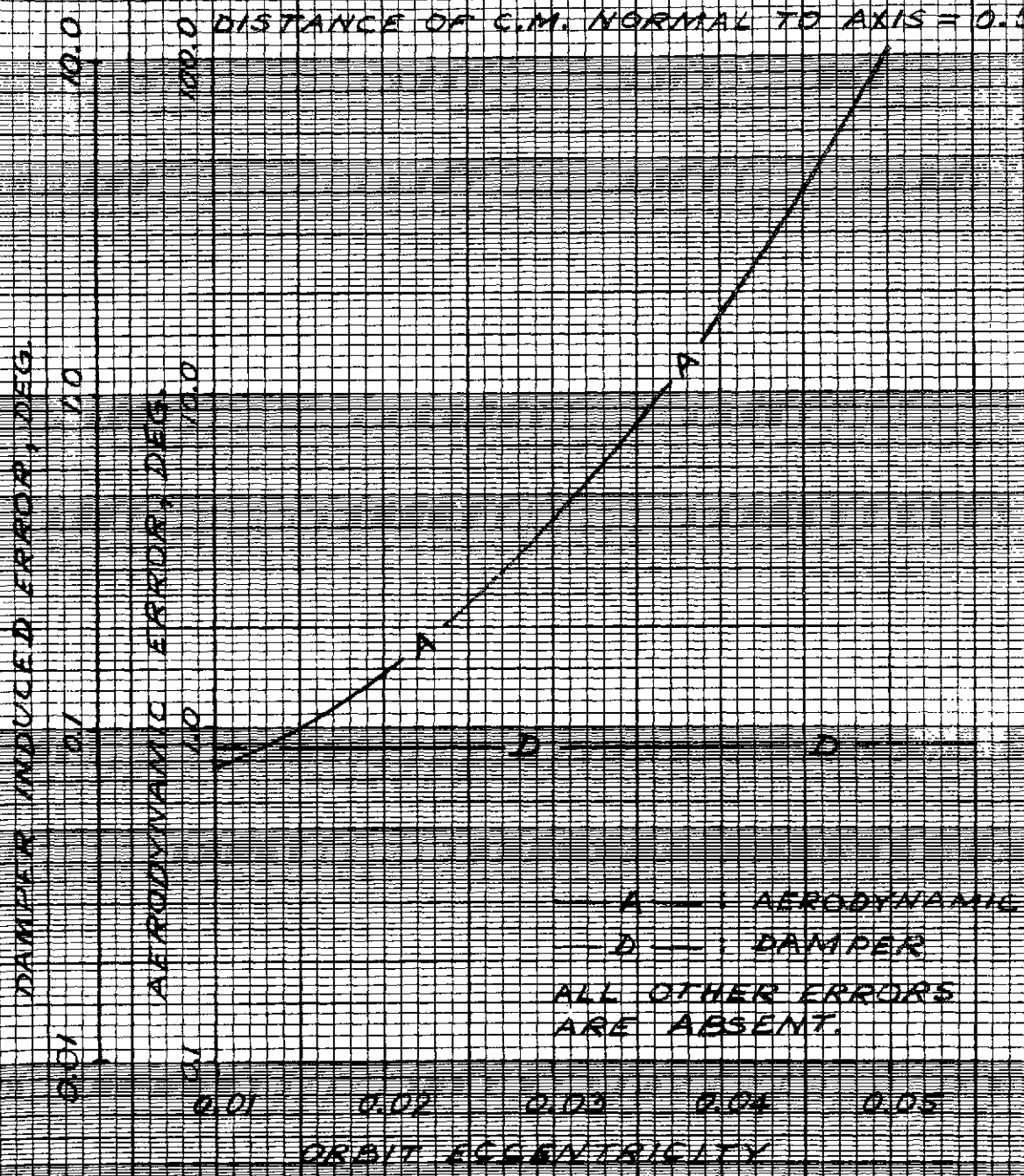


AXIAL C.M. OFFSET, FT.

FIGURE 3.15

EFFECT OF ORBIT ECCENTRICITY ON
PITCH ERROR DUE TO RITCH TORQUE
(CONSTANT COMPONENT)

C.M. IS 6 INS. AWAY FROM CENTER (AXIAL)
DAMPING COEFF. = 0.4 LB. FT. SEC. / RAD.
DISTANCE OF C.M. NORMAL TO AXIS = 0.9



A — AERODYNAMIC
D — DAMPER
ALL OTHER ERRORS
ARE ABSENT.

FIGURE 3.16

EFFECT OF ORBIT ECCENTRICITY ON
PITCH ERROR DUE TO PITCH TORQUE
(ORBITAL FREQ. COMPONENT)

C.M. IS 6 INS. OFF CENTER (AXIAL).

DAMPING COEFF. = 0.4 LB. FT. SEC. / RAD.

DISTANCE OF C.M. NORMAL TO AXIS = 0.0

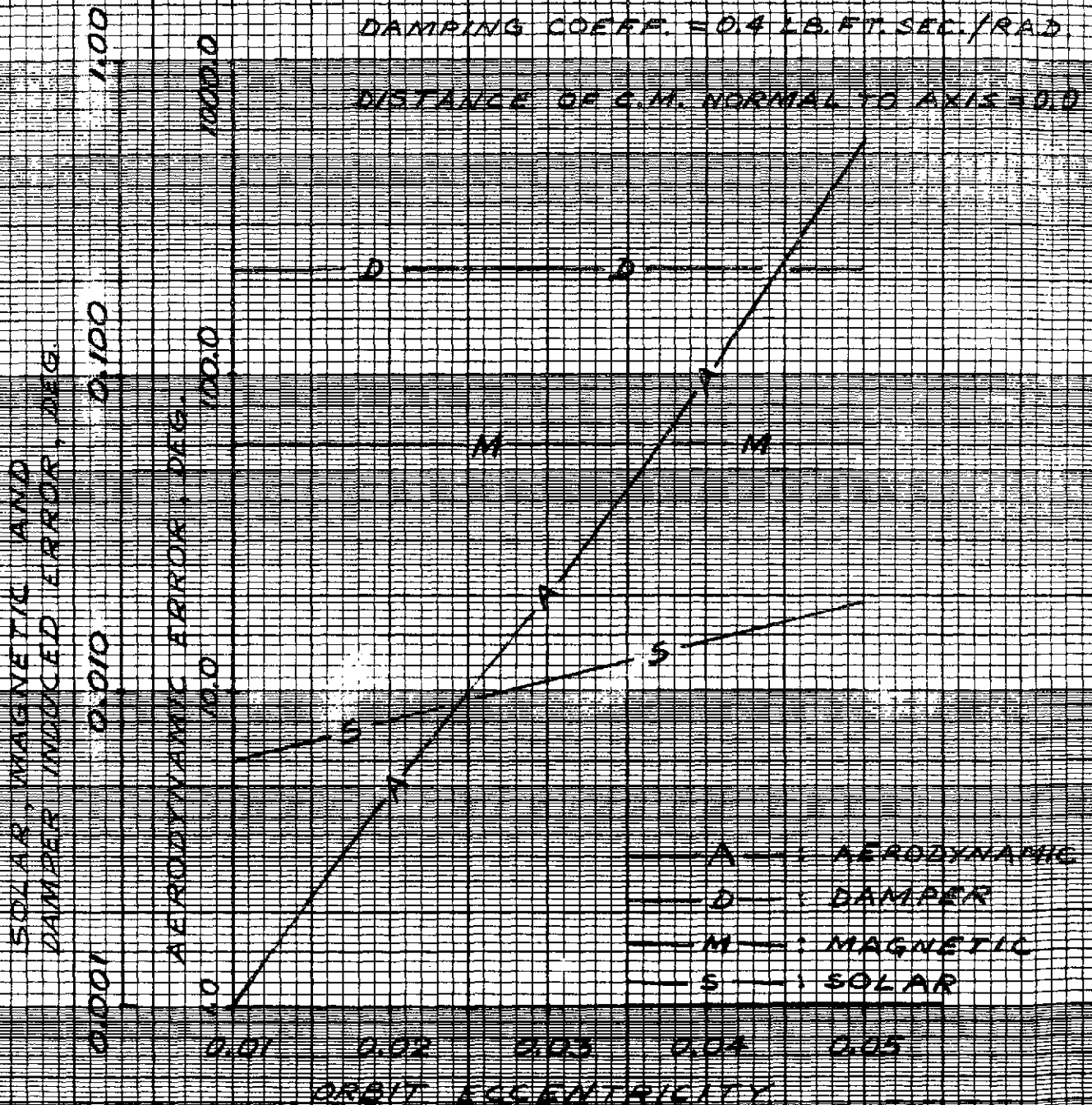


FIGURE 3.17

EFFECT OF ORBIT ECCENTRICITY ON
 PITCH ERROR DUE TO PITCH TORQUE
 (TWICE ORBITAL FREQ. COMPONENT)

C.M. IS 6 INS. OFF CENTER.

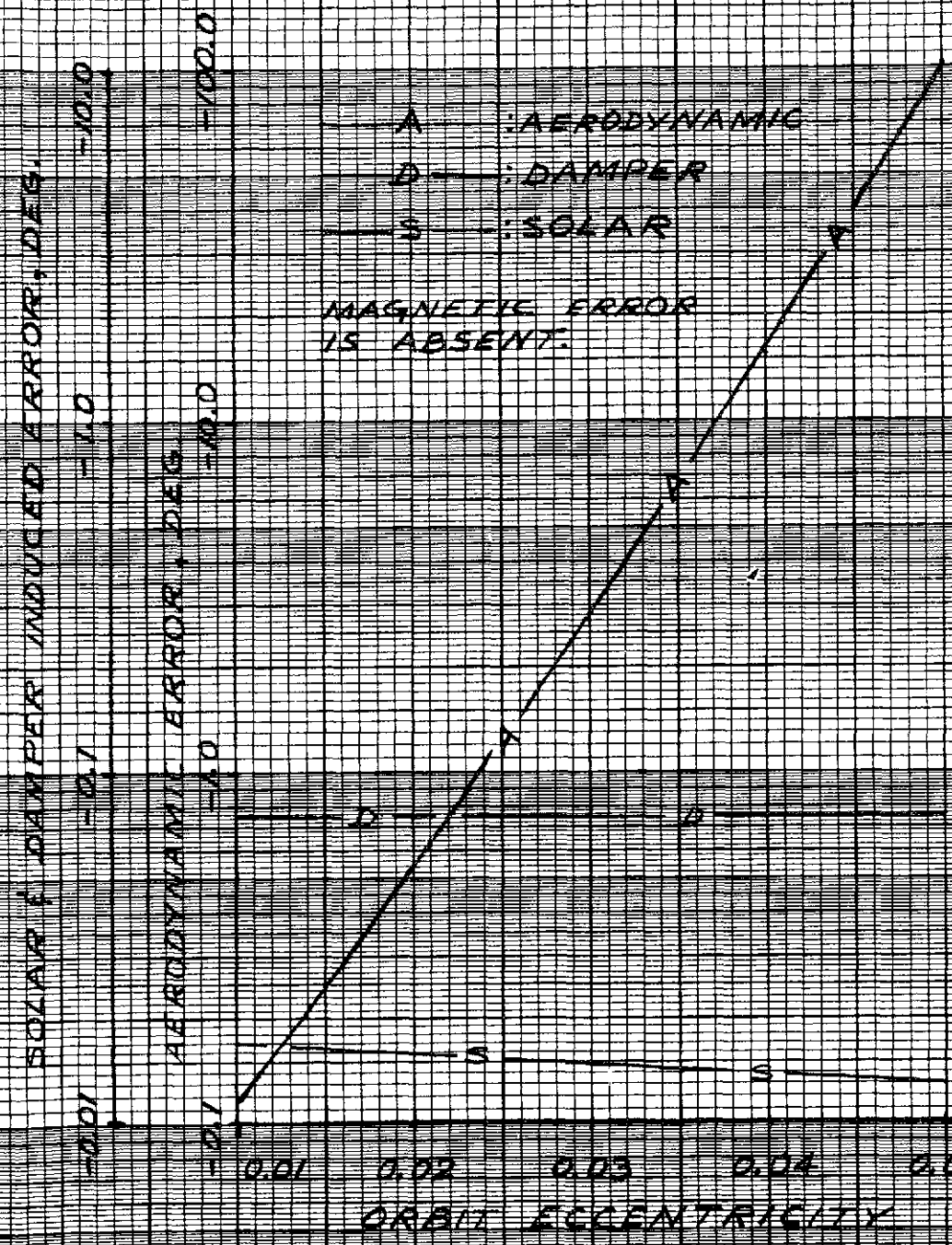


FIGURE 3.18

EFFECT OF ORBIT ECCENTRICITY ON
ROLL ERROR DUE TO ROLL TORQUE
(CONSTANT COMPONENT)

C.M. IS 6 INS. OFF CENTER.

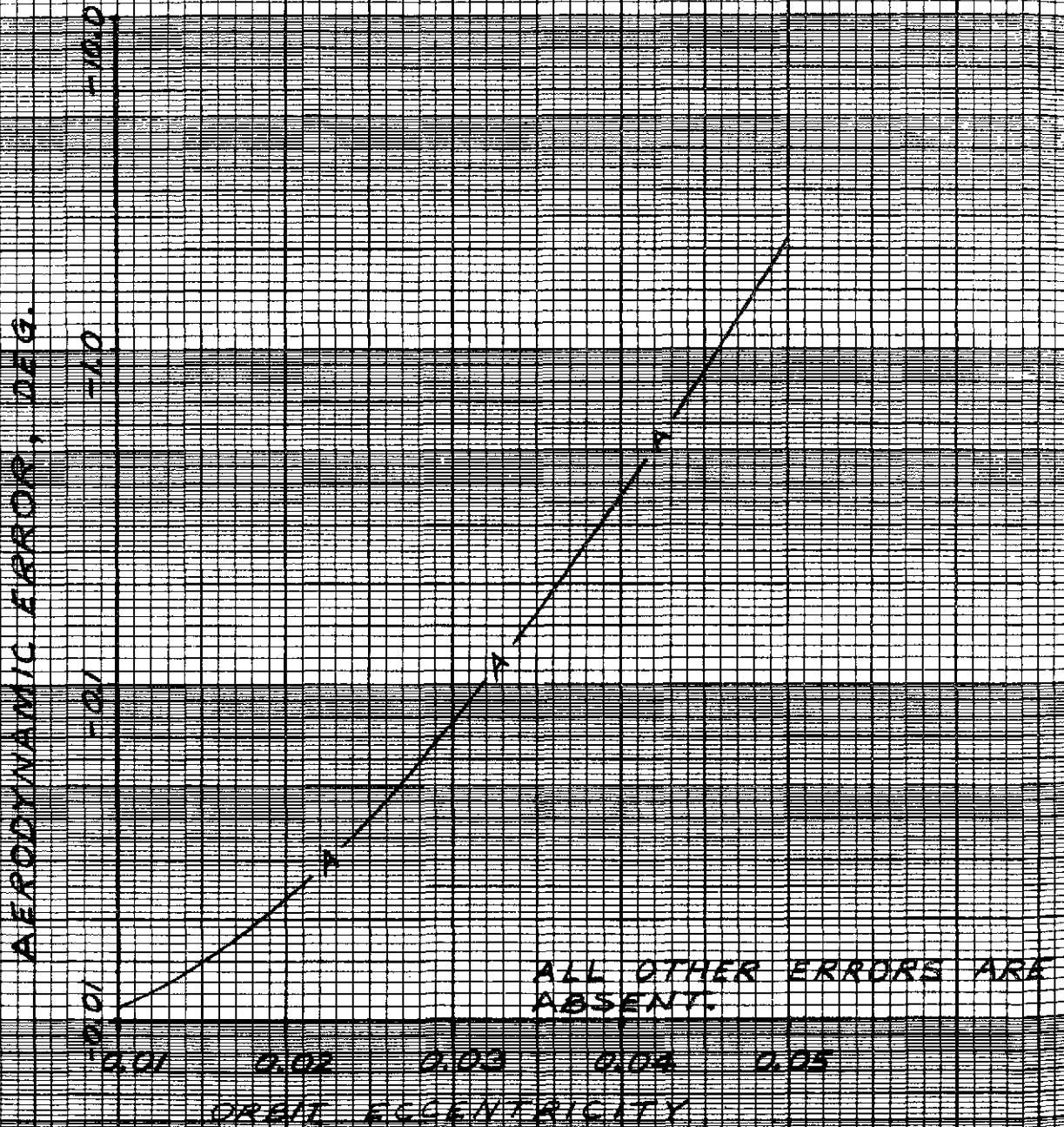


FIGURE 3.19

EFFECT OF ORBIT ECCENTRICITY ON
 ROLL ERROR DUE TO ROLL TORQUE
 (ORBITAL FREQ. COMPONENT)

C.M. IS 6 INS. OFF CENTER.

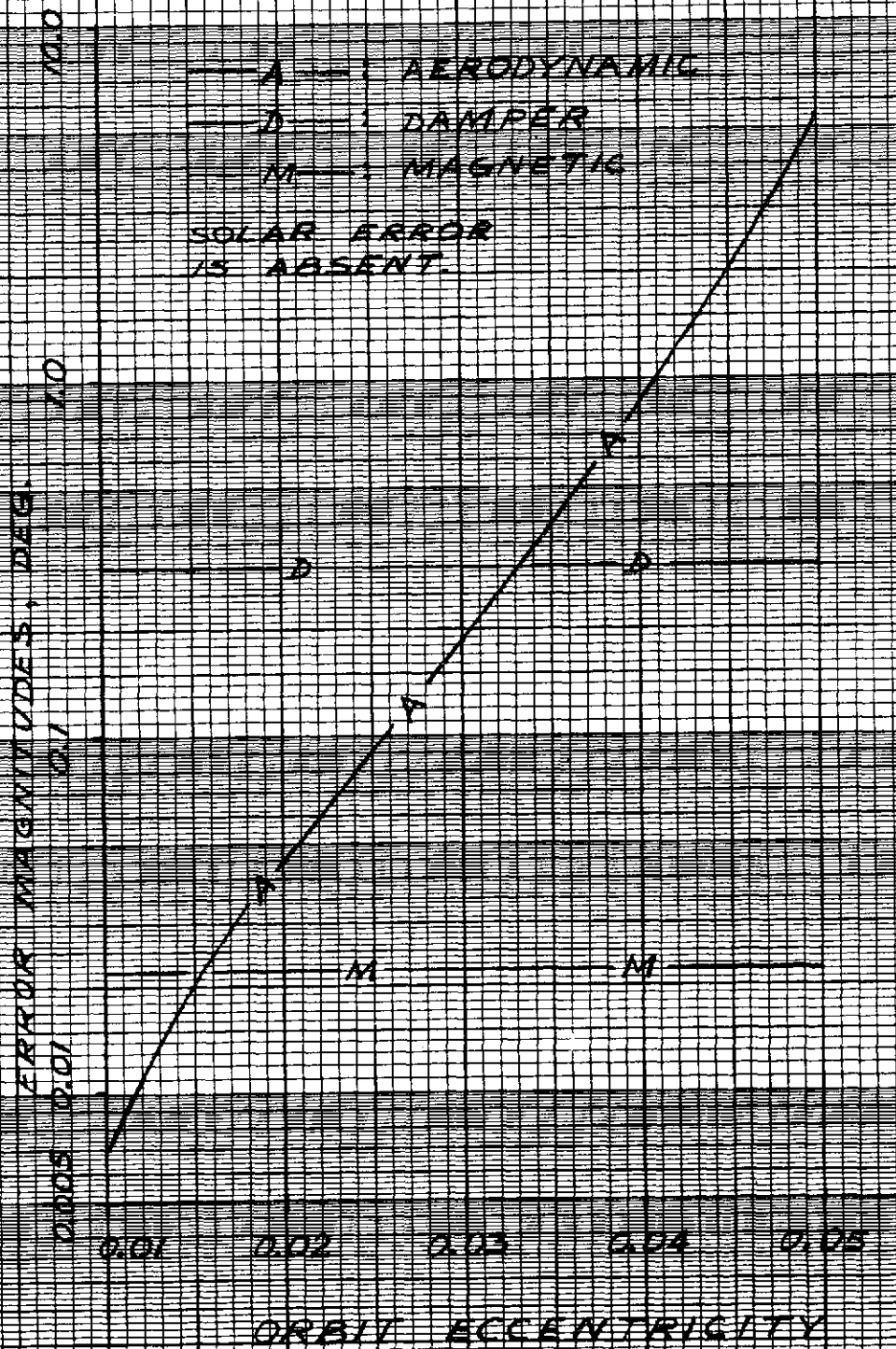


FIGURE 3.20

EFFECT OF ORBIT ECCENTRICITY ON
ROLL ERROR DUE TO ROLL TORQUE
(TWICE ORBITAL FREQ. COMPONENT)

C.M. IS 6 INS. OFF CENTER.

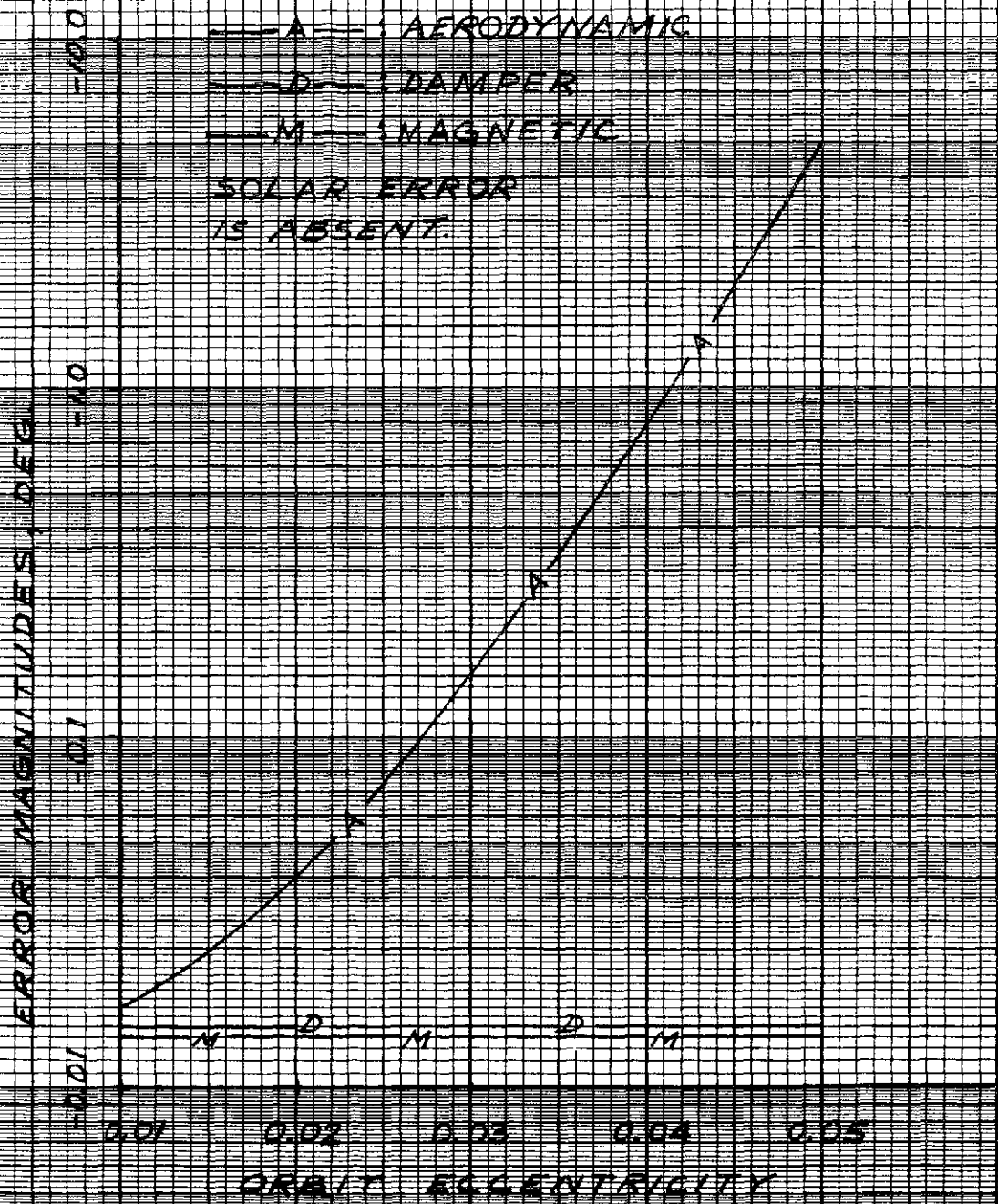


FIGURE 3.21

EFFECT OF ORBIT ECCENTRICITY ON
ROLL ERROR DUE TO YAW TORQUE
(ORBITAL FREQ. COMPONENT)

NOTE: CONST. COMPNTS ARE ABSENT.
C.M. IS 6 INS. OFF CENTER.

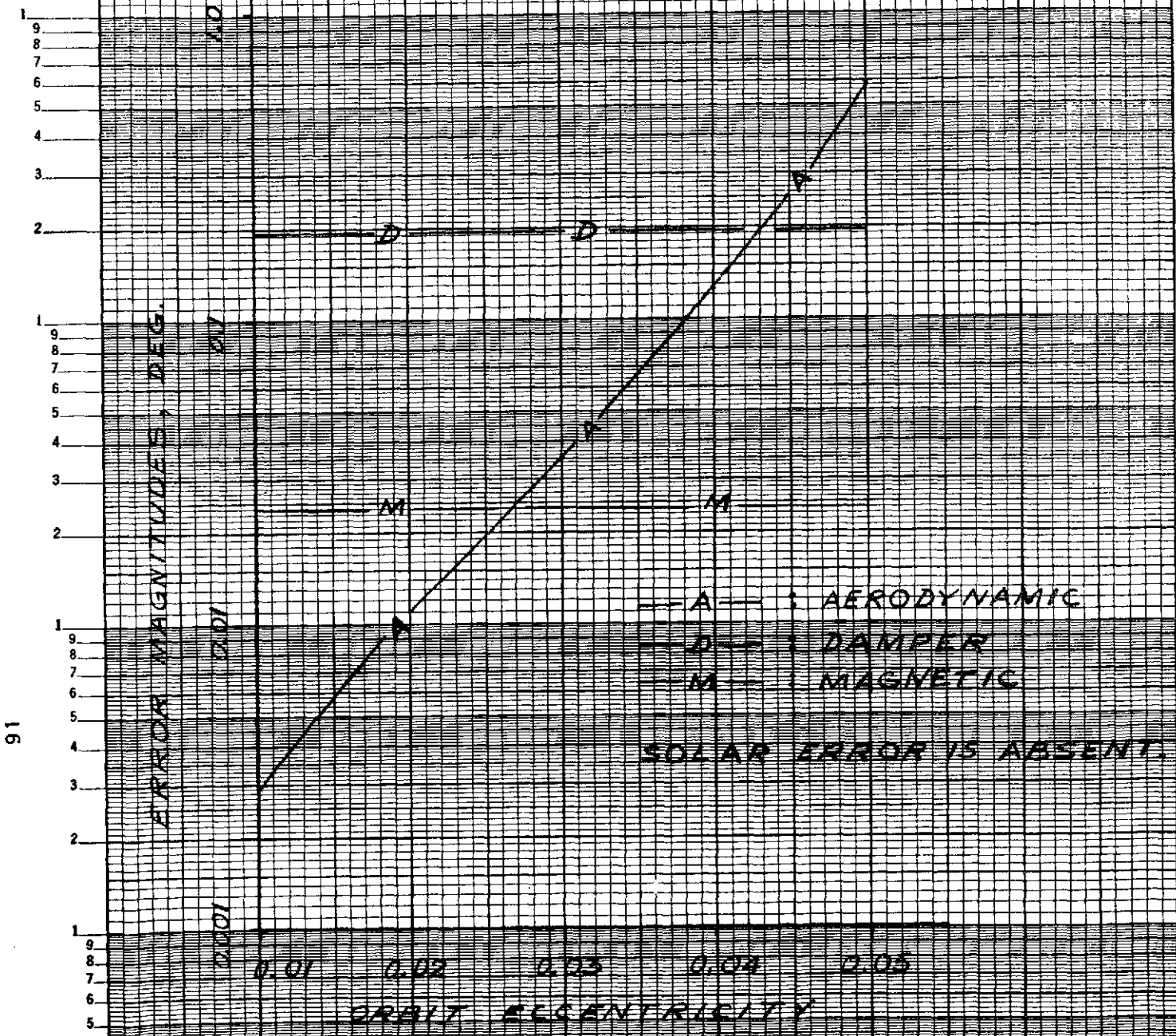


FIGURE 3.22

EFFECT OF ORBIT ECCENTRICITY ON
ROLL ERROR DUE TO YAW TORQUE
(TWICE ORBITAL FREQ. COMPONENT)

C.M. IS 6 INS. OFF CENTER.

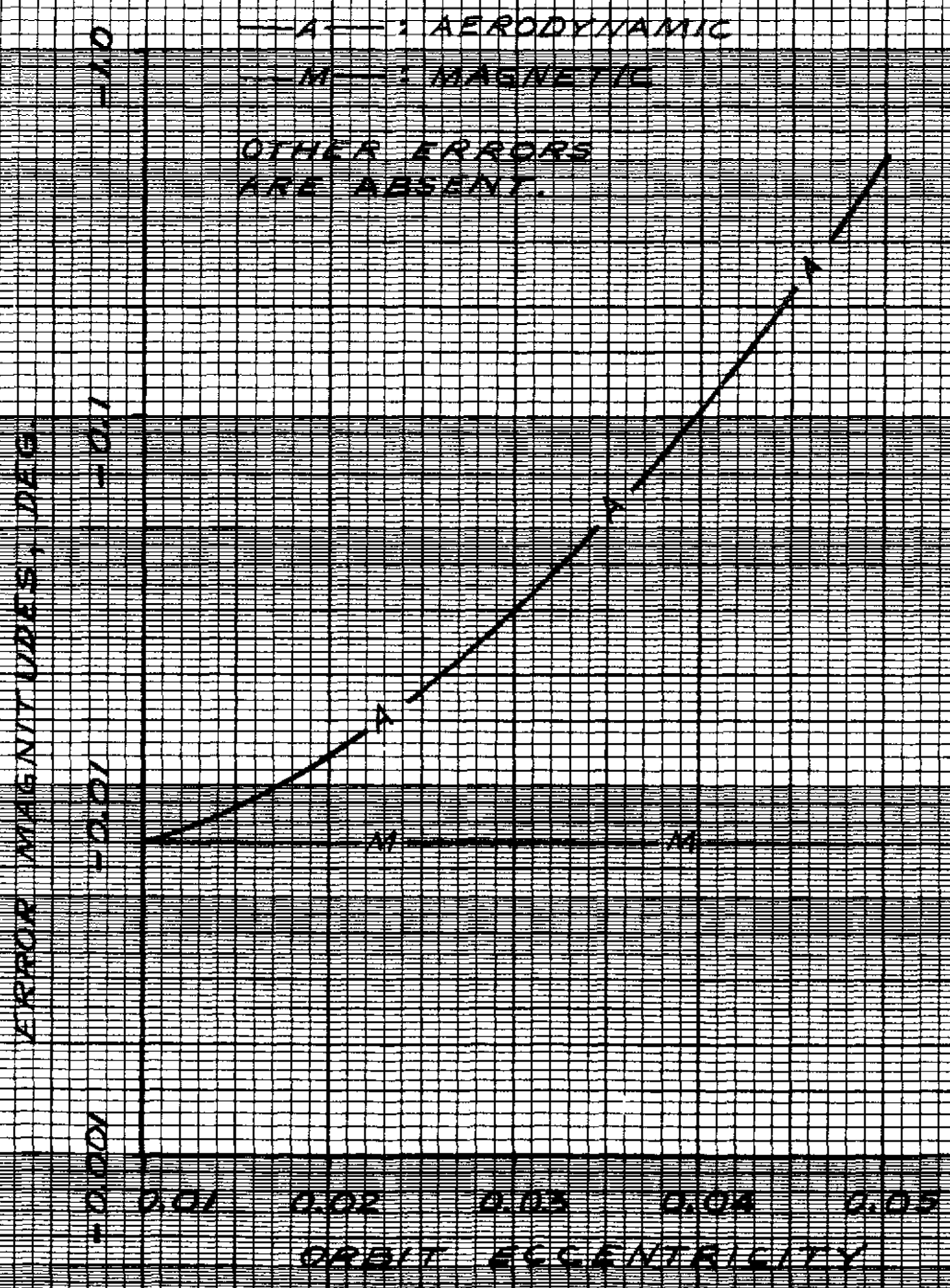


FIGURE 3.23

PITCH AND ROLL ERRORS AT ORBITAL FREQ. & CONSTANT PITCH ERROR - DEG

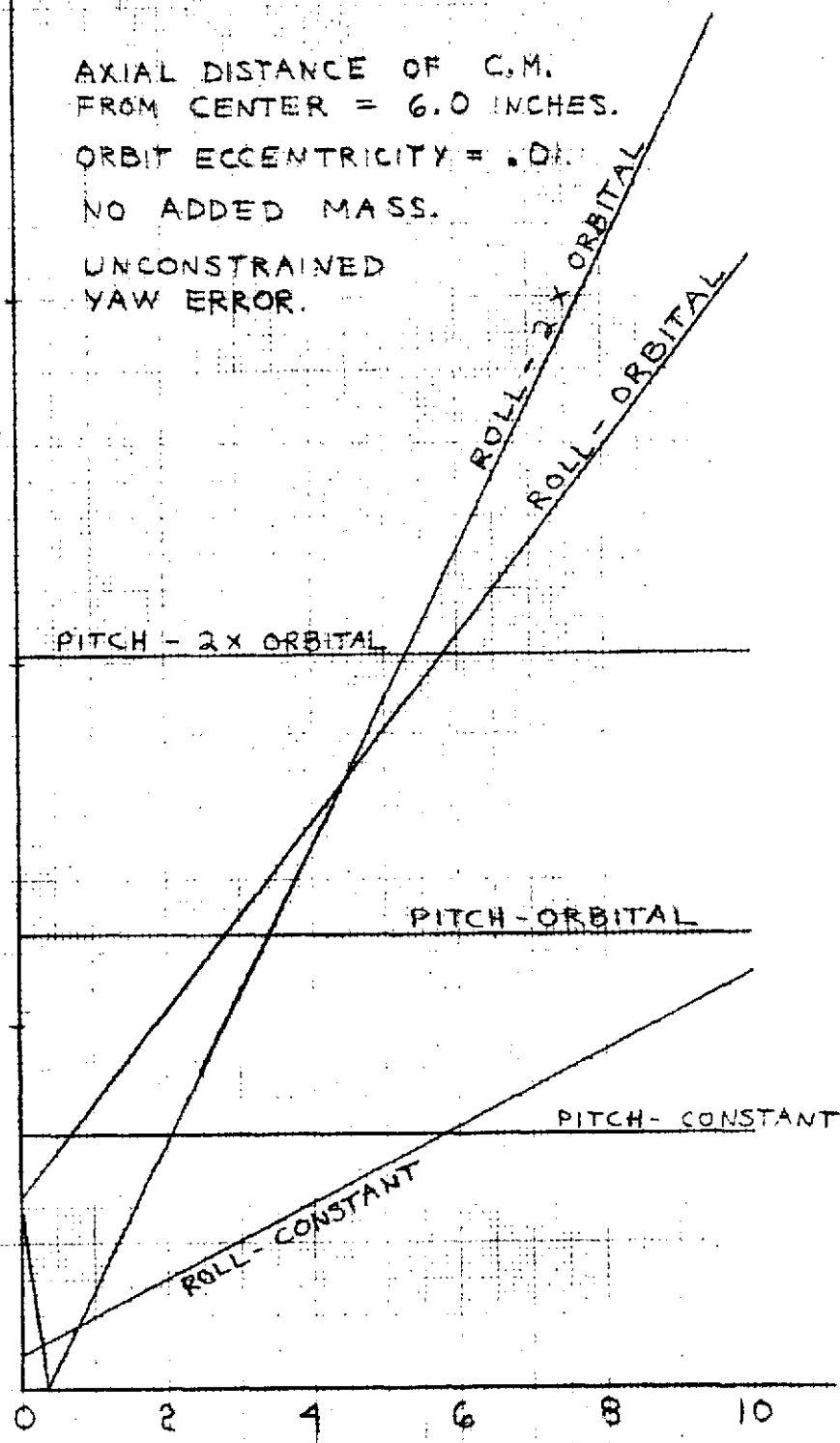
A
B
2
1
0

PITCH AND ROLL ERRORS AT TWICE ORBITAL FREQ. & CONSTANT ROLL ERROR - DEG

0.4
0.3
0.2
0.1
0

EFFECT OF A SHIFT OF THE C.M. NORMAL TO THE CYLINDER AXIS ON PITCH AND ROLL ERROR

AXIAL DISTANCE OF C.M. FROM CENTER = 6.0 INCHES.
ORBIT ECCENTRICITY = .01.
NO ADDED MASS.
UNCONSTRAINED YAW ERROR.



DISTANCE OF CM NORMAL TO AXIS - INCHES

FIGURE 3.24

ORIGINAL PAGE IS OF POOR QUALITY

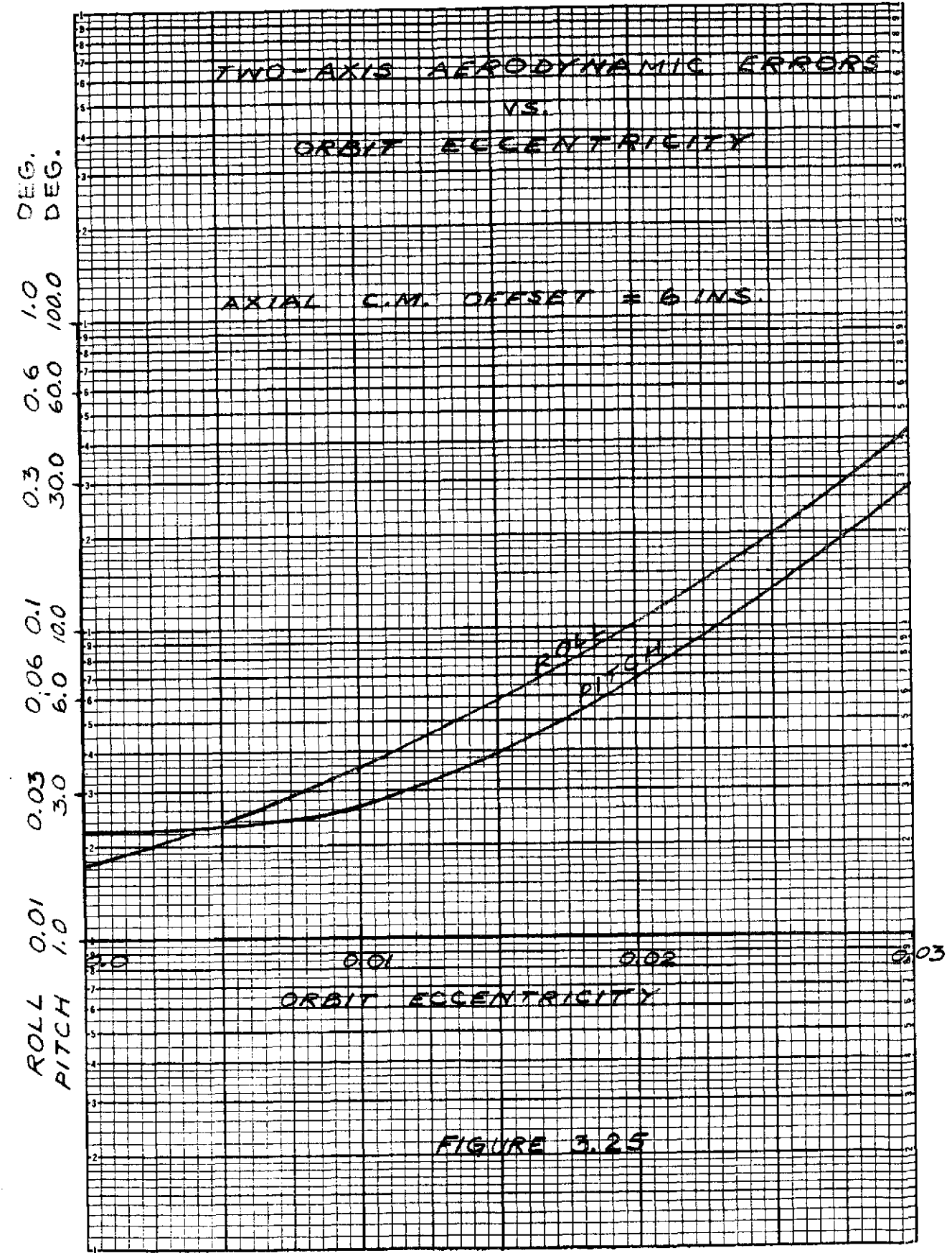


FIGURE 3.25

3.1.5.3 Argument of Perigee / Ascending Node

Figures 3.26, 3.27 and 3.28 show the effect on the pitch error of orbit position relative to the sun. Because of its large error, only pitch has been considered. These error estimates were calculated at autumnal equinox, which places the diurnal bulge on the equator. Therefore, by changing the ascending node position, the effect of both ascending node and argument of perigee (best case and worst case positions) are determined.

Three eccentricities were considered: 0, 0.01 and 0.02. The center of mass/center of pressure offset was again selected to be .152 m (six inches).

The differences between the worst case and best case performance is low at zero eccentricity (approximately .21 deg.), but increases rapidly with increasing eccentricity reaching a difference of 4.7 deg. at an eccentricity of 0.02. For values of eccentricity anticipated for the shuttle (Section 3.4), the effects of ascending node and argument of perigee on spacecraft performance are small.

3.2 GARBER INSTABILITY

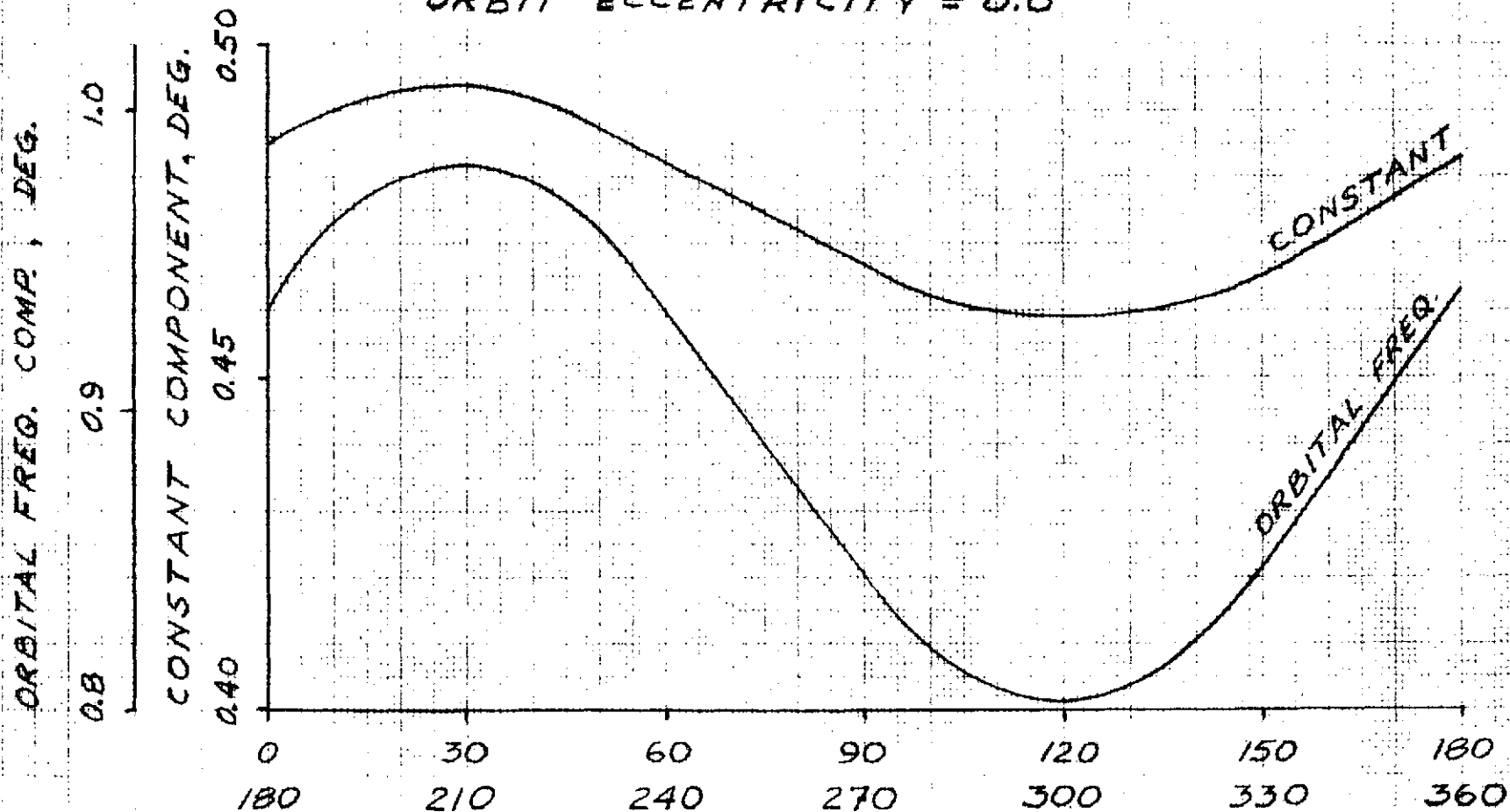
All gravity gradient spacecraft have a first order instability which was identified by T. Garber of Rand.⁽⁴⁾ This instability is caused by a constant torque on the pitch axis, which produces a constant pitch error. This error causes the roll axis to go unstable, typically with a long period exponential. The instability appears in the linearized equations of motion when the linearization is performed about bias pitch, roll and yaw positions. Only pitch biases produce the instability, however.

The pitch bias position at which the spacecraft goes unstable is a function of configuration and damping. Increasing the damping will increase the pitch

EFFECT OF THE ASCENDING NODE POSITION ON THE
AERODYNAMIC PITCH ERROR DUE TO PITCH TORQUE

AXIAL C.M. OFFSET = 6.0 INS.

ORBIT ECCENTRICITY = 0.0



POSITION OF THE ASCENDING NODE FROM MIDNIGHT, DEG.

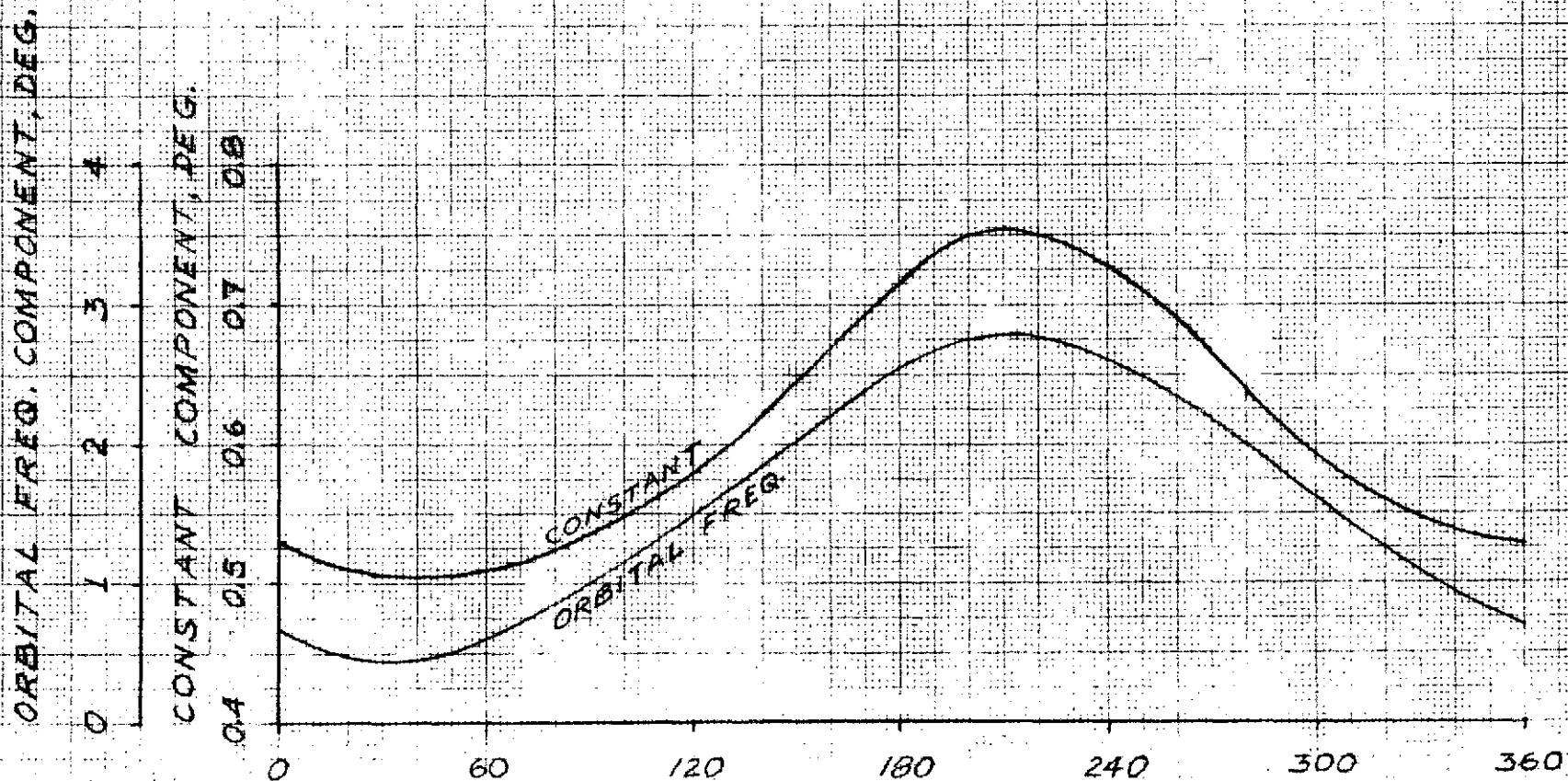
FIGURE 3.26

EFFECT OF THE ASCENDING NODE POSITION ON THE
AERODYNAMIC PITCH ERROR DUE TO PITCH TORQUE

AXIAL C.M. OFFSET = 6.0 INS.

ORBIT ECCENTRICITY = 0.01

THE PERIGEE IS AT THE ASCENDING NODE.



POSITION OF THE ASCENDING NODE FROM MIDNIGHT, DEG.

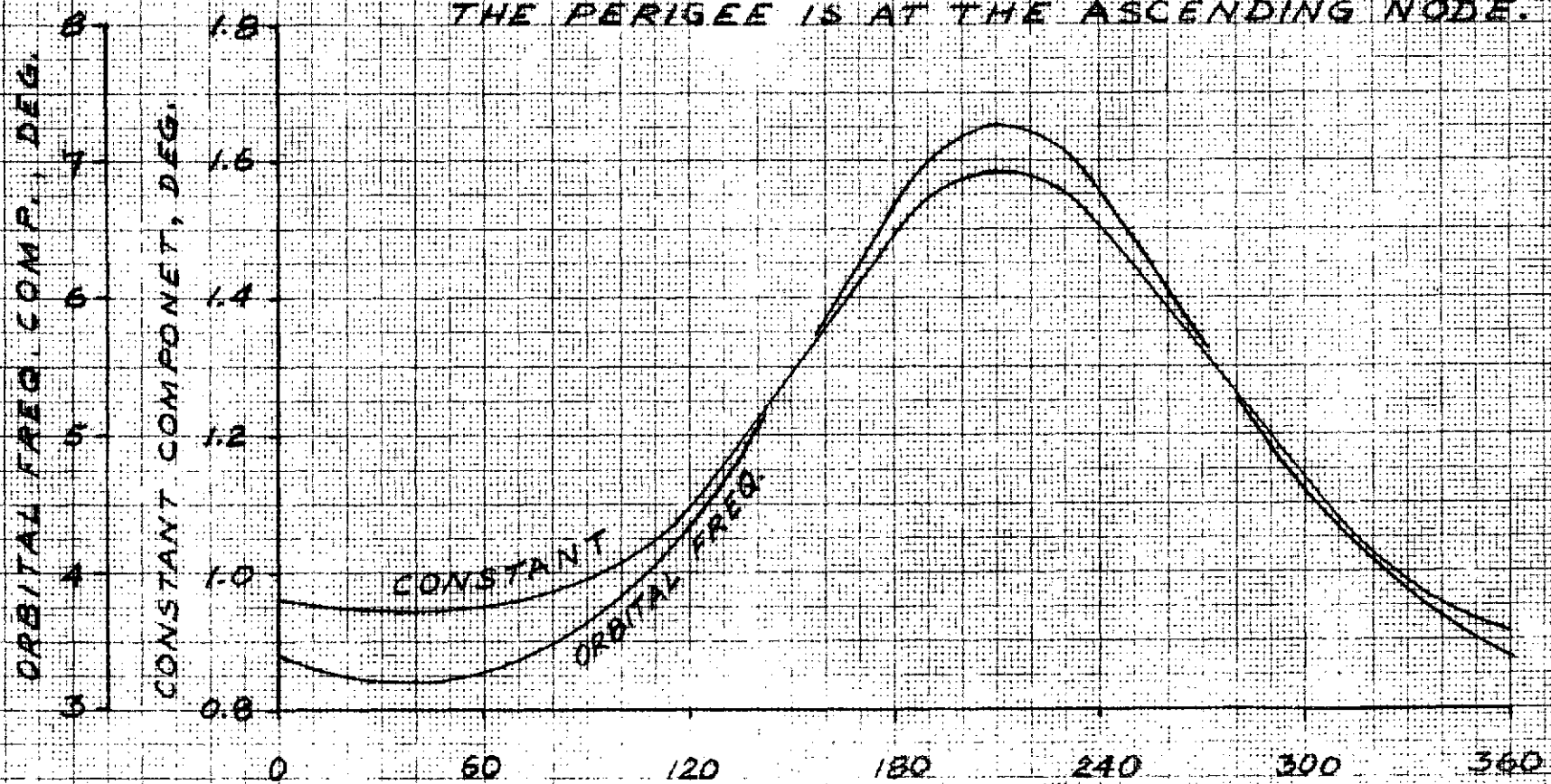
FIGURE 3.27

EFFECT OF THE ASCENDING NODE POSITION ON THE
AERODYNAMIC PITCH ERROR DUE TO PITCH TORQUE

AXIAL C.M. OFFSET = 6 INS

ORBIT ECCENTRICITY = 0.02

THE PERIGEE IS AT THE ASCENDING NODE.



POSITION OF THE ASCENDING NODE FROM MIDNIGHT, DEG.

FIGURE 3.28

error at which the instability occurs. Only two disturbances cause constant pitch errors; the magnetically anchored rate damper and aerodynamics. The damper causes a pitch bias, but also supplies damping, and within the limits of the current spacecraft designs, produces no instability. The major source of constant torque is therefore aerodynamics (Figures 3.6 and 3.16).

Table 3.1 shows the pitch errors at which Garber instability occurs as a function of damping coefficient. At the lowest level of damping coefficient, a three degree pitch bias is required. The required pitch bias increases with damping coefficient up to a damping level of 1.08 n.m.sec (0.8 lb-ft-sec), at which point it drops abruptly. The reason for this drop, as well as a discussion as to its validity, is given in appendix A. Based upon the estimate of the aerodynamic torque, however, Garber instability will not occur.

3.3 TRANSIENT AND CAPTURE PERFORMANCE

3.3.1 TRANSIENT PERFORMANCE

To determine the damping and steady state characteristics of the damper, the equations of motion of the damper and the spacecraft must be solved simultaneously. Linearization of the equations is the normal analytical approach, but the magnetic field orientation changes as a function of orbit position and linearization is only approximate (Appendix A). Consequently, a dynamic pitch planar analysis is used for most damping calculations, with several simplifying assumptions about the magnetic field model. With this approach, a simple relationship between damping constant, magnet strength, spacecraft

Table 3.1

Effects of Damping on the
Garber Stability Boundaries

Magnet Strength = 225000 pole-cms

Damping Coefficient		Pitch Bias
n-m-sec	lb-ft-sec	deg
0.542	0.4	3
0.678	0.5	4
0.813	0.6	5
0.950	0.7	6
1.08	0.8	4 *
1.22	0.9	7

* See Appendix A

moment of inertia ratio, and damping time constant can be determined. The relationship requires only two non-dimensional terms: $\frac{b}{I_{zz}\omega_o}$ and $\frac{M}{I_{zz}}$, where b is the damping coefficient, I_{zz} is spacecraft moment of inertia, ω_o is orbital rate, and M is the damper magnetic moment (in pole-cm). Selection of these terms defines the damping time constant in terms of orbits, which remains the same irrespective of altitude.

Figure 3.29 shows the relationship between pitch damping time and damper characteristics for the LDEF. The curve represents the pitch performance of a spacecraft in a polar orbit about a simple magnetic dipole. More intricate linear analyses, as well as digital simulations, have indicated the analysis is a good approximation for high inclinations, and gives a rough estimate of the performance at the lower inclinations.

Three magnetic strengths for the damper are shown in this figure. A magnet strength of 225,000 pole-cm is compatible with an existing GE damper design. The figure indicates that for damping coefficients higher than 2.71 n.m.sec (2.0 lb-ft-sec/rad), this magnet is pulled off the Earth's field, and the damping performance degrades drastically. Larger magnets improve the damping, but only at high damping coefficients, which produce higher damping.

These figures were developed assuming the damper has no moment of inertia. Analyses were also performed assuming that the damper had the anticipated moments of inertia. The analyses, contained in appendix A, indicate similar performance, except for instabilities on the roll damping curve.

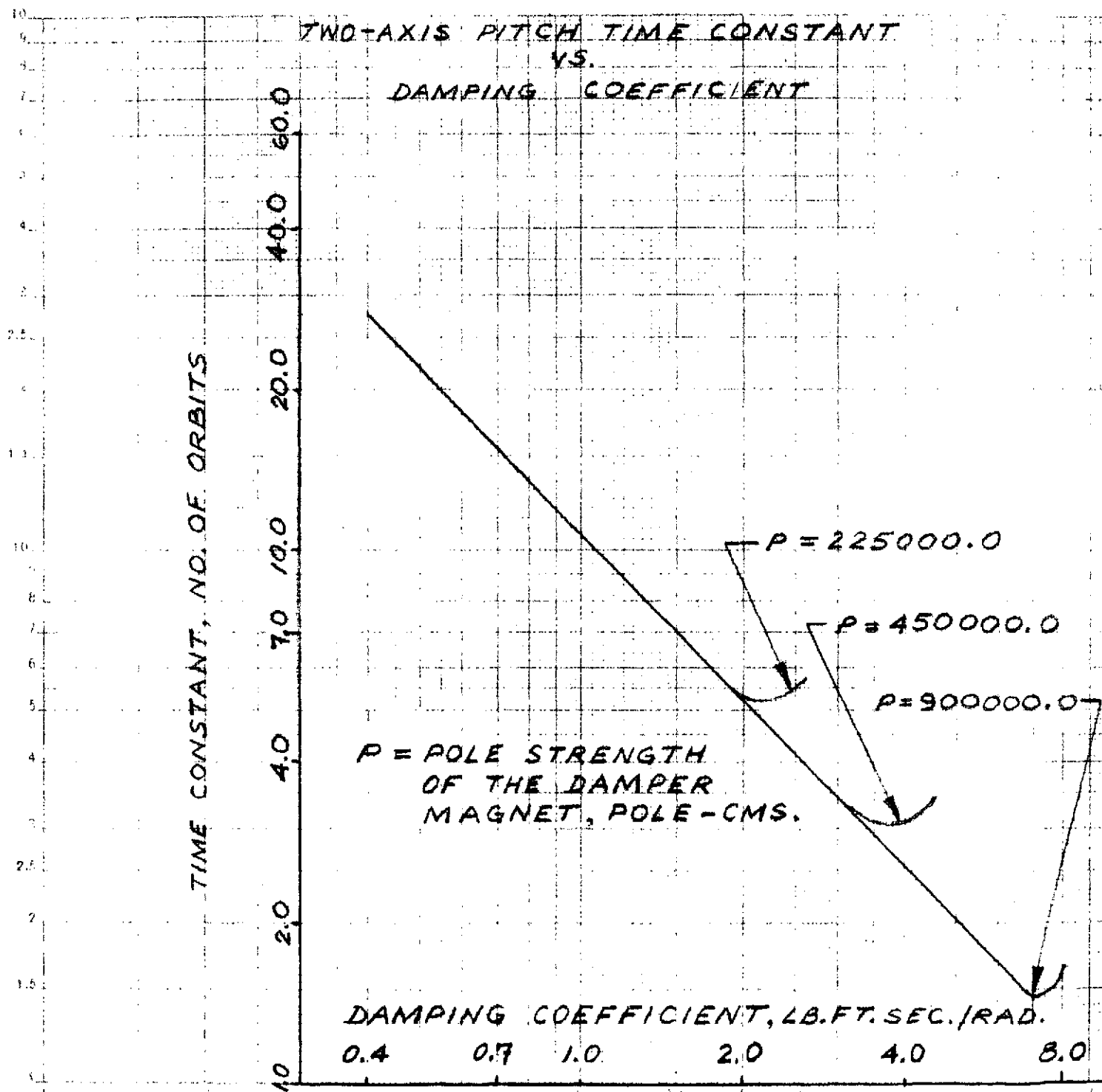


FIGURE 3.29

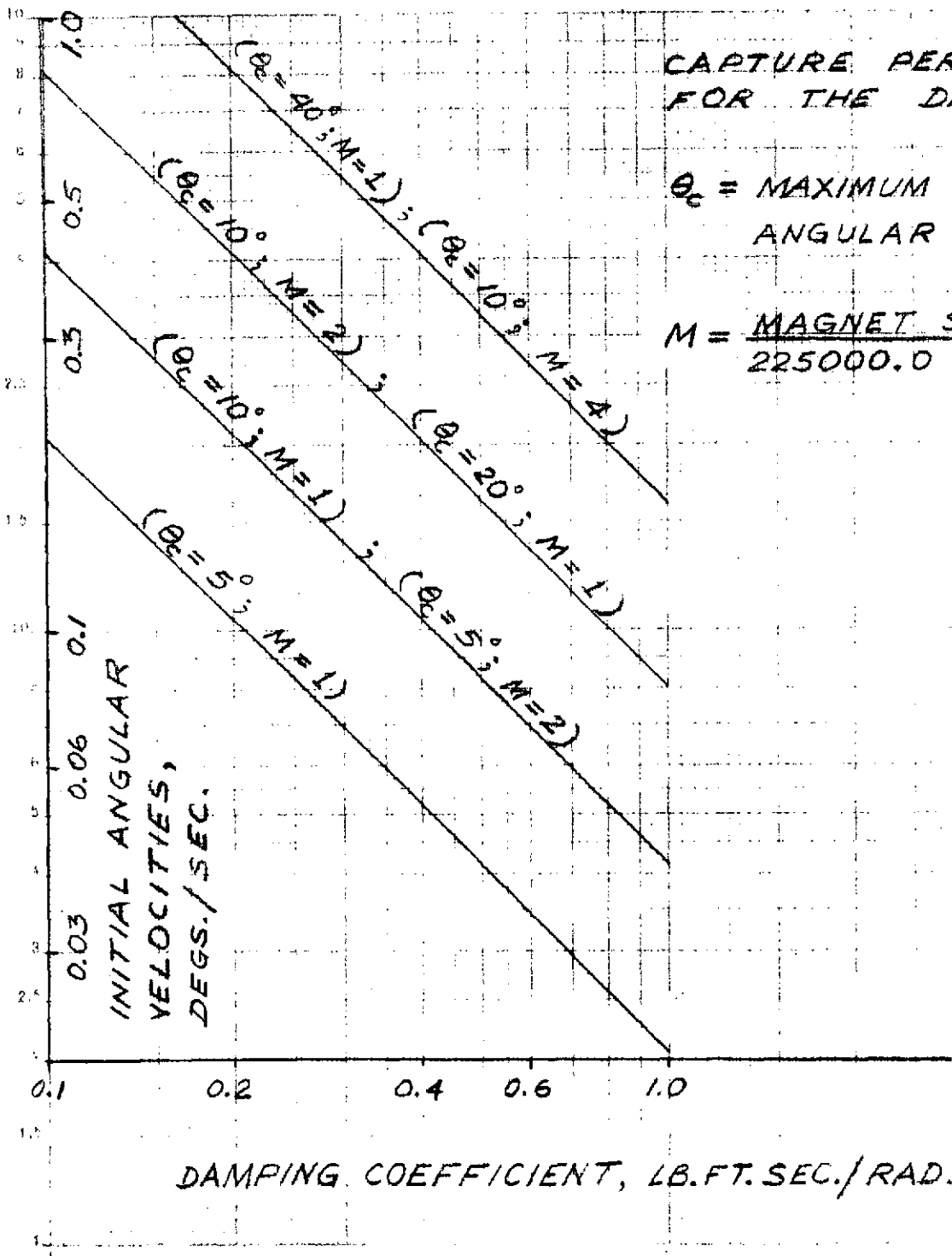
ORIGINAL PAGE IS
OF POOR QUALITY

3.3.2 CAPTURE PERFORMANCE

It is evident that as long as the magnet stays anchored to the Earth's magnetic field, it will damp out any oscillations that the spacecraft is subjected to (see Section 5.1.2, however). But the damper magnet may be pulled away from the magnetic field by initial angular rates which exceed its design capability. The maximum angular deviations of the magnet from the Earth's field are inversely proportional to the magnet strength and directly proportional to the damping coefficient and the spacecraft rates. Past experience has demonstrated that the magnet strength should be such that the damper magnet does not deviate by more than approximately 40.0 degrees from the Earth's magnetic field (a conservative value).

Figure 3.30 shows the maximum allowable spacecraft angular rates as a function of the damping coefficient for a given magnet strength and maximum angular deviation of the magnet. It indicates that for a magnet strength of 225,000 pole-cms and a spacecraft angular rate of 0.25 degs/sec, a damping coefficient of 0.882 n.m.sec (0.65 lb-ft-sec) is required to produce an angular deviation of 40 degrees.

An additional design constraint for the magnet arises from the magnitudes of the decentering forces it has to tolerate. The existing GE designs can provide 35.2 dynes of centering force per kilogram (16 dynes/pound) of the magnet mass. Figure 3.31 shows the centrifugal decentering force to be withstood by the damper magnet on the LDEF spacecraft. It shows that for maximum angular rates of 0.25 degs/sec the decentering force is less than 3.52 dynes/kg (1.6 dynes/lb), even if the damper is offset from the center of mass of LDEF by as much as 1.97 m (six feet). Thus, the centrifugal forces are well under the limit of 35.2 dynes/kg (16 dynes/lb).



CAPTURE PERFORMANCE FOR THE DAMPER

θ_c = MAXIMUM MAGNET ANGULAR DISPLACEMENT

$M = \frac{\text{MAGNET STRENGTH}}{225000.0 \text{ POLE-CMS.}}$

FIGURE 3.30

EFFECT OF THE DISTANCE THE DAMPER IS OFFSET FROM THE CENTER ON THE CENTRIFUGAL FORCE ON THE DAMPER PER POUND OF ITS WEIGHT

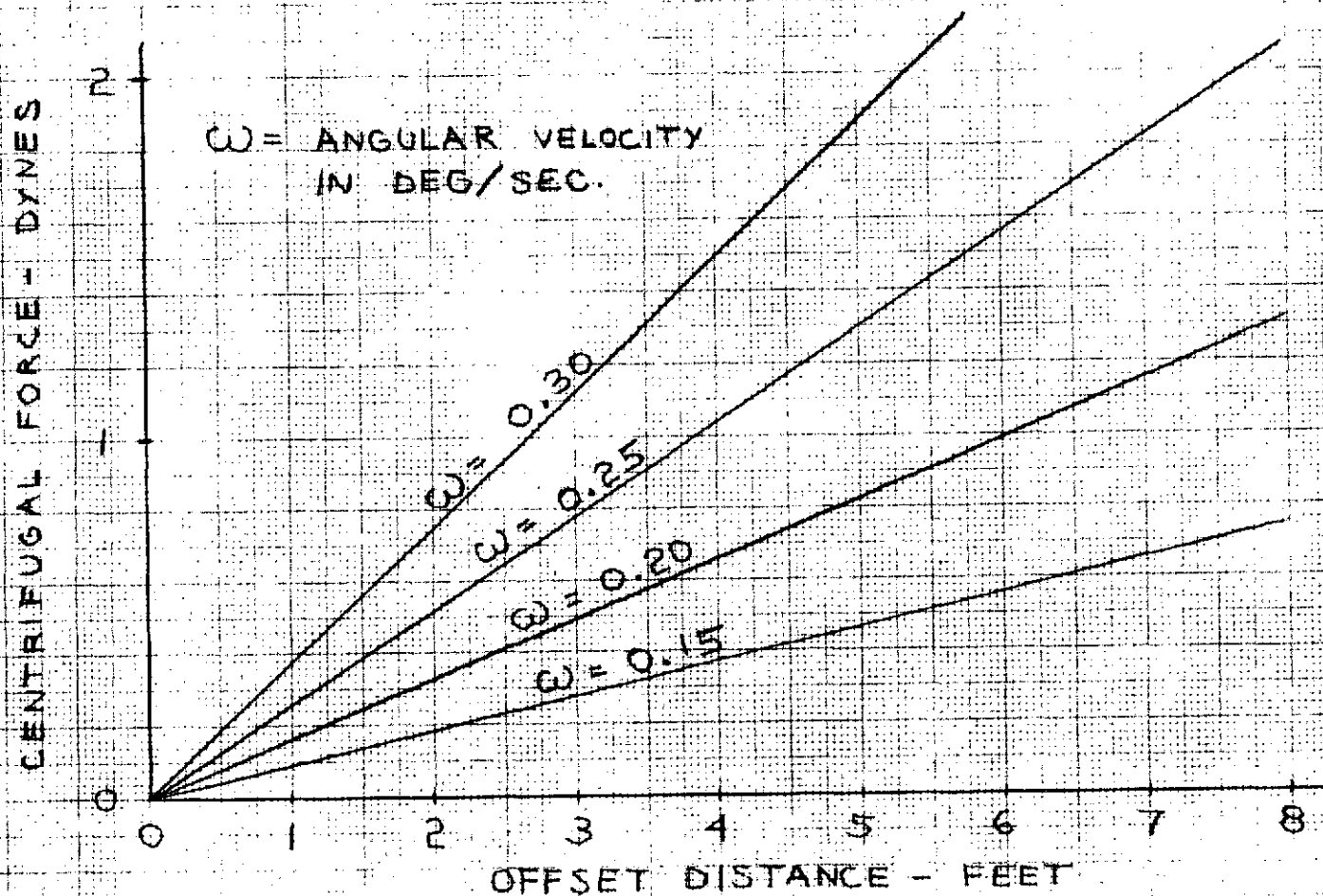


FIGURE 3.31

3.4 CONFIGURATION OPTIMIZATION

Optimization of the two axis LDEF configuration consists of identifying as closely as possible the magnitudes and frequencies of the external torques, estimating the spacecraft performance, and selecting the damper characteristics required to damp the spacecraft. The damper selected must also prevent the Garber instability from occurring, and induce only small spacecraft oscillations. The disturbance torques and their effect on the spacecraft performance are contained in Section 3.1, on a parametric basis. It is necessary to define, within the range of parameters considered, the conditions the spacecraft will encounter. Aerodynamics is the largest source of error for the LDEF; depending upon the actual value of center of pressure/center of mass offset and orbit eccentricity. An offset of 0.152 m (6 inches) was selected as the nominal value, as discussed in Section 3.1.5. The eccentricity of the orbit depends upon the value that can be achieved by the shuttle. The shuttle specification⁽³⁾, indicates an insertion capability of ± 4 nm on the orbit, which at 500 Km (270 nm) produces an eccentricity of .00082. Taking a conservative value of 0.002, the eccentricity error is .43 deg., and the aerodynamic pitch error (worst case) is 1.9 degrees. The solar torque error, with the same offset, is less than .01 degrees in pitch, and less than 0.1 degrees in roll. The magnetic error (for a 1000 pole-cm magnetic dipole in all axes) is .06 degrees in pitch, and .07 degrees in roll.

The damping coefficient for the magnetically anchored rate damper was selected based upon the desired damping time, Garber instability and steady state

error. Consideration was also given to the required damper characteristics for the three axis configuration (Section 4.0). It is evident from Figure 3.30, that a dipole of 225,000 pole-cm is adequate for the anticipated worst case acquisition conditions. Since this value is compatible with existing damper designs, the magnet strength was accepted.

The damping coefficient was selected based upon a tradeoff between damping time constant and steady state attitude error, factoring in the Garber instability restrictions. The limitations on the selection of damping coefficient provided by the Garber instability are shown in Table 3.1. Since the constant pitch error caused by aerodynamics is 0.5 degrees, and the lowest instability angle is three degrees, instability will not occur for any of the damping coefficients considered. Hence, only the damping time/steady state tradeoff is important. Previous experience with low altitude spacecraft (NRL, GEOS, etc.) has indicated a damping time constant on the order of twenty orbits provides acceptable damping performance with reasonable damper induced errors. Consequently, a damping coefficient of 0.692 n.m.sec (0.51 lb-ft-sec) was selected, providing a linear damping time constant of 22.5 orbits and steady state pitch and roll errors of 0.39 degrees and 0.63 degrees, respectively. The error budget for the configuration which combines all of these errors, is shown in Table 3.2. The errors are arrived at by root-sum-squaring all the error sources with the same frequency components, and then adding "across" the frequencies. The approach is conservative and produces somewhat larger errors than would actually be encountered.

Table 3.2

Linear Error Breakdown				
Two Axis Configuration				
Spacecraft Parameters				
Orbit Eccentricity = 0.002				
Position of the Ascending Node and Perigee = 2:00 P.M.				
C.M. Offset Along Pitch Axis = 1.0 ins.				
C.M. Offset Along Roll Axis = 1.0 ins.				
C.M. Offset Along Yaw Axis = 6.0 ins.				
Damping Coefficient = 0.51 lb-ft-sec/rad				
Spacecraft Magnetics = 1000.0 pole-cms/axis				
Torque	Error Axis	Error Freq. Orbit Freq.	Error Magnitude Deg.	
			Frequency Components	Total
Orbit Eccentricity	Pitch	1	.432	.432
Aerodynamic	Pitch	0	.521	1.902
		1	1.270	
		2	.111	
	Roll	0	.008	.283
		1	.258	
		2	.017	

Table 3.2 (cont'd)

Torque	Error Axis	Error Freq. Orbit Freq.	Error Magnitude Deg.	
			Frequency Components	Total
Damper	Pitch	0	0.113	.483
		1	0.274	
2		-0.096		
Roll	Roll	0	0.0	.648
		1	0.629	
		2	-0.019	
Solar	Pitch	0	0.0	.019
		1	0.005	
2		-0.014		
Roll	Roll	0	0.004	.026
		1	0.013	
		2	-0.009	
Magnet	Pitch	0	0.0	.06
		1	0.060	
2		0.0		
Roll	Roll	0	0.021	.069
		1	0.048	
		2	0.0	

Total Pitch Error

2.03 degrees

Total Roll Error

.79 degrees

SECTION 4.0

LINEARIZED ANALYSIS - THREE AXIS CONFIGURATION

The linearized analysis for the three axis configuration was divided into the same four parts as the two axis configuration analyses; Steady State Performance, Garber Instability, Transient and Capture Performance, and Configuration Optimization.

4.1 STEADY STATE PERFORMANCE ANALYSES

To provide three axis attitude control, the spacecraft must have three different moments of inertia; the largest on the pitch axis, the smallest on the yaw axis, and the intermediate on the roll axis. Attitude stabilization is provided directly by gravity gradient on the pitch and roll axes, and by "dynamic torques" on the yaw axis. The "torques" result from the fact that the spacecraft prefers to rotate about its maximum moment of inertia, and will move toward that orientation when forced to rotate at orbital rate by gravity gradient torques.

To obtain a three axis control configuration for the LDEF, mass was added to the spacecraft in the roll-yaw plane. Four equal masses were placed symmetrically at the points farthest from the pitch axis (Figure 4.1). Since the three axis configuration has the same envelope and shape as the two axis configuration, the magnitude and frequency of the disturbance torques are virtually unchanged. The change in performance from the two axis configuration is due almost entirely to added mass, resulting in increased moment of inertia (Figure 4.2) and altered frequency response. The largest effect is on the yaw response to constant torques, which is reduced from the infinite

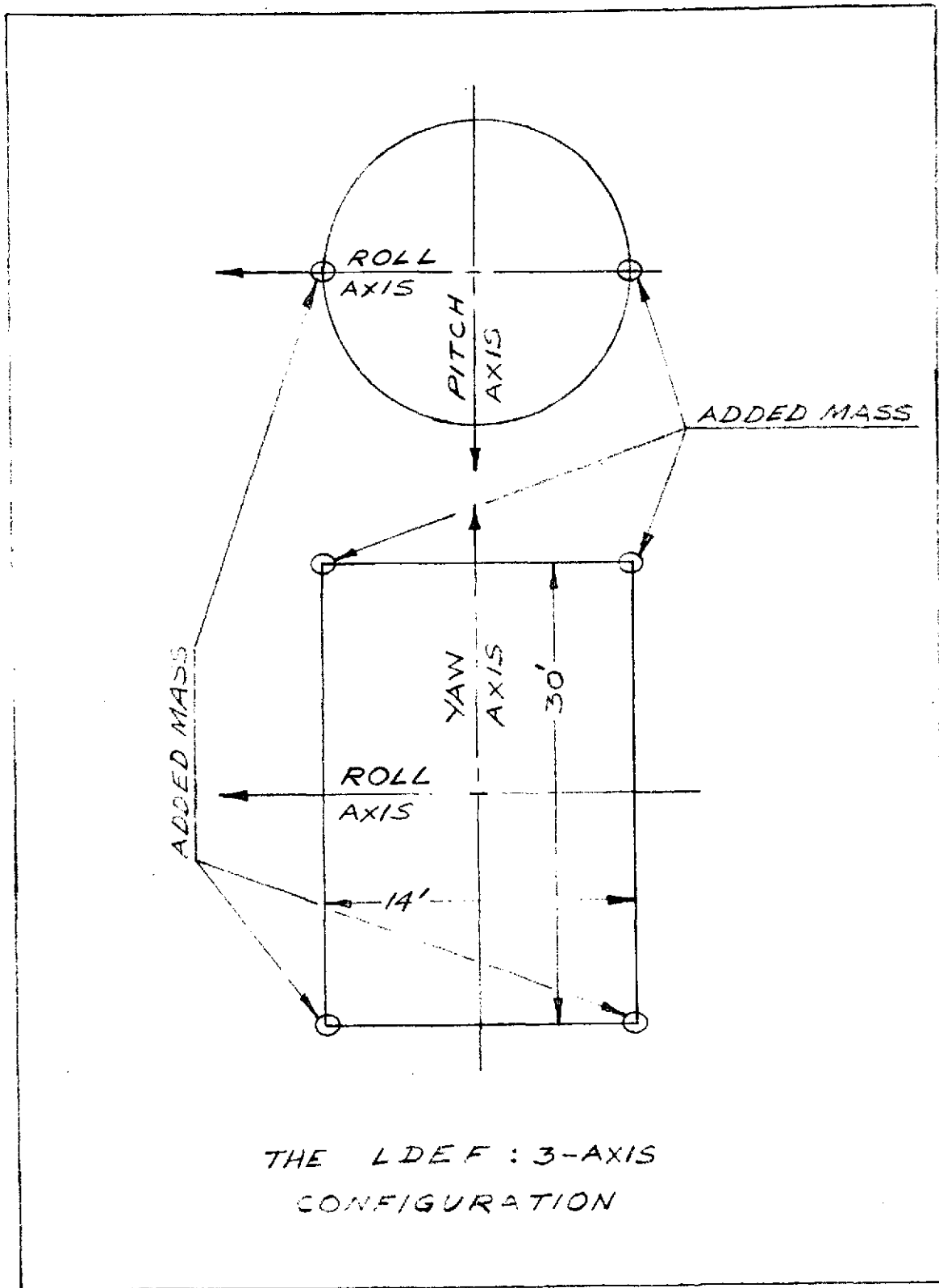


FIGURE 4.1

ORIGINAL PAGE IS
OF POOR QUALITY

SPACECRAFT MOMENTS OF INERTIA

MOMENT OF INERTIA, 1000 SLUG-FT²

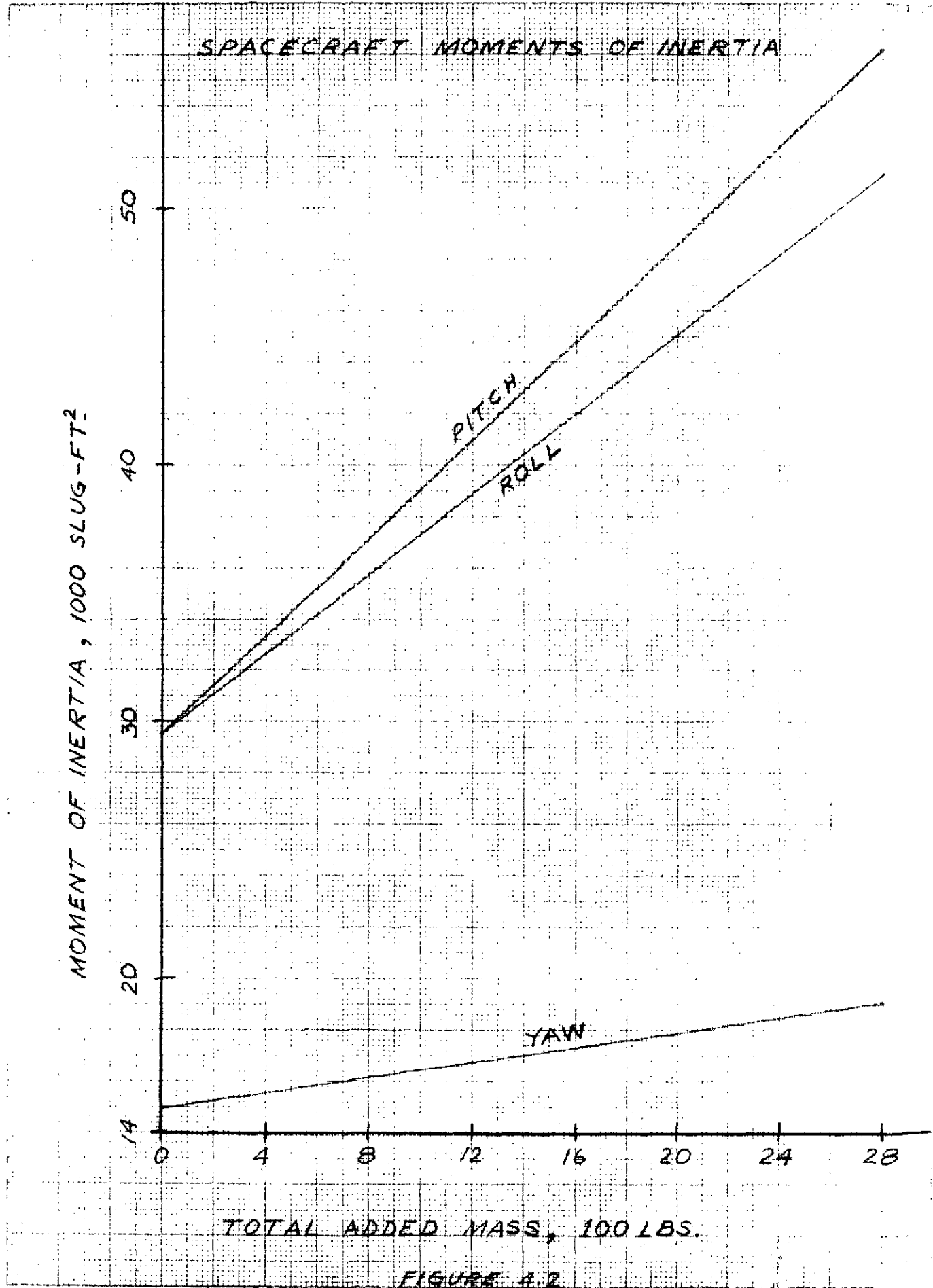
50
40
30
20
14

PITCH
ROLL

YAW

TOTAL ADDED MASS, 100 LBS.

FIGURE 4.2



response of the two axis configuration. The yaw response to orbital frequency is only slightly improved, since the large yaw moment of inertia of the LDEF already provides good frequency response.

As indicated in the previous paragraph, the disturbance torques affecting the three axis configuration are the same as those affecting the two axis configuration. It is therefore only necessary to evaluate the errors produced on the three axis configuration by these torques. The largest source of torque is aerodynamic pressure, as indicated in Section 3.1.5, and the largest contributor to aerodynamic torque is a center of mass/center of pressure offset. The effect of an axial offset of the center of mass is the same or less for the three axis configuration as the two axis configuration. Figures 4.3, 4.4 and 4.5 show the pitch, roll and yaw performance of the spacecraft with an axial offset of .152 m (six inches); the value selected as nominal in Section 3.4. The effect of a radial center of pressure /center of mass offset is, however, much more severe on a three axis configuration than a two axis configuration, primarily because of yaw. The errors are largest on yaw, which is the weakest axis. Its restoring torque, for 182 kg (400 lb) of added mass is 174 dyne-cm/degree compared to 15,200 dyne-cm/degree for pitch.

The effect of a center of pressure/center of mass offset along a radius (normal to the centerline axis) is shown in Figures 4.6 through 4.9 as a function of added mass. For convenience, all the errors for each axis were added, as opposed to root sum squaring. The most significant improvement is the reduction in "constant yaw error" with increasing mass. The primary purpose of adding the mass is to provide a yaw restoring torque.

THREE - AXIS PITCH ERRORS VS. ADDED MASS

AXIAL C.M. OFFSET = 6 INCHES.

ORBIT ECCENTRICITY = 0.

I_z = PITCH MOMENT OF INERTIA

I_y = ROLL MOMENT OF INERTIA

I_{y_0} = 29,000 SLUG-FT²

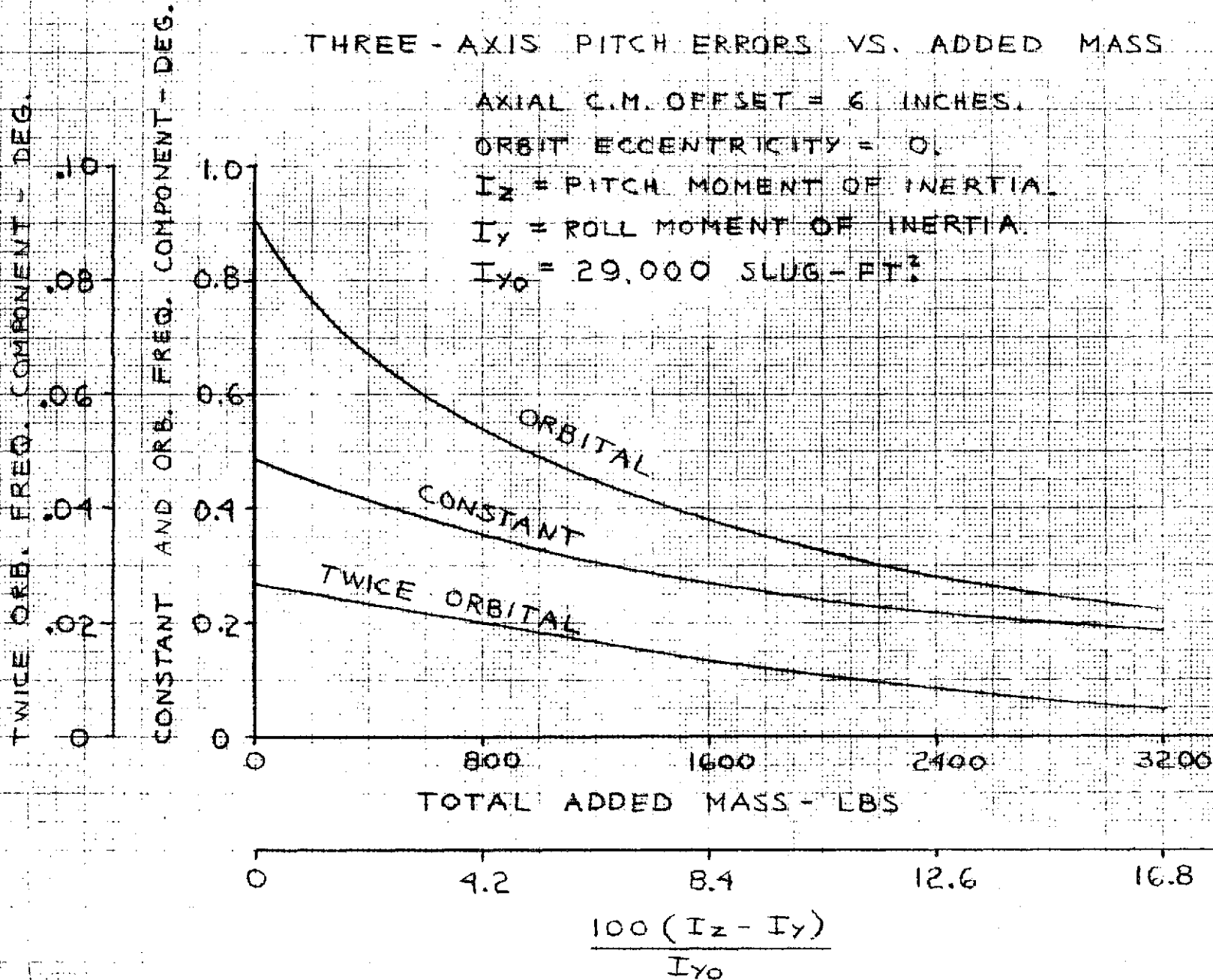


FIGURE 1.3

THREE-AXIS ROLL ERRORS VS. ADDED MASS

AXIAL C.M. OFFSET = 6 INCHES.

ORBIT ECCENTRICITY = 0.

I_z = PITCH MOMENT OF INERTIA.

I_y = ROLL MOMENT OF INERTIA.

$I_{y0} = 29,000$ SLUG-FT²

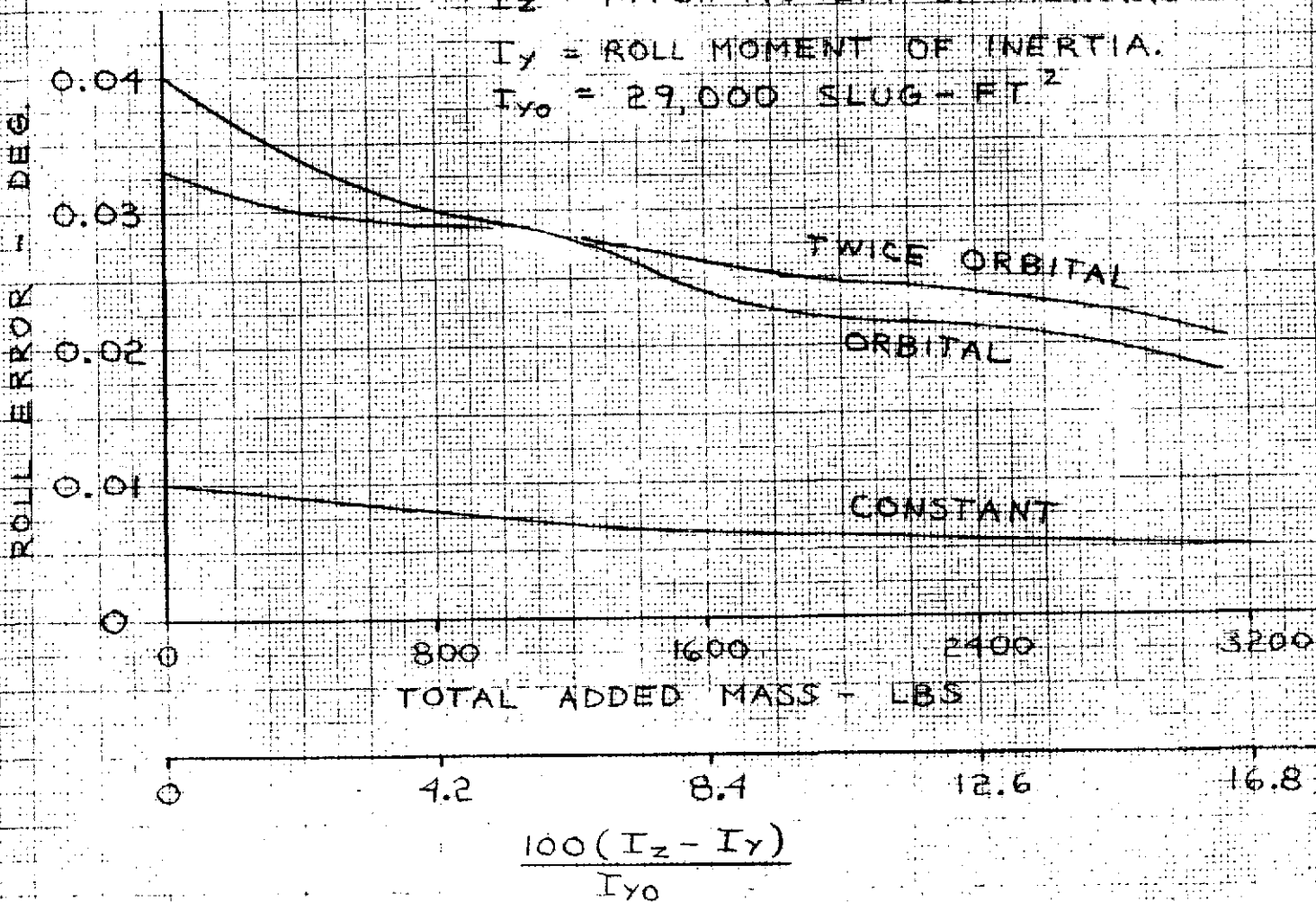


FIGURE 4.4

-55-

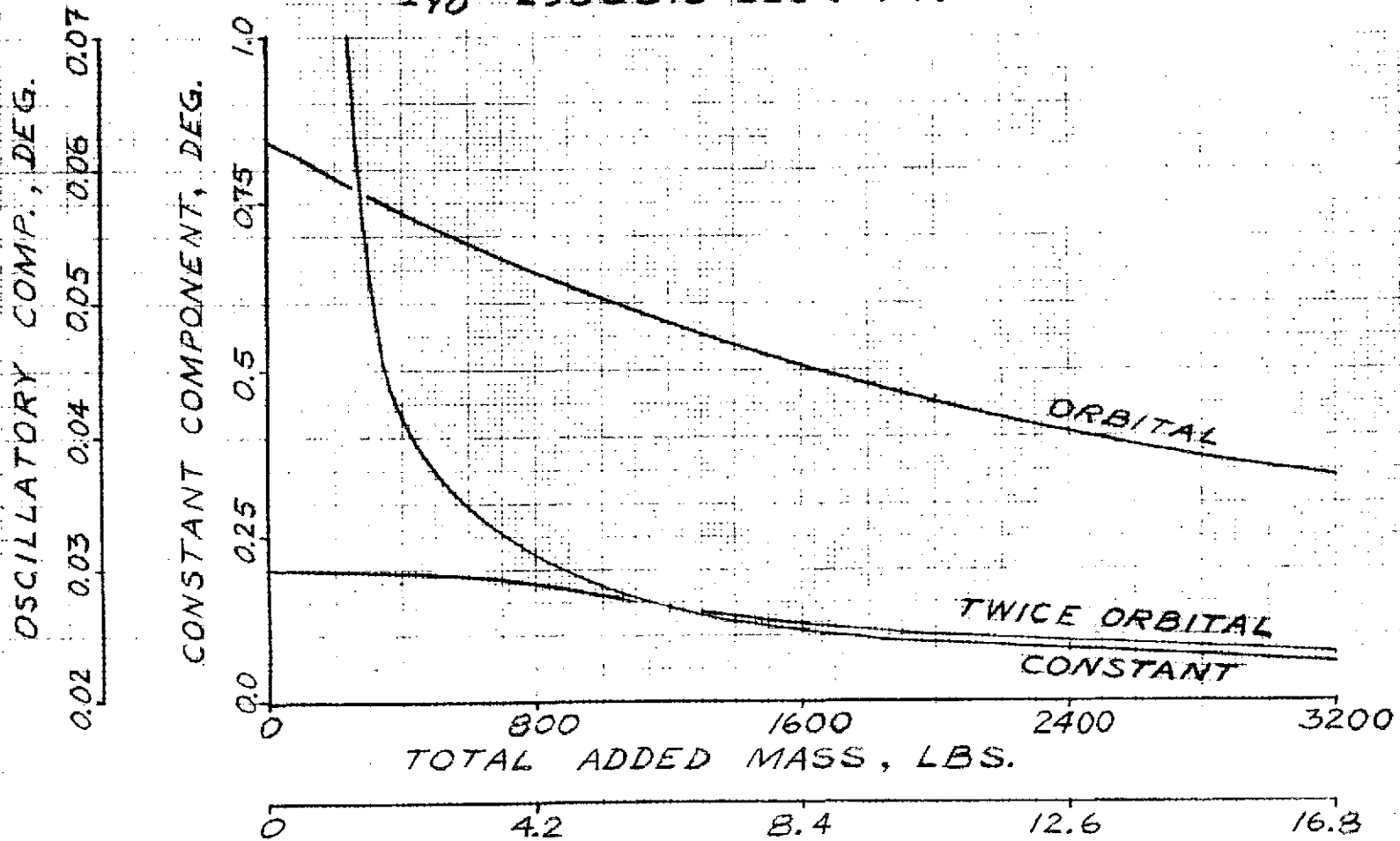
THREE-AXIS YAW ERRORS VS. ADDED MASS.

AXIAL C.M. OFFSET = 6 INS.

ORBIT ECCENTRICITY = 0.0

I_z = PITCH M.I. ; I_y = ROLL M.I.

I_{y0} = 29000.0 SLUG-FT.²



$$100(I_z - I_y)/I_{y0}$$

FIGURE 4.5

ATTITUDE ERRORS VS. RADIAL C.M. OFFSET

TOTAL ADDED MASS = 400 LBS.

ORBIT ECCENTRICITY = 0.

AXIAL C.M. OFFSET = 6 INCHES

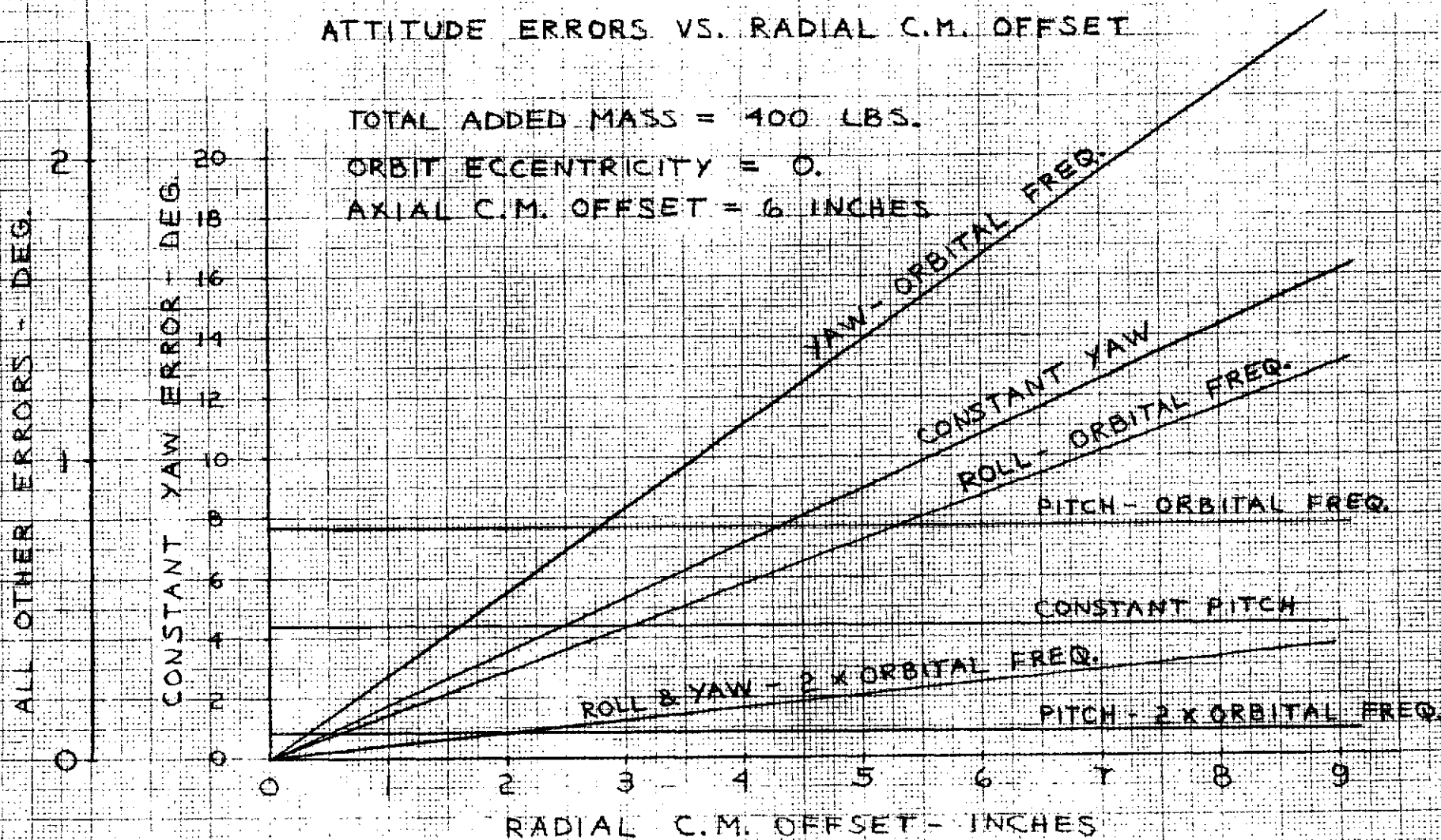


FIGURE 4.6

ATTITUDE ERRORS VS. RADIAL C.M. OFFSET

TOTAL ADDED MASS = 800 LBS.
 AXIAL C.M. OFFSET = 6 INCHES.
 ORBIT ECCENTRICITY = 0.

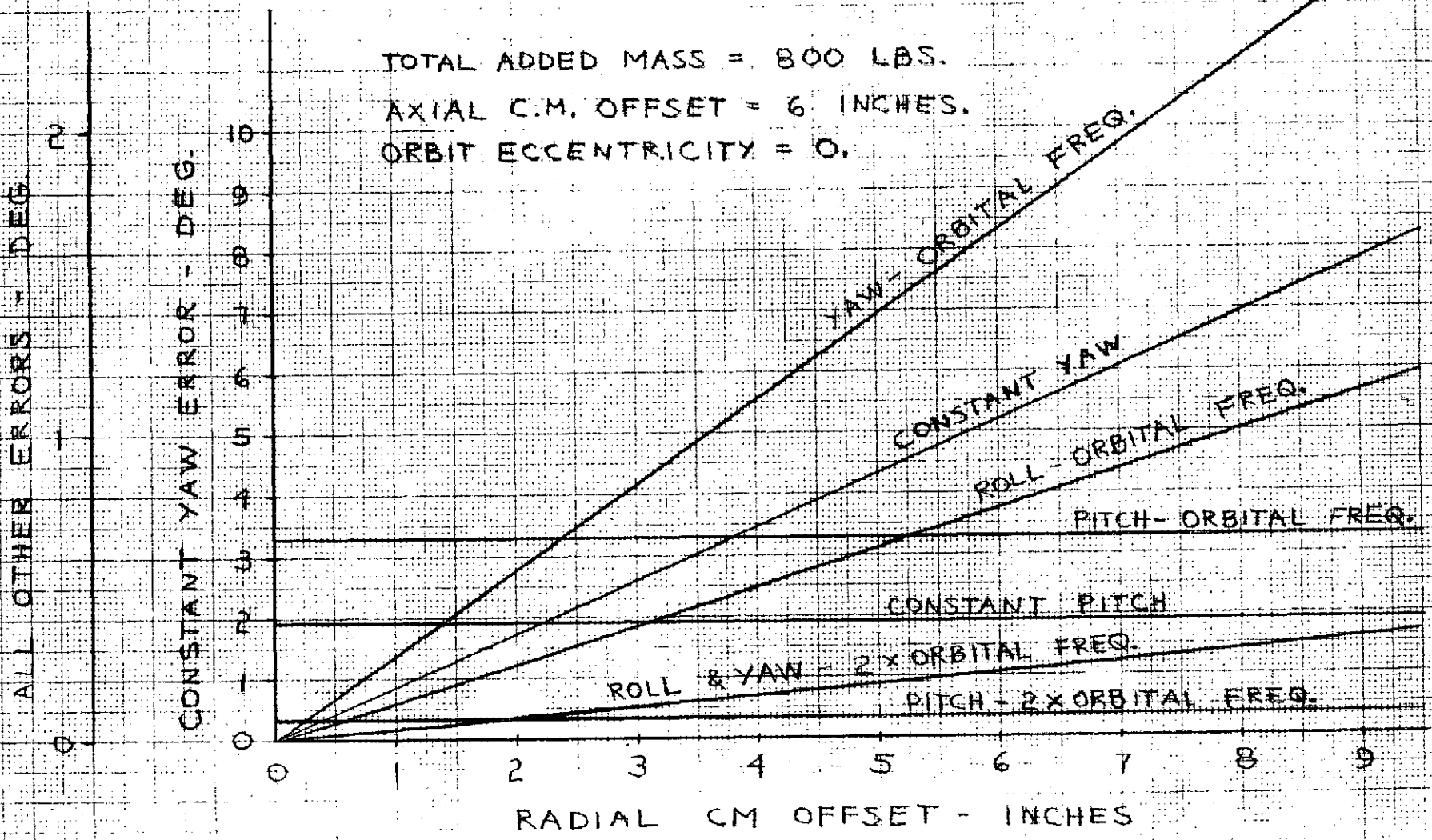


FIGURE 4.7

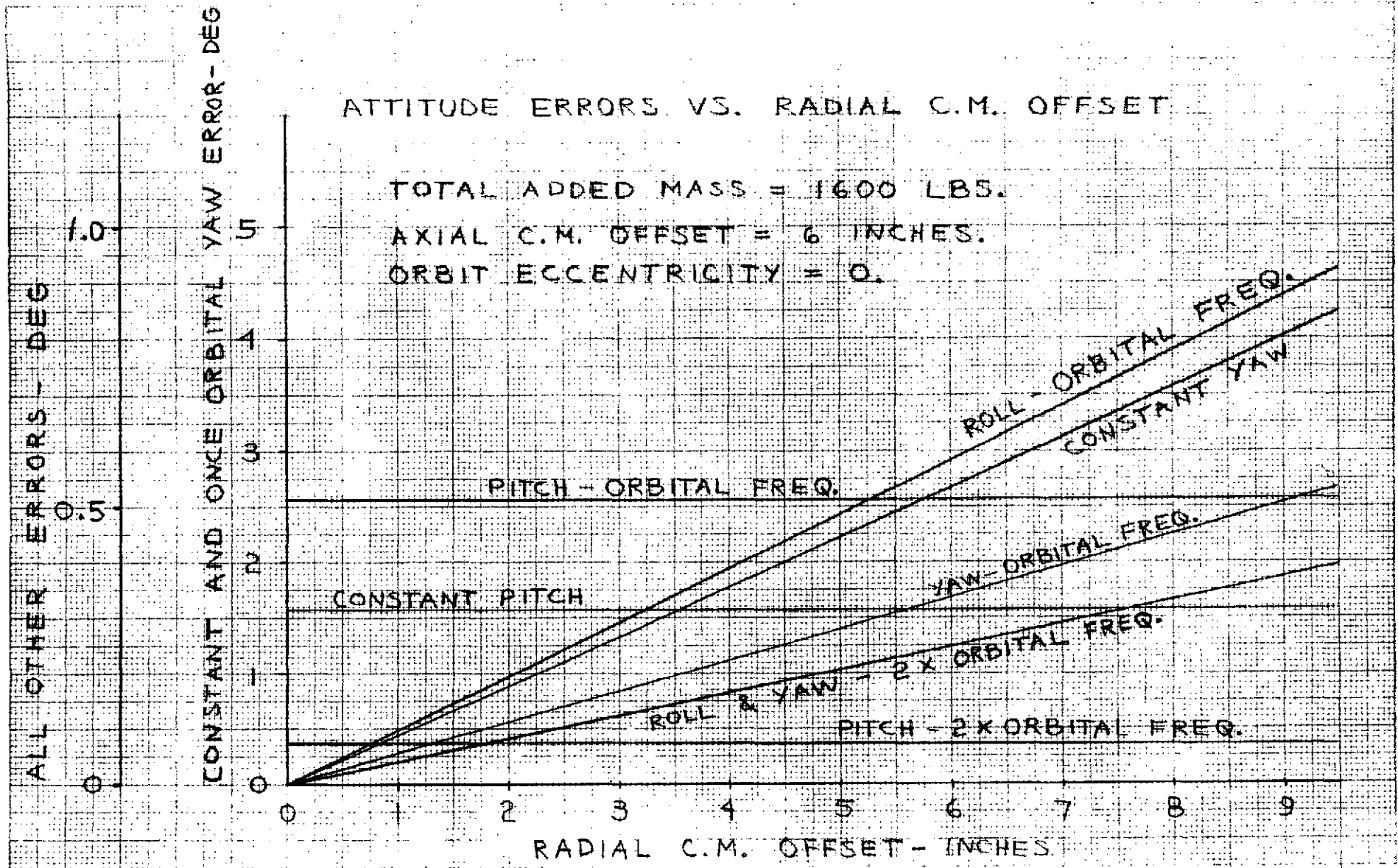


FIGURE 4.8

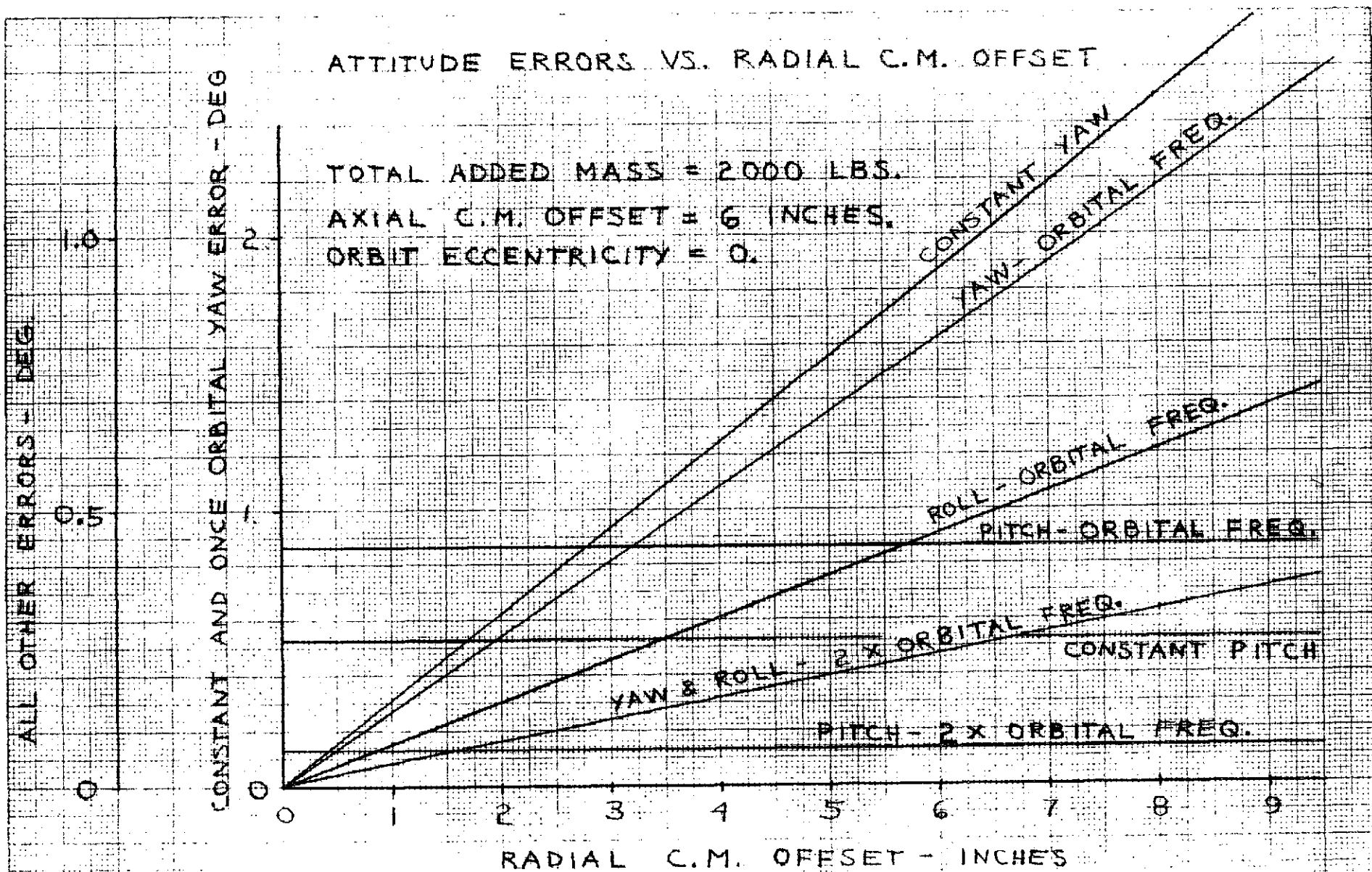


FIGURE 4.9

-70-

This restoring torque is directly proportional to the difference between the pitch and roll moments of inertia. Since the geometry of the spacecraft is fixed, and the masses are placed in the optimum position, the difference between pitch and roll is directly proportional to the mass. Hence, the yaw gravity gradient torque is linear with added weight, and the yaw error is inverse with added weight. This effect is evident in Figures 4.6 through 4.9, where the yaw error decreases directly as the added weight increases. With 182 kg (400 pounds) of added mass, for example, a .152 m (six inch) center of pressure/center of mass offset produces a constant yaw error of approximately 10.1 degrees. At 908 kg (2000 pounds), the error is only 1.94 degrees. When the added weight contributes significantly to the LDEF moment of inertia, a decrease in the yaw sinusoidal errors appears (pitch and roll, also).

4.2 GARBER INSTABILITY

Each of the configurations analyzed in Section 4.1 was evaluated for Garber instabilities. The results are shown in Table 4.1. It is evident from this table that the increased moments of inertia reduce the effectiveness of the damping, and lowers the pitch bias at which the instability occurs. The result was anticipated since increasing the spacecraft moment of inertia without increasing the damping coefficient, reduces the effective damping, and consequently lowers the instability point. The lowest allowable pitch bias is three degrees for any level of damping considered. The relationship

EFFECTS OF MASS ADDITION AND DAMPING ON
 THE GARBER STABILITY BOUNDARIES.
 MAGNET STRENGTH = 22500 POLE-CMS.

		DAMPER COEFFICIENT, LB.-FT.-SEC./RAD.						
		0.4	0.5	0.6	0.7	0.8	0.9	
TOTAL ADDED MASS, LBS.		PITCH BIAS AT WHICH INSTABILITY OCCURS, DEG.						
		0	3	4	5	6	4	7
		400	3	4	5	5	5	6
		800	3	3	4	5	5	6
		1200	3	3	4	4	5	5
		1600	3	3	4	4	5	4
		2000	3	3	3	4	5	5
		3200	2	3	3	3	3	3

TABLE 4.1

between the Garber stability boundaries and the spacecraft performance is summarized in Figure 4.10 which indicates that Garber instability is not a problem.

4.3 TRANSIENT AND CAPTURE PERFORMANCE

4.3.1 TRANSIENT PERFORMANCE

The transient analysis performed for the two axis configuration was also performed for the three axis configuration. The results are shown in Figures 4.11, 4.12 and 4.13. The general relationship between damping coefficient and damping time constant established in Section 3.3 is retained, but the curves are shifted, showing reduced damping with increased mass. Here again, the reduced damping is the result of increased moment of inertia for the same damping coefficient. The effect of increased magnet size is the same for the three axis configuration as the two axis configuration.

4.3.2 CAPTURE PERFORMANCE

The spacecraft configuration is irrelevant to the damper as far as capture is concerned (see Section 5.1.2, however). The spacecraft will ultimately capture if the magnet is anchored to the magnetic field. Hence, the analysis performed in Section 3.3.2 for the two axis configuration is directly applicable to the three axis configuration.

4.4 CONFIGURATION OPTIMIZATION

Optimization of the three axis LDEF configuration consists of selecting the amount of mass which must be added to provide yaw stabilization; and selecting the damper characteristics to provide appropriate damping and stability.

EFFECT OF MASS ADDITION ON THE ATTITUDE ERRORS

ORBIT ECCENTRICITY = 0.0

AXIAL DISTANCE OF C.M. FROM CENTER = 6 INS.

(B; M; D) = GARBER STABILITY BOUNDARY

B = DAMPING CONSTANT, LB. FT. SEC./RAD.

M = ADDED MASS/100.0, LBS.

D = DAMPER MAGNET STRENGTH/225000.0,
POLE - CMS.

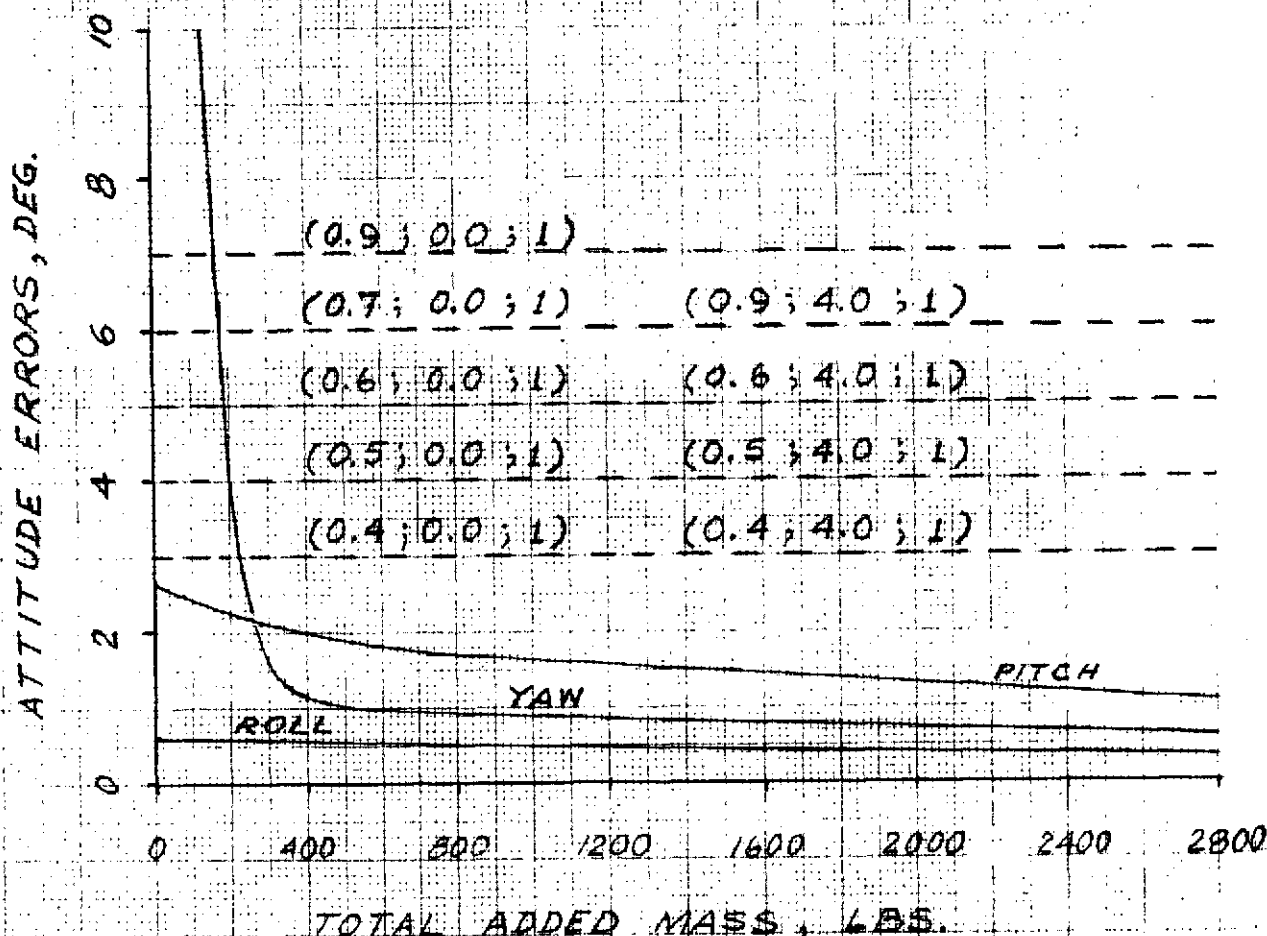
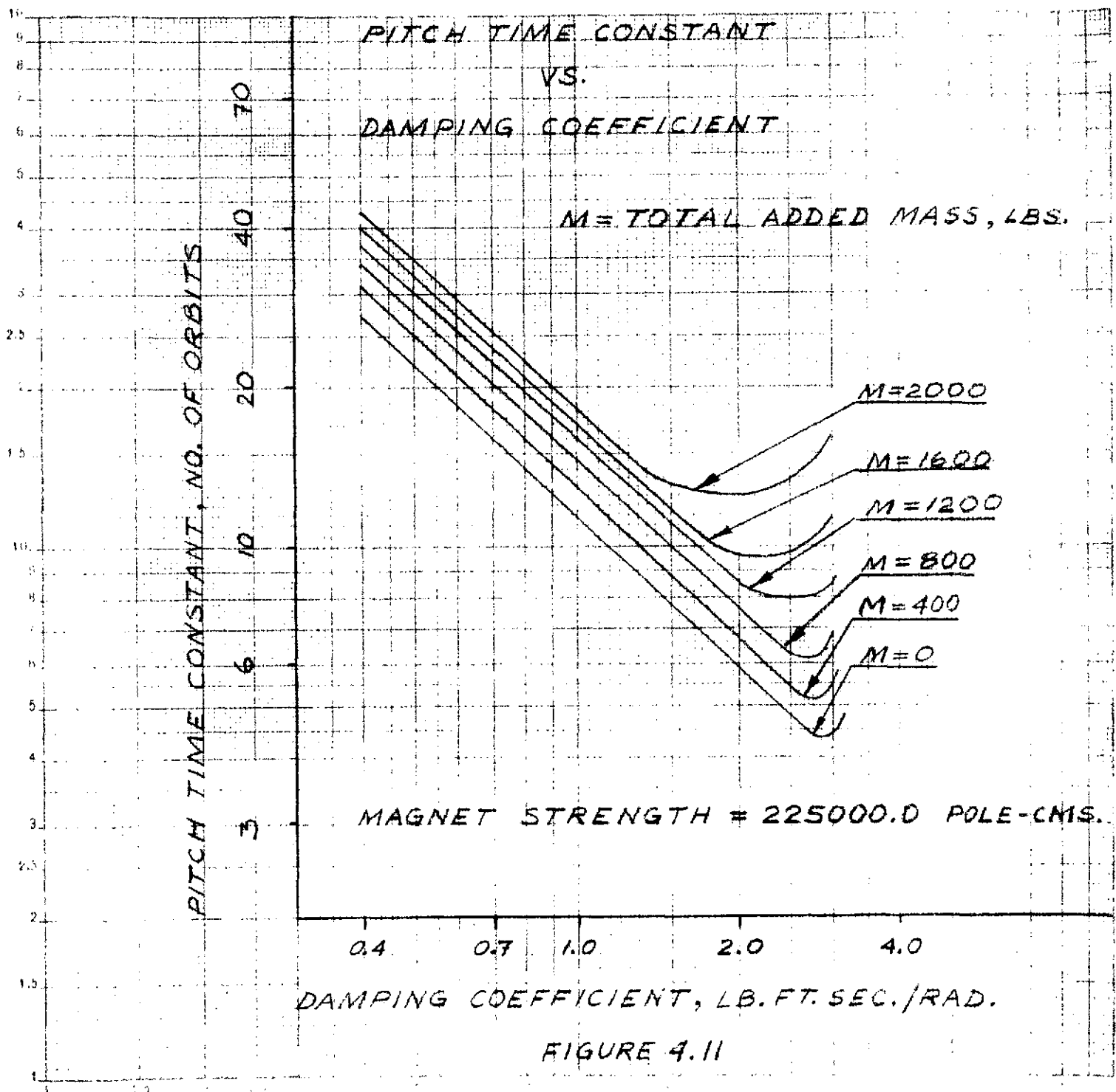
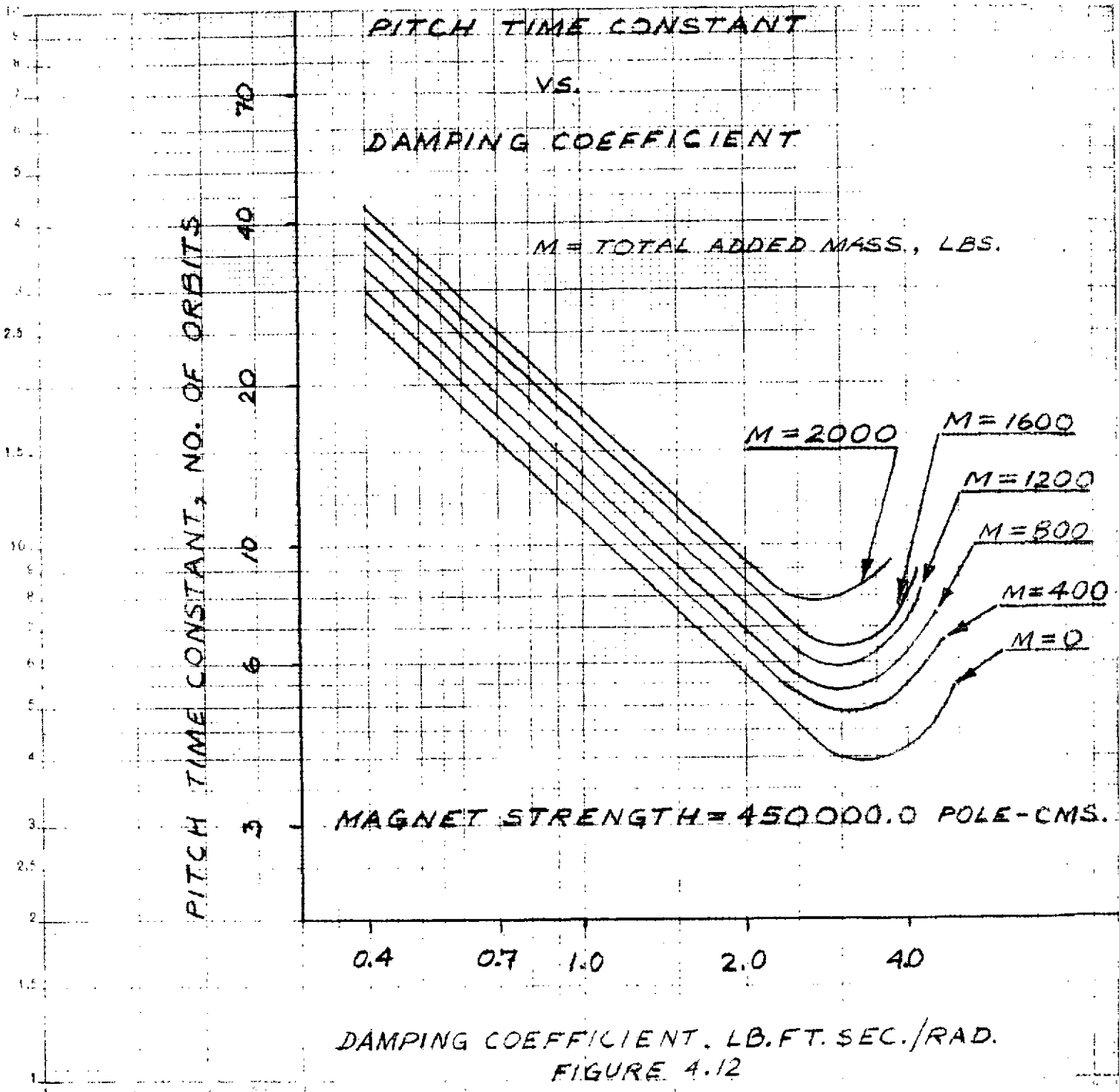


FIGURE 4.10



ORIGINAL PAGE IS
OF POOR QUALITY

2 X 2 CYCLES



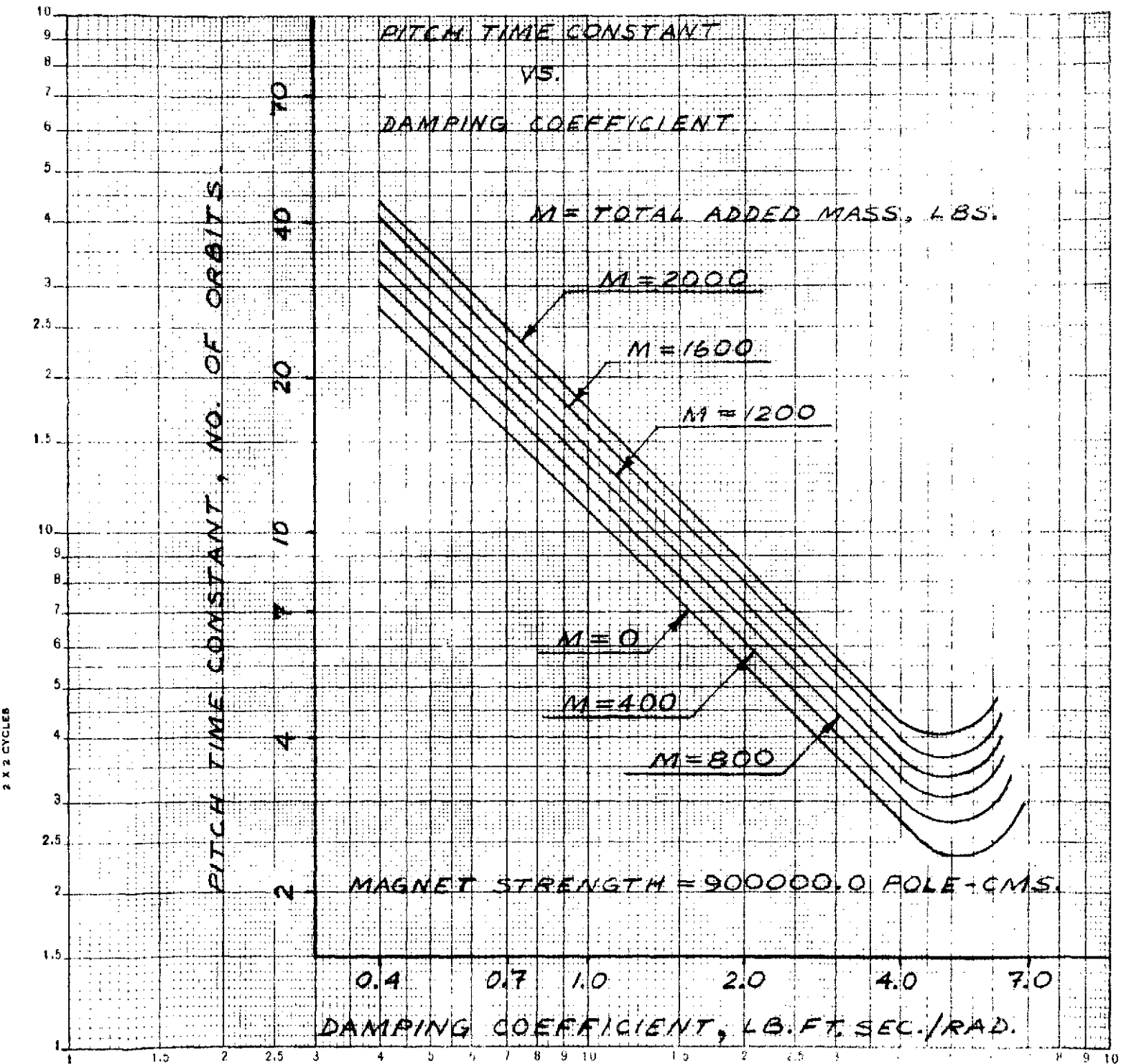


FIGURE 4.13

An evaluation of the disturbance torques acting on the two axis configuration (Section 3.4) led to the selection of a 0.152 m (six inch) center of pressure/center of mass offset, for a 0.002 orbit eccentricity value. These values have only a small impact in yaw, however, as indicated in Figure 4.5. The principal source of yaw error is a center of pressure/center of mass offset normal to the cylinder axis, along a radius. The worst position is along the spacecraft pitch axis (Figure 3.2), which maximizes the yaw torque due to aerodynamic pressure. For offsets of .101 m (four inches) or less, reasonable performance can be obtained by adding 182 kg (400 lb) to 364 kg (800 lb) of additional mass. From discussions with Langley Research Center, an offset of .025 m (one inch) can be achieved by weight balancing. To obtain a 0.025 m (one inch) offset by coefficient of drag differences, however, would require a temperature difference of several hundred degrees between the left and right side of the spacecraft, or a completely different shape on the two sides. Neither of these conditions is likely, but to be conservative, an additional inch was added to the center of mass location to produce a two inch center of pressure/center of mass offset. With this offset, 182 kg (400 pounds) of additional mass will provide yaw control to within nine degrees. The variation of aerodynamic error with center of pressure/center of mass offset along a radius is shown in Figure 4.14.

The selection of damping coefficient was relatively straightforward in view of the small change in moment of inertia between the two axis configuration and the three axis configuration (with 182 kg). With the same damping coefficient as the two axis configuration (0.692 n.m.sec), the linear damping time constant is 24 orbits. The damper characteristics for the two axis configuration was therefore selected for the three axis configuration. The error breakdown for the three axis configuration is shown in Table 4.2.

EFFECT OF A SHIFT OF THE C.M. NORMAL TO THE CYLINDER AXIS ON THE ATTITUDE ERRORS.

AXIAL DISTANCE OF C.M. FROM CENTER = 6 INCHES.
TOTAL ADDED MASS = 400 LBS.
ORBIT ECCENTRICITY = 0

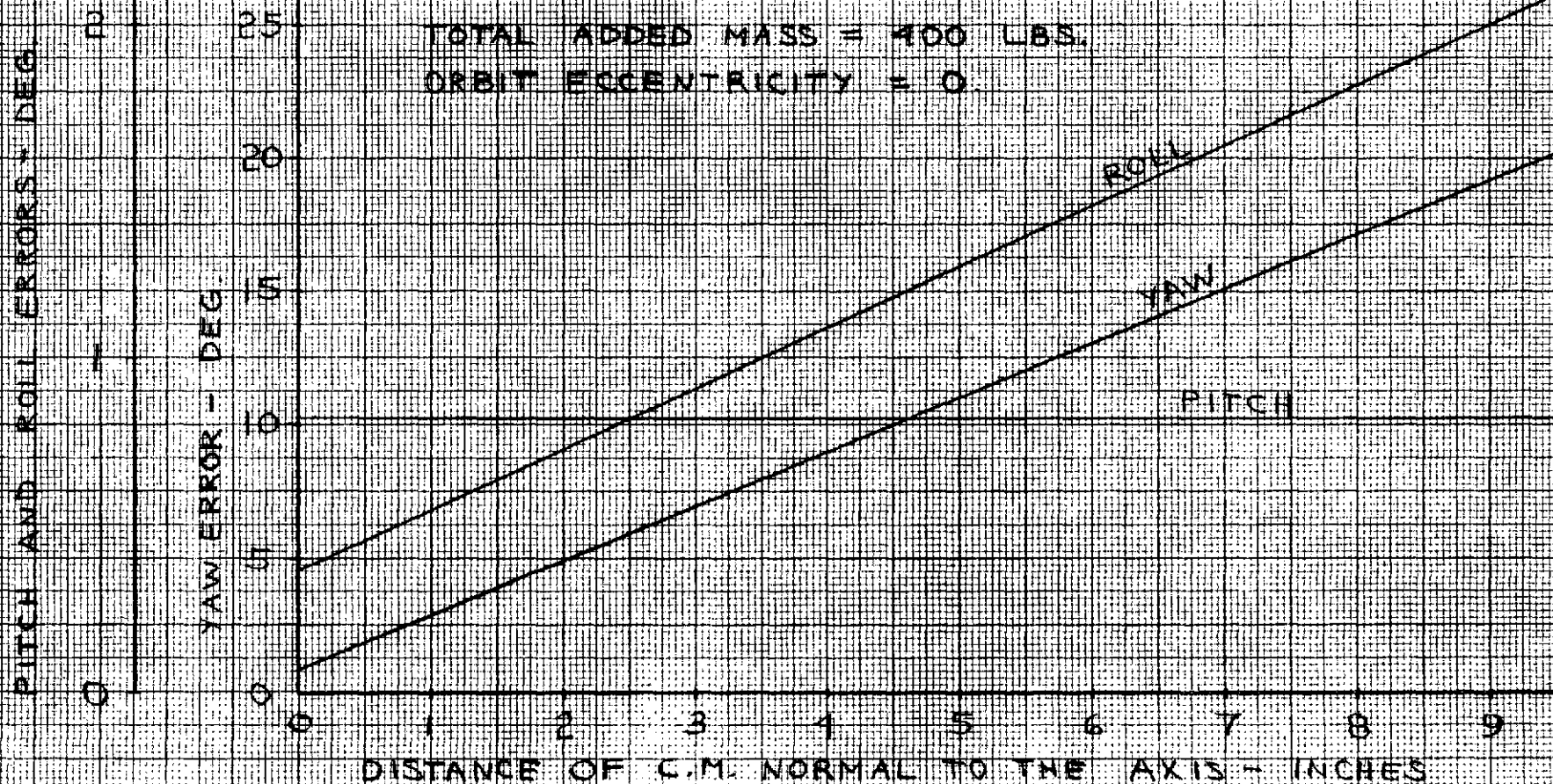


FIGURE 4.14

Table 4.2

Linear Error Budgets Three Axis Configuration				
Spacecraft Parameters				
Orbit Eccentricity = 0.002				
Position of the Ascending Node and Perigee = 2:00 P.M.				
C.M. Offset Along Pitch Axis = 2.0 ins.				
C.M. Offset Along Yaw Axis = 6.0 ins.				
Damping Coefficient = 0.51 lb-ft-sec/rad				
Spacecraft Magnetics = 1000.0 pole-cms/axis				
Torque	Error Axis	Error Freq. Orbit Freq	Error Magnitude, Deg.	
			Frequency Components	Total
Orbit Eccentricity	Pitch	1	.40	.40
Aerodynamic	Pitch	0	.46	1.61
		1	1.06	
		2	.10	
	Roll	0	.01	.52
		1	.43	
		2	.08	
	Yaw	0	7.64	8.67
		1	.87	
		2	.16	

Table 4.2 (cont'd)

Torque	Error Axis	Error Freq. Orbit Freq.	Error Magnitude, Deg.	
			Frequency Components	Total
Damper	Pitch	0	.10	.42
		1	.23	.42
		2	.09	
	Roll	0	.0	
		1	.53	.55
		2	.02	
Yaw	0	.0		
	1	.89	.89	
	2	.0		
Solar	Pitch	0	.0	
		1	.0	.01
		2	.01	
	Roll	0	.0	
		1	.01	.02
		2	.01	
Yaw	0	.19		
	1	.02	.22	
	2	.01		
Magnet	Pitch	0	.0	
		1	.05	.05
		2	.0	
	Roll	0	.0	
		1	.04	.06
		2	.02	
Yaw	0	.34		
	1	.07	.43	
	2	.02		

Table 4.2 (cont'd)

Total Pitch Error	1.75 deg
Total Roll Error	.68 deg
Total Yaw Error	9.06 deg

A comment about the moment of inertia distribution for the three axis configuration appears warranted at this point. The basic LDEF spacecraft has been assumed to have exactly $39,300 \text{ kg-m}^2$ ($29,000 \text{ slug-ft}^2$) in the pitch and roll axes. With the addition of 182 kg (400 lb), the difference between the pitch and roll moments of inertia reaches only 825 kg-m^2 (609 slug-ft^2). This value is small compared to the basic spacecraft, and it is estimated that the value falls below the packaging accuracy capability. Consequently, the spacecraft is likely to have three different moments of inertia, the differences of which exceed the value necessary to provide good yaw control. If the moments of inertia can be controlled to be favorable (pitch a maximum, yaw a minimum), and the moment of difference between pitch and roll equal to greater than the value calculated for 182 kg of added mass, the added mass is unnecessary. The exact moment of inertia difference is not critical to performance, and if the pitch moment of inertia is approximately the same as the two axis configuration, damping will not be significantly affected.

SECTION 5.0

PERFORMANCE PREDICTION

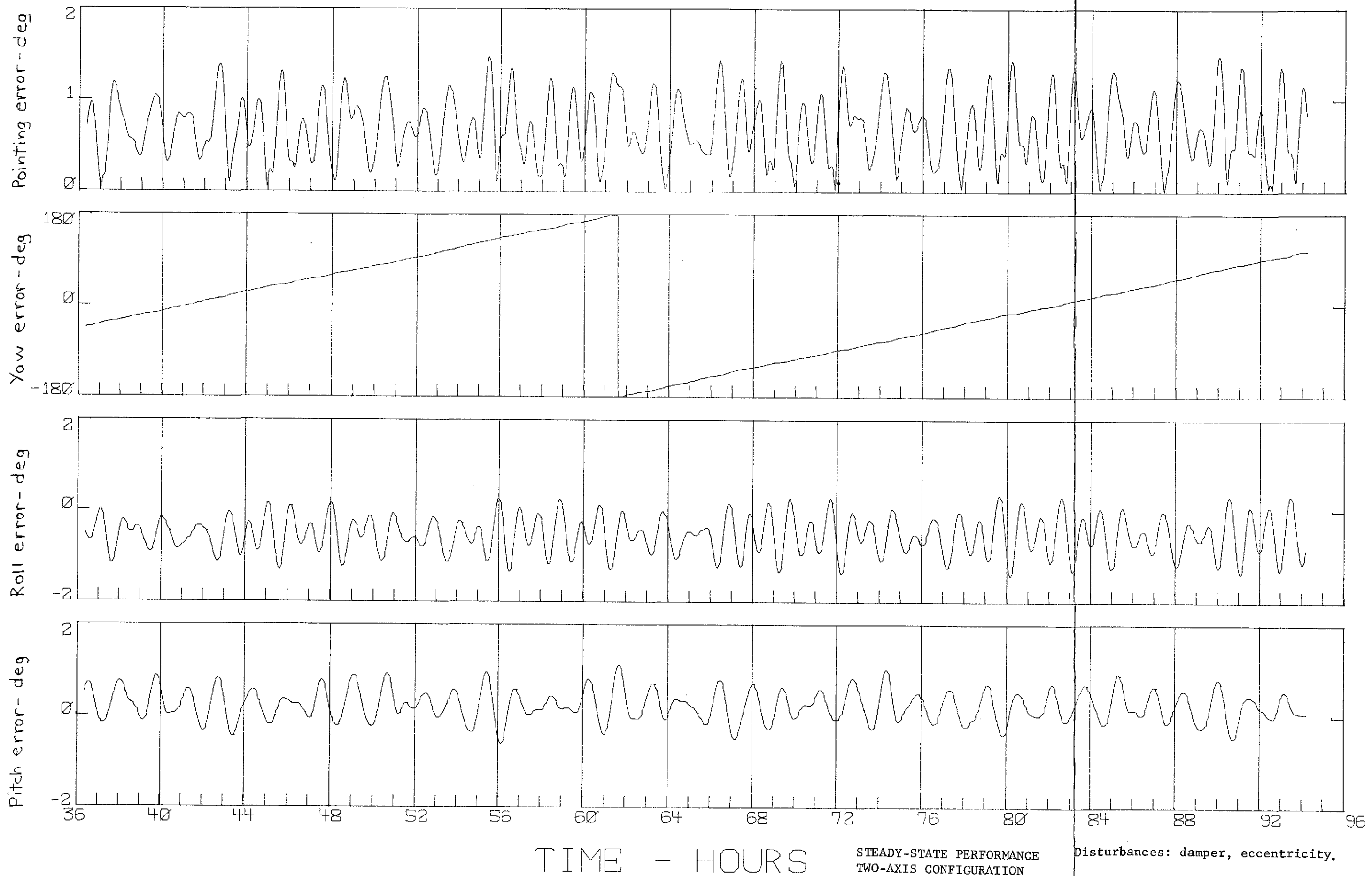
Performance Prediction consists of simulating the LDEF configuration using a three axis digital computer program. The purpose of the simulation is to verify the conclusions drawn from the linear analyses. Capture is also simulated, because of its non-linear dynamics.

The computer program used to make the simulations is a large digital computer program which simulates the dynamics of the spacecraft in three axes using Euler dynamical equations. The attitude of the spacecraft is specified by Euler parameters. Solar torque, aerodynamic torque, magnetic torque and damper torque are included in the simulation for both circular and eccentric orbits. The torques are calculated as a function of spacecraft attitude and orbit position.

5.1 TWO AXIS CONFIGURATION

5.1.1 STEADY STATE PERFORMANCE

Several computer simulations were made to determine the behavior of the spacecraft once steady state is achieved. The first simulation included only the magnetically anchored rate damper and orbit eccentricity, and was selected to illustrate the behavior of the magnetically anchored rate damper in steady state. Figure 5.1 shows the last fifty eight hours of the simulation. Only the end of the simulation is shown to eliminate transients caused by errors in initial conditions. The damping coefficient in the simulation is .697 n.m.sec (.51 lb-ft-sec). The orbit eccentricity is 0.002, with perigee located at the base of the diurnal bulge.



STEADY-STATE PERFORMANCE
TWO-AXIS CONFIGURATION

Disturbances: damper, eccentricity.

Damping coefficient = 0.51 ft-lb-sec.

TIME - HOURS

ORIGINAL PAGE IS
OF POOR QUALITY

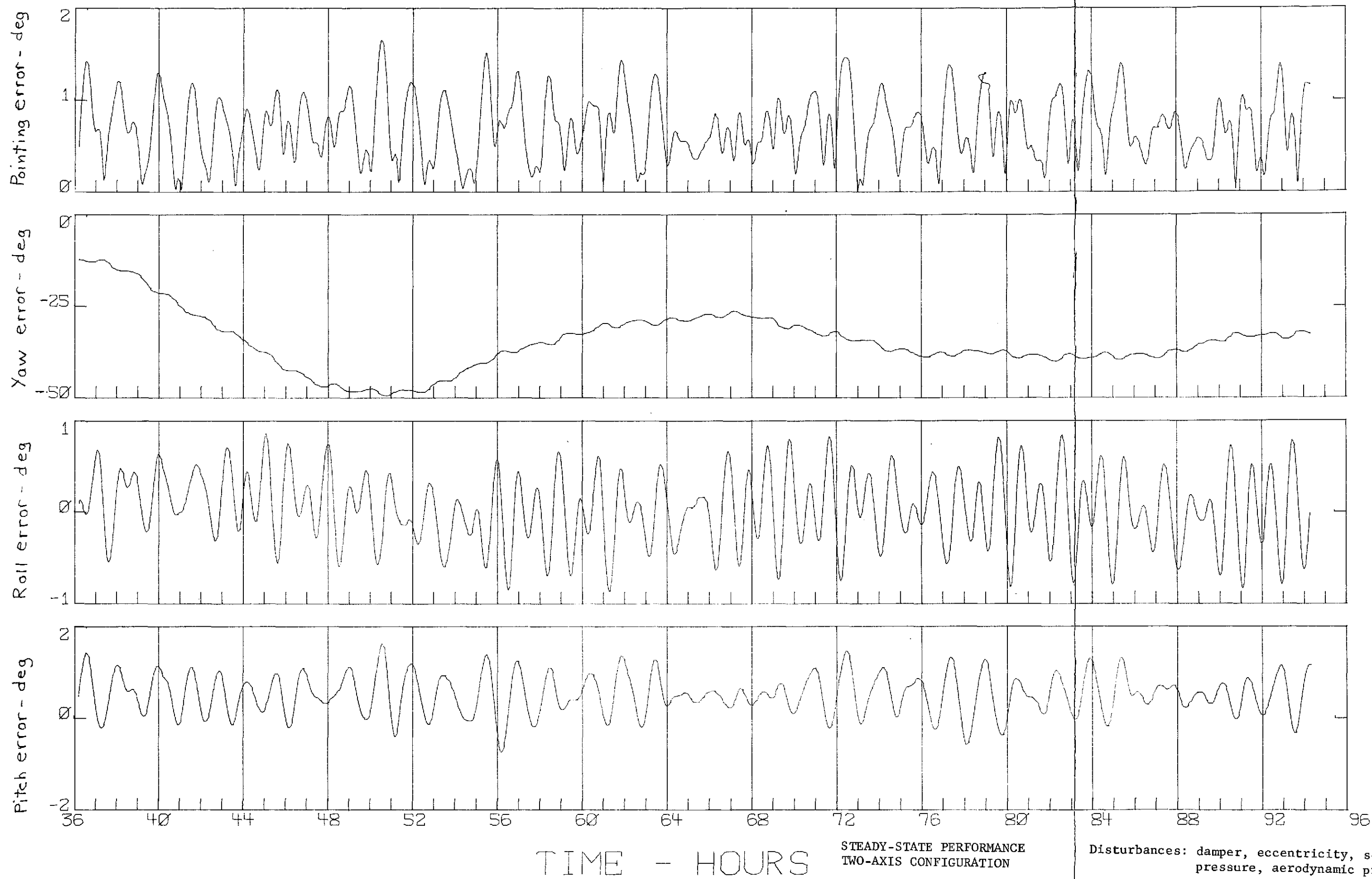
FIGURE 5.1

The error breakdown, Table 3.2, indicates the pitch axis will show a pitch bias of 0.1 degrees and an oscillation of 0.61 degrees. Figure 5.1 indicates a bias of 0.25 degrees, with an oscillation of 0.63 degrees. There is a long period of oscillation on the spacecraft pitch axis, with a period of approximately twelve hours. This is the effect of the rotation of the earth on the magnetic field.

The behavior of the spacecraft in roll is very different from the linear estimate. The largest difference is a pronounced bias of approximately 0.5 degrees, not indicated by the linear analysis. The roll bias and the yaw rotation (obvious in Figure 5.1) are directly connected. If the roll bias were the cause of the yaw rate, a roll bias of 0.5 degrees would produce a yaw rate of 5.55×10^{-4} deg/sec (orbital rate times the sine of 0.5 degrees); approximately 180 degrees in 90 hours. The yaw plot indicates a rate of 1.23×10^{-3} deg/sec (180 degrees in 40.5 hours). Considering that the yaw rate is causing a roll bias, a yaw rate of 1.23×10^{-3} deg/sec will cause a coupling torque of 6.66×10^{-4} lb-ft, which will induce a roll error of 0.534 degrees. It is apparent that it is the rate about yaw which is causing the roll bias, rather than the reverse. Figure 5.2 confirms the analysis since the bias disappeared when yaw stopped rotating. The cause of the yaw rotation appears to be the result of a linear instability caused by the damper (appendix A). The instability is in yaw, and manifests itself as a steady yaw rate. The effect on steady state is not serious, since the overall effect of the instability is to cause the spacecraft to assume a biased attitude (and rate). The roll error (exclusive of the bias) is 0.63 degrees, in good agreement with the linear estimate.

Figure 5.2 shows the steady state performance of the two axis configuration with all error sources (solar torque, aerodynamic torque, damper, and orbit eccentricity) except magnetic torques. The error breakdown for this case indicates a pitch error of 2.03 degrees and a roll error of 0.79 degrees. The roll error shown in Figure 5.2 is approximately 0.8 degrees (note the bias has disappeared), in good agreement with the linearized estimate. The pitch axis, however, has a peak error of approximately 1.5 degrees, nearly 0.5 degrees below the anticipated value. This reduced error is primarily the result of reduced oscillation amplitude. The bias has increased approximately 0.4 degrees between Figures 5.1 and 5.2, compared to the linear estimate of 0.52 degrees.

A significant difference between Figures 5.1 and 5.2 is the position assumed by the yaw axis. The spacecraft is weathervaning as a result of a center of mass offset of one inch along each of the roll and pitch axes. The weathervaning eliminated the observed effect of the yaw instability, but it cannot be established that the instability is eliminated. The instability may, for example, cause a yaw bias from the weathervaning null. The overall agreement with the linearized estimate, however, is reasonably good, since, as indicated earlier, the linearized estimate is conservative. Additional steady state runs were unnecessary because of the excellent performance, even in the worst case, and the close correlation between the linearized analysis and the simulation. However, an additional simulation was made using a damping coefficient of 1.38 n.m.sec (1.0 lb-ft-sec) to determine the effect of a higher damping coefficient. Figure 5.3 shows the results, and indicates a peak error of 1.9 degrees in the pitch axis, and 1.2 degrees in the roll axis. This is an increase of .4 degrees in pitch, and .3 degrees in roll due to the damper, in agreement with the linearized analysis (Figure 3.3).

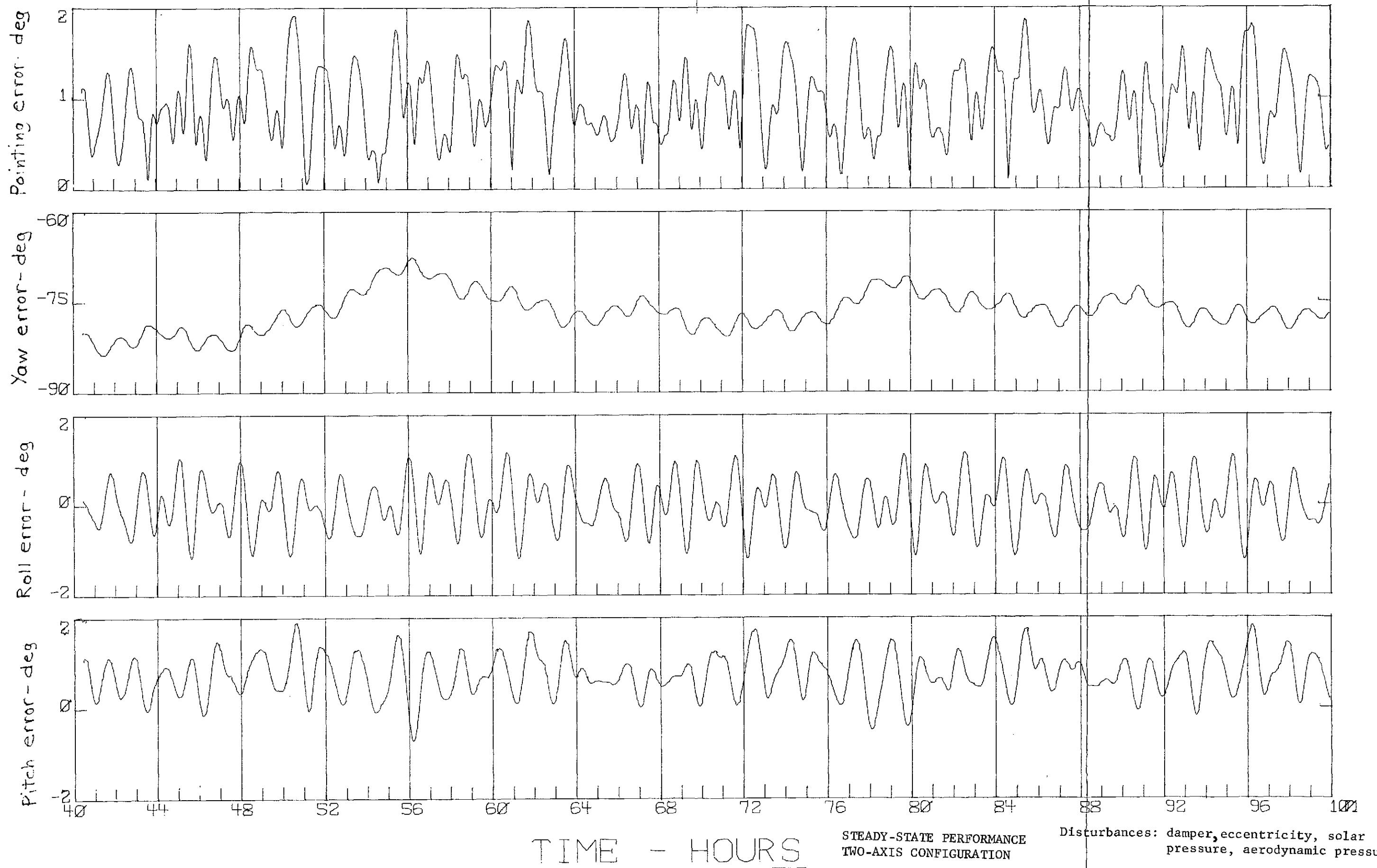


STEADY-STATE PERFORMANCE
TWO-AXIS CONFIGURATION

Disturbances: damper, eccentricity, solar pressure, aerodynamic pressure.

Damping coefficient = 0.51 ft-lb-sec.

FIGURE 5.2



STEADY-STATE PERFORMANCE
TWO-AXIS CONFIGURATION

Disturbances: damper, eccentricity, solar pressure, aerodynamic pressure.

Damping coefficient = 1.0 ft-lb-sec.

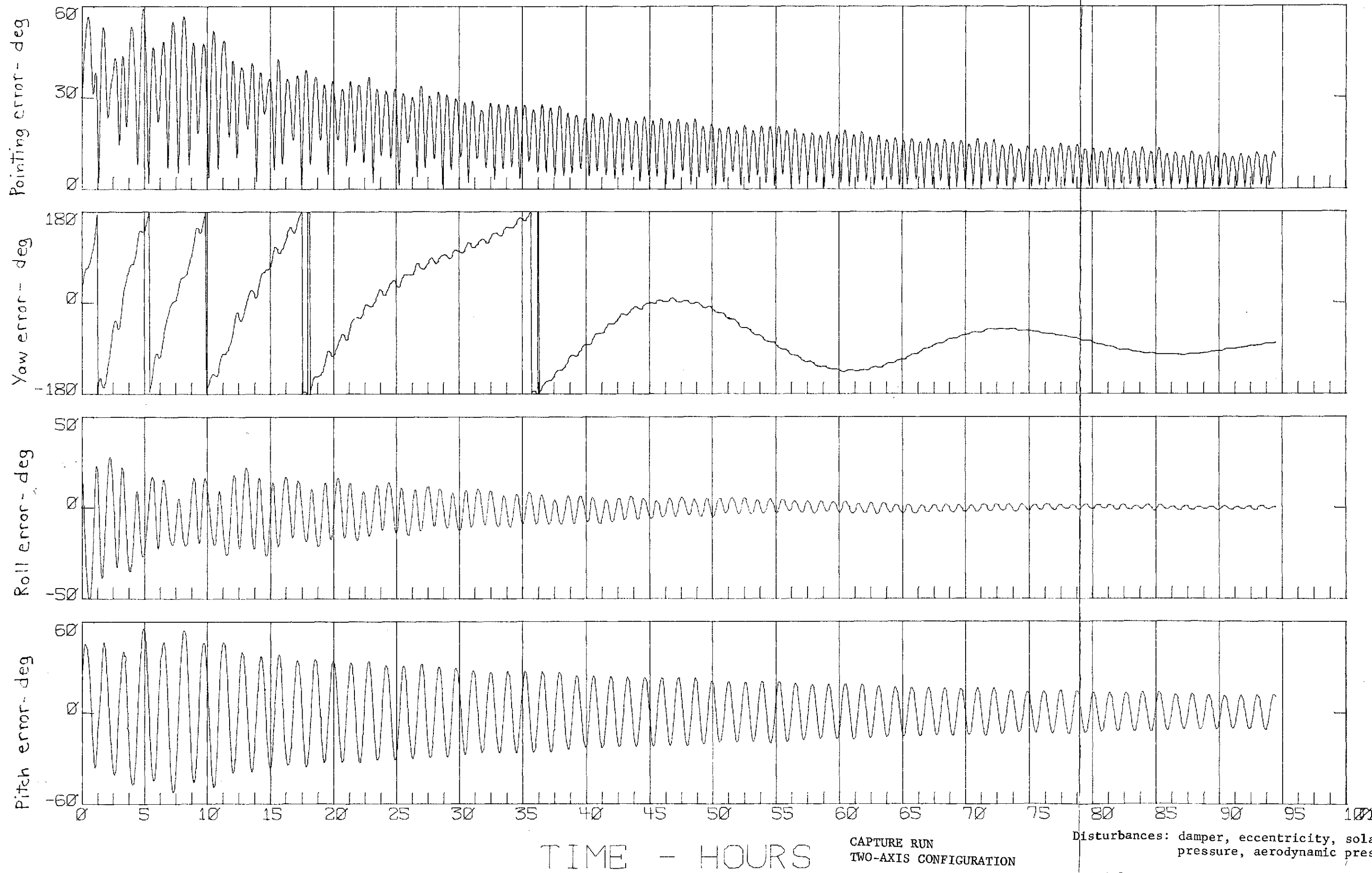
TIME - HOURS

5.1.2 TRANSIENT AND CAPTURE PERFORMANCE

The transient and capture simulations were performed with two sets of initial conditions. The first set placed 0.04 deg/sec rate and fifteen degrees attitude error on all axes. The conditions were selected (from Langley inputs) to verify that the spacecraft would stabilize rightside up. The conditions also provided an excellent run for the calculation of damping time constant.

The results of the simulation are shown in Figure 5.4. The spacecraft does capture upright, reaching a peak pointing error of 59 degrees at five hours. The local vertical at the end of the simulation is 11.3 degrees, indicating a transient decay time of 90 hours. This is not in agreement with the linearized estimate (23 orbits), and is directly attributable to the behavior of pitch. The time constant for pitch is 43 orbits, nearly twice the anticipated value. In general, pitch damping falls off with decreasing orbit inclination, and some increase in damping time is normally anticipated. Correlation with other simulations had indicated that to an inclination of 45 degrees, the reduction is minor. However, the majority of the previous simulations were for two axis configurations with pitch and roll moments of inertia much larger than yaw (factor of 100). A brief comparison with the results obtained from a study performed for Marshal Spaceflight Center indicated closer correlation with LDEF simulation results. Other simulations performed during this study (Section 5.2.2) indicated similar results. Hence, the linear time constant is 43.8 orbits.

The second set of initial conditons was a capture condition with initial rates of 0.25 deg/sec on all axes, and 15 degrees of attitude error. The rates are the maximum separation rates anticipated for the Remote Manipulator for



CAPTURE RUN
TWO-AXIS CONFIGURATION

Disturbances: damper, eccentricity, solar pressure, aerodynamic pressure.

Initial rates = .04 deg/sec per axis.

Damping coefficient = 0.51 ft-lb-sec.

FOLDOUT FRAME 2

TIME - HOURS

ORIGINAL PAGE IS
OF POOR QUALITY

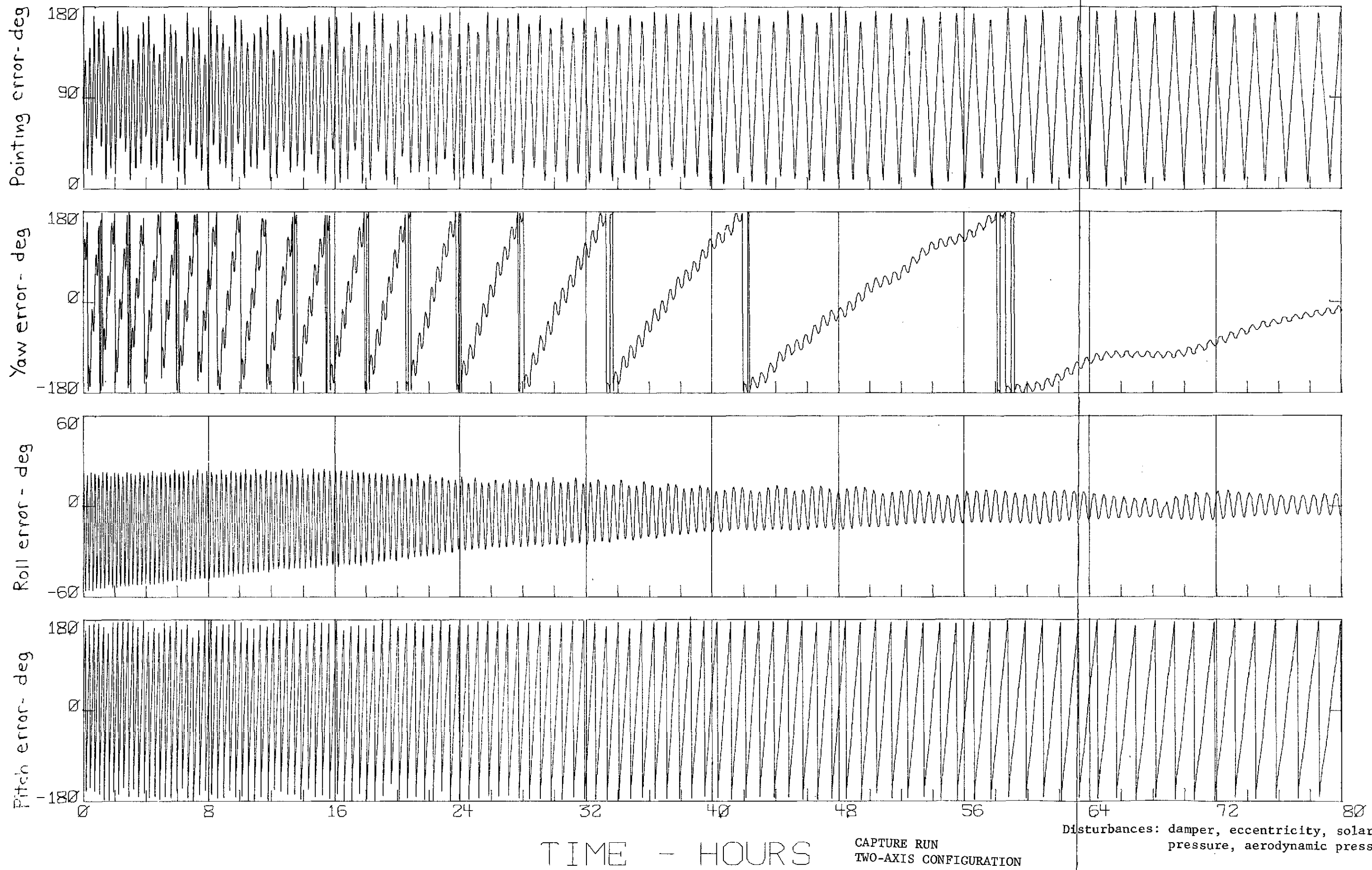
FIGURE 5.4

the space shuttle. Figure 5.5 shows the results of the simulation, and indicates that the spacecraft tumbled for 150 hours. Increasing the damping from .692 n.m.sec (0.51 lb-ft-sec) to 1.36 n.m.sec (1.0 lb-ft-sec) did not improve the damping (Figure 5.6). It is evident from Figure 5.6, that the spacecraft is not damping after the first 60 hours. An analysis of the results indicated that the primary cause of the prolonged tumble is a spacecraft resonant condition associated with large amplitude oscillations. Since gravity gradient torques are a function of the angle between the local vertical and the minimum moment of inertia, a gravity gradient spacecraft will act as a spring mass system. At low amplitude oscillations, the natural frequency of the spacecraft in pitch for the two axis configuration is 1.23 times orbital. At large amplitudes, however, the gravity gradient "spring constant" reduces, and the natural frequency of the spacecraft falls below the low amplitude natural frequency. At oscillation amplitudes of ninety degrees, the configuration's natural frequency is nearly orbital (the frequency can be estimated from Figure 5.5). As a consequence, the configuration is extremely sensitive to torques which disturb the spacecraft at orbital frequency, and the damper (as well as aerodynamics) drives the spacecraft and prevents it from settling. The problem can be eliminated by altering the natural frequency of the spacecraft through appropriate moment of inertia change. Altering the damping coefficient, however, is not effective since the level of damping is too low to significantly impact the natural frequency.

5.2 THREE AXIS CONFIGURATION

5.2.1 STEADY STATE PERFORMANCE

The three axis configuration was simulated in a manner similar to the two



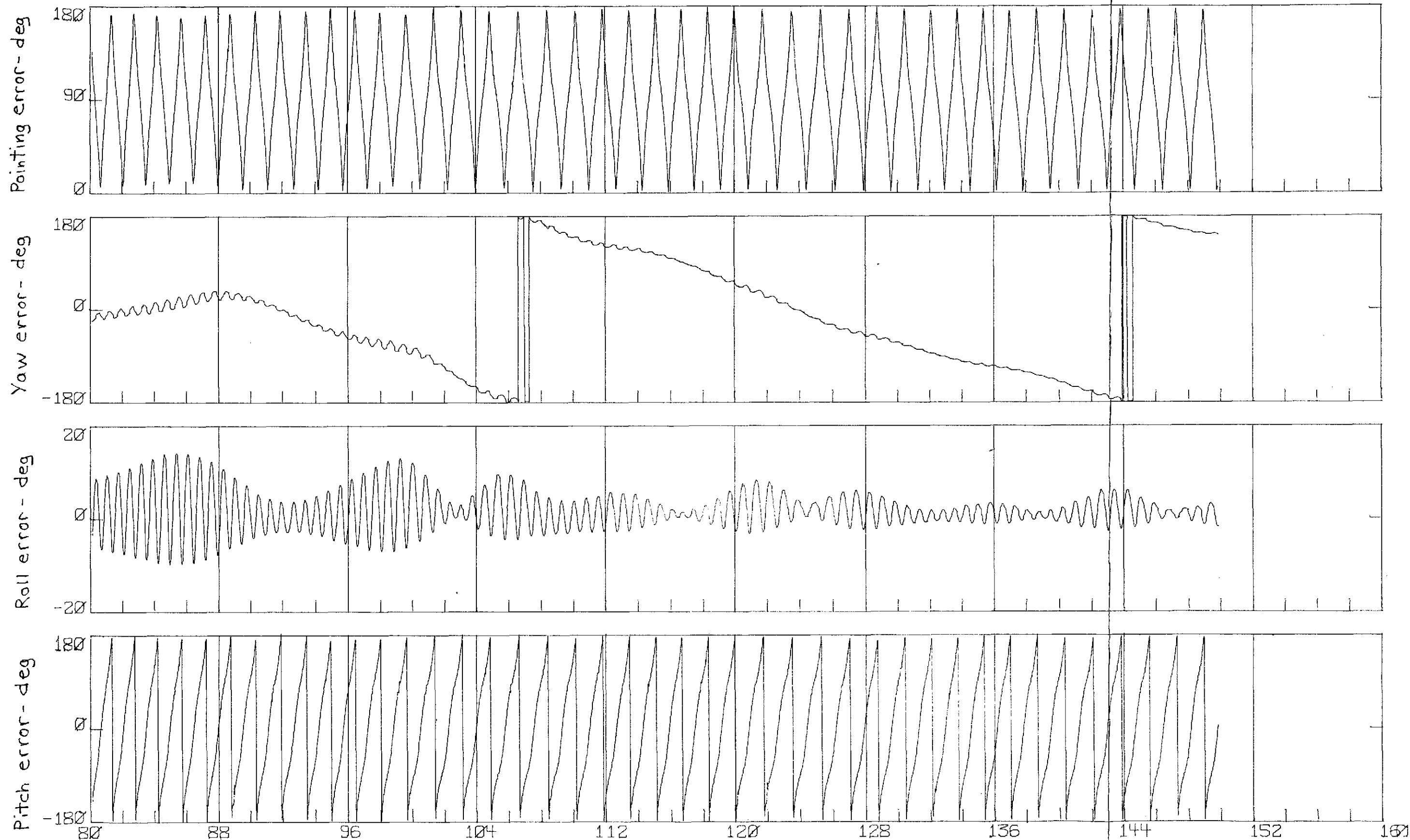
Disturbances: damper, eccentricity, solar pressure, aerodynamic pressure.

Initial rates = .25 deg/sec per axis.

Damping coefficient = 0.51 ft-lb-sec.

FOLDOUT FRAME 2

FIGURE 5.5



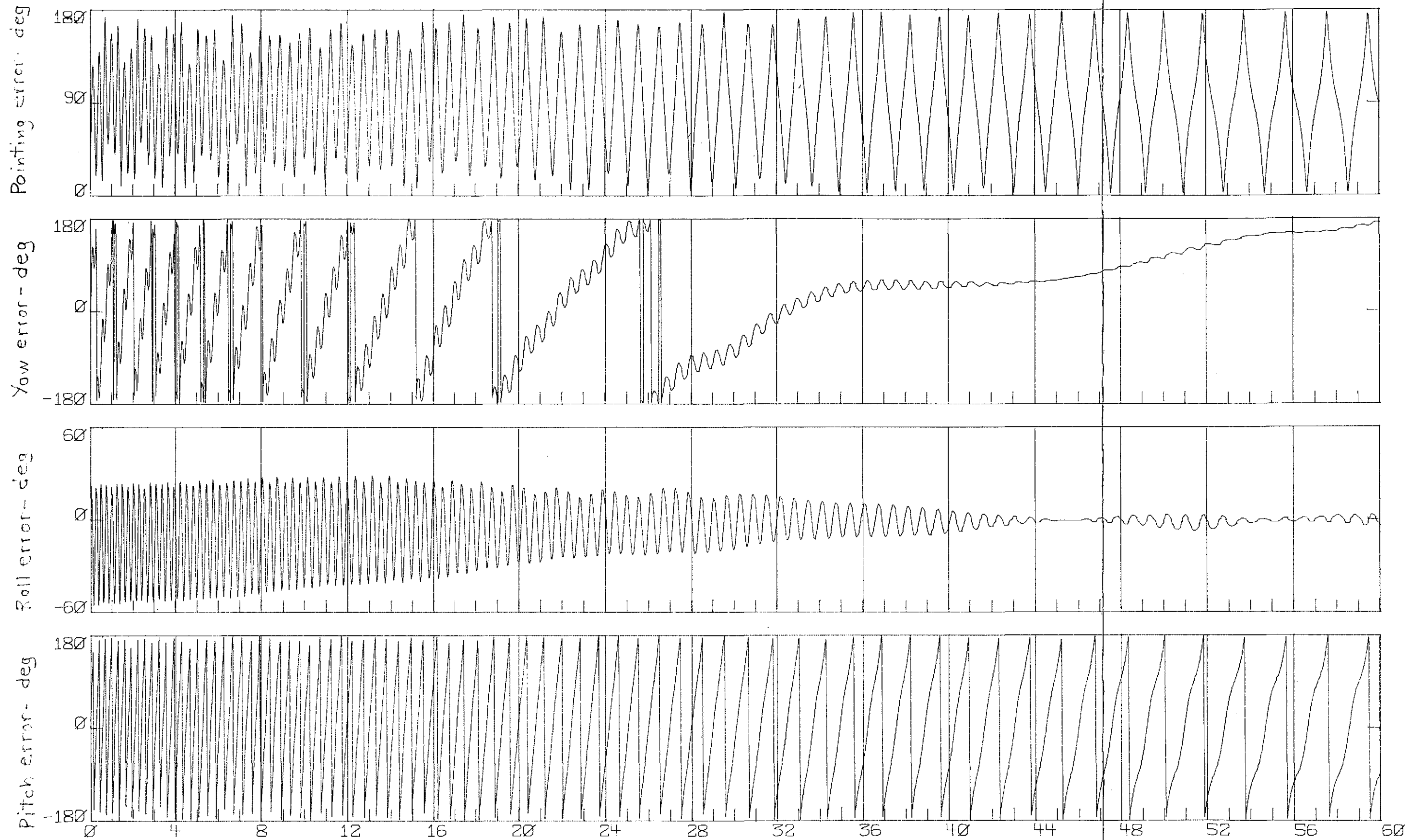
TIME - HOURS

CAPTURE RUN
TWO-AXIS CONFIGURATION

Disturbances: damper, eccentricity, solar pressure, aerodynamic pressure.
Initial rates = .25 deg/sec per axis.
Damping coefficient = 0.51 ft-lb-sec.

ORIGINAL PAGE IS
OF POOR QUALITY

FIGURE 5.5 (cont'd)



TIME - HOURS

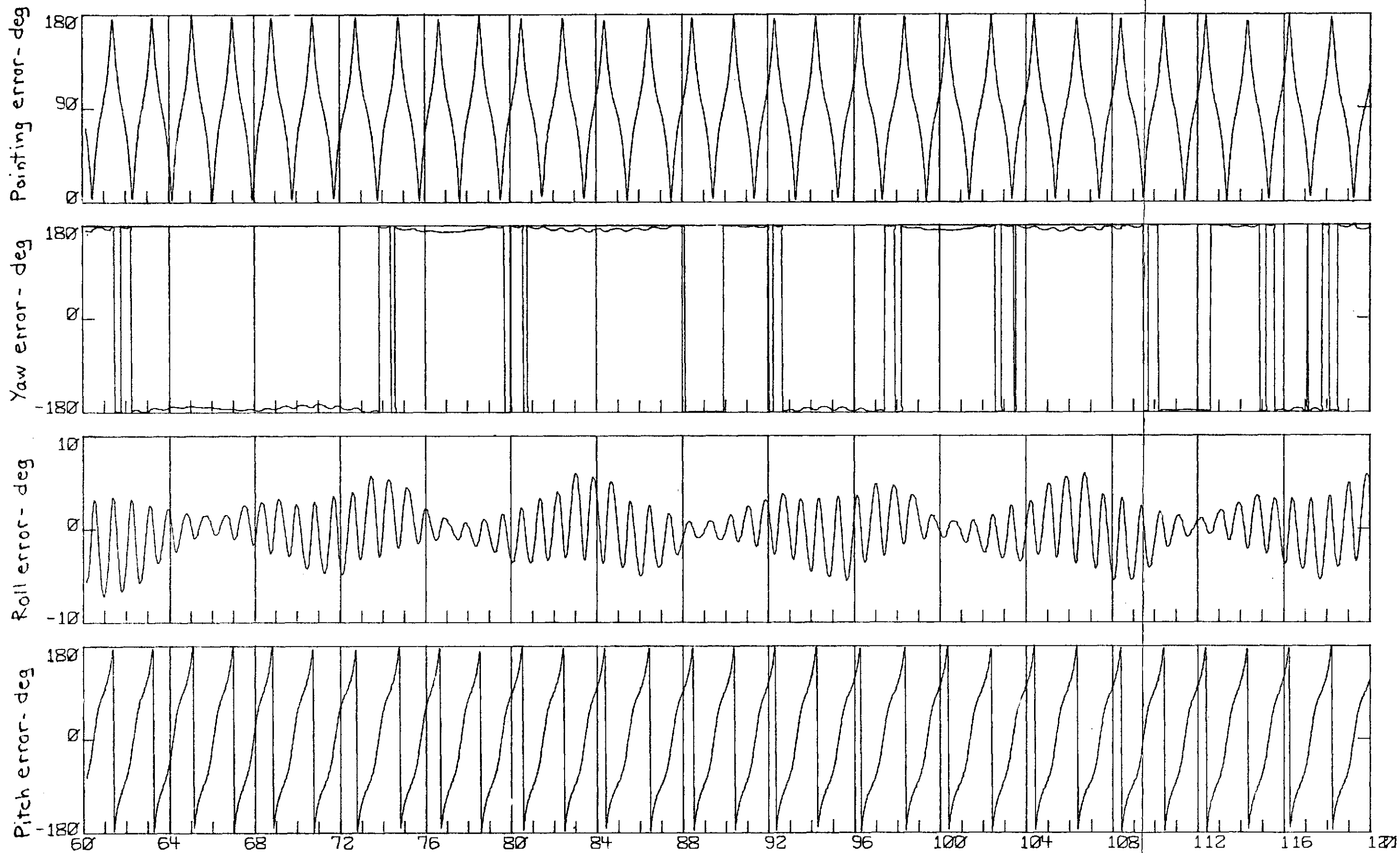
CAPTURE RUN
TWO-AXIS CONFIGURATION

Disturbances: damper, eccentricity, solar pressure, aerodynamic pressure.

Initial rates = .25 deg/sec per axis.

Damping coefficient = 1.0 ft-lb-sec.

FIGURE 5.6



TIME - HOURS

CAPTURE RUN
TWO-AXIS CONFIGURATION

Disturbances: damper, eccentricity, solar pressure, aerodynamic pressure.

Initial rates = .25 deg/sec per axis.

Damping coefficient = 1.0 ft-lb-sec.

FIGURE 5.6 (cont'd)

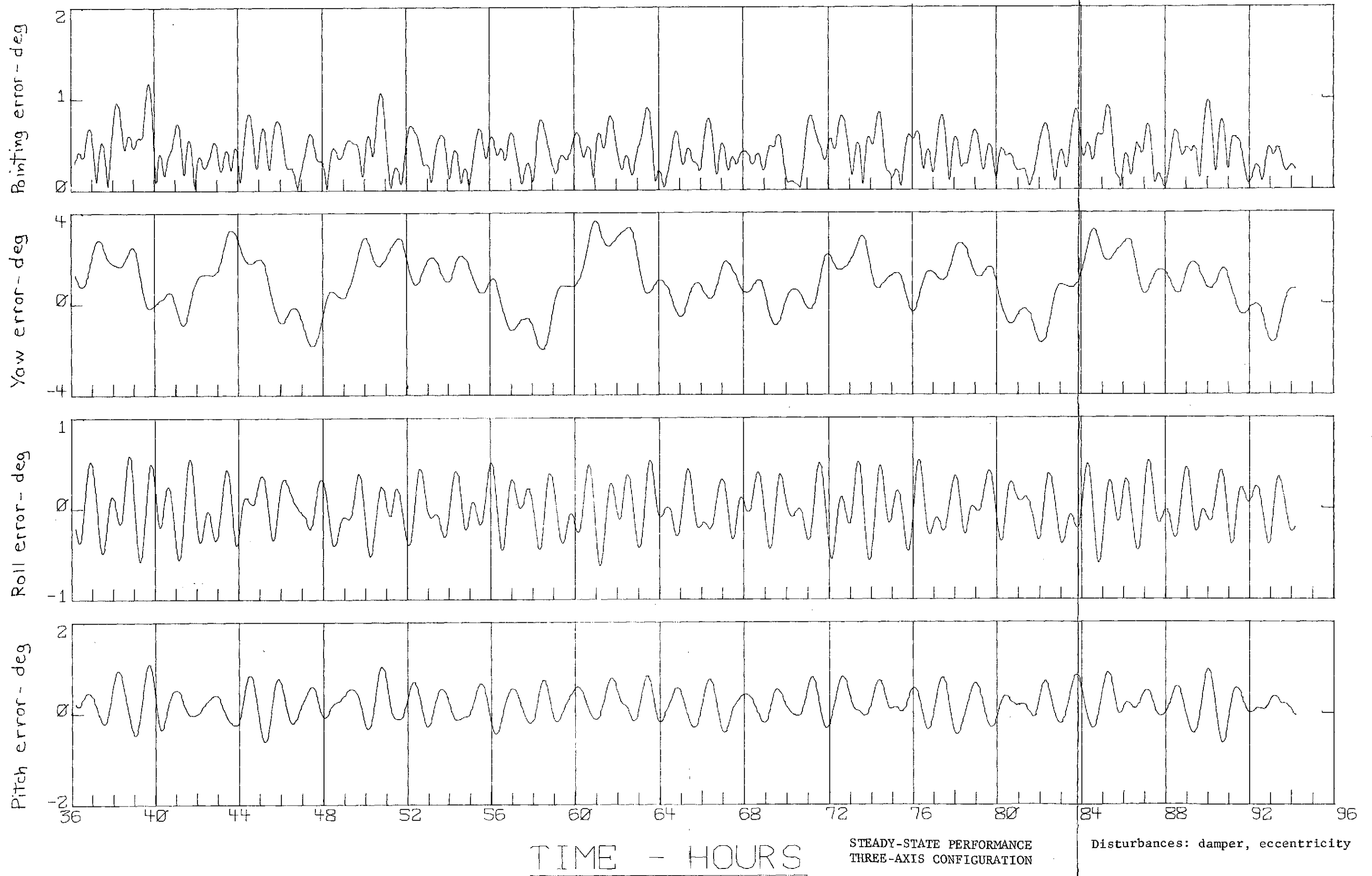
FOLDOUT FRAME 1

FOLDOUT FRAME 2

axis configuration. The first simulation included only the magnetically anchored rate damper (damping coefficient of .692 n.m.sec (.51 lb-ft-sec) and orbit eccentricity (.002). Figure 5.7 shows the last fifty-eight hours of the simulation, and indicates pitch, roll and yaw errors of 0.82 deg, 0.47 deg, and 3.3 degrees, respectively. The error breakdown indicates pitch, roll and yaw errors of 0.65 deg, .55 deg, and .89 deg for this case. The pitch and roll estimates are in reasonable agreement, but the yaw axis simulation results are significantly different from the linearized estimate. The difference in the yaw performance is primarily the result of a low frequency oscillation (twelve hours) associated with the rotation of the earth. The once orbital frequency, superimposed on the long cycle, has an amplitude of 0.65 degrees, which is in good agreement with the linearized estimate.

The performance of the three axis configuration with all disturbances, is shown in Figure 5.8. The peak pitch, roll and yaw errors are 0.94 deg, 0.47 deg, and 8.2 deg. The linearized error budget indicates 1.75 deg, 0.68 deg, and 9.06 deg for the same conditions. The better agreement in yaw between the linearized estimate and the simulation is probably the result of aerodynamic torque suppressing the low frequency yaw disturbance. The low pitch error appears to be the result of phasing of the disturbances since there is an obvious difference in behavior between Figures 5.7 and 5.8, but little increase in oscillation amplitude.

As with the two axis configuration, a steady state run was made with a damping coefficient of 1.36 n.m.sec (1.0 lb-ft-sec). The results, shown in Figure 5.9, indicate pitch, roll and yaw errors of 1.7 deg, 1.2 deg, and 10.5 degrees. The long period oscillation on the yaw axis is more pro-



STEADY-STATE PERFORMANCE
THREE-AXIS CONFIGURATION

Disturbances: damper, eccentricity

Damping coefficient = 0.51 ft-lb-sec.

ORIGINAL PAGE IS
OF POOR QUALITY

FIGURE 5.7

FOLDOUT FRAME 2

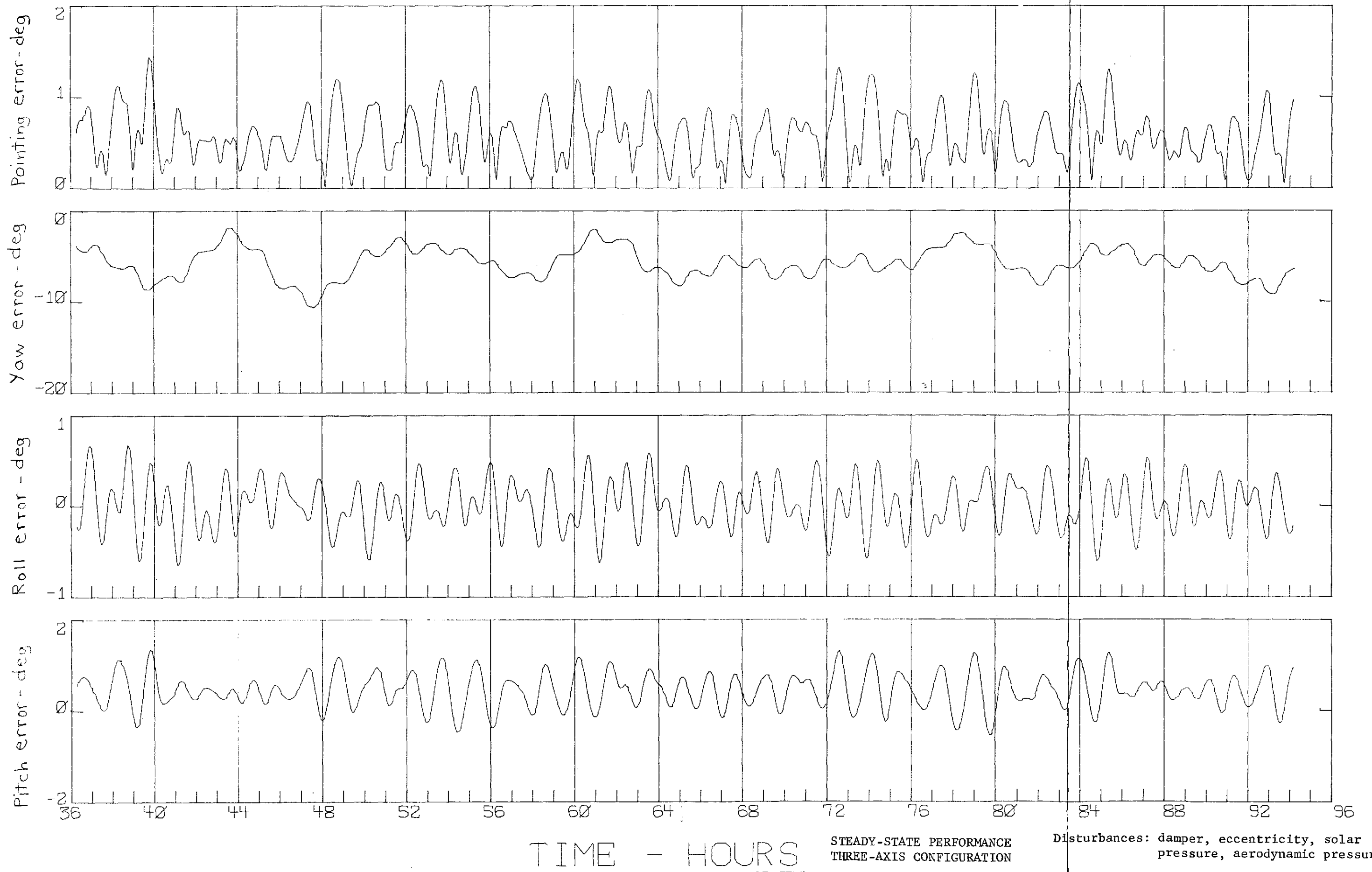
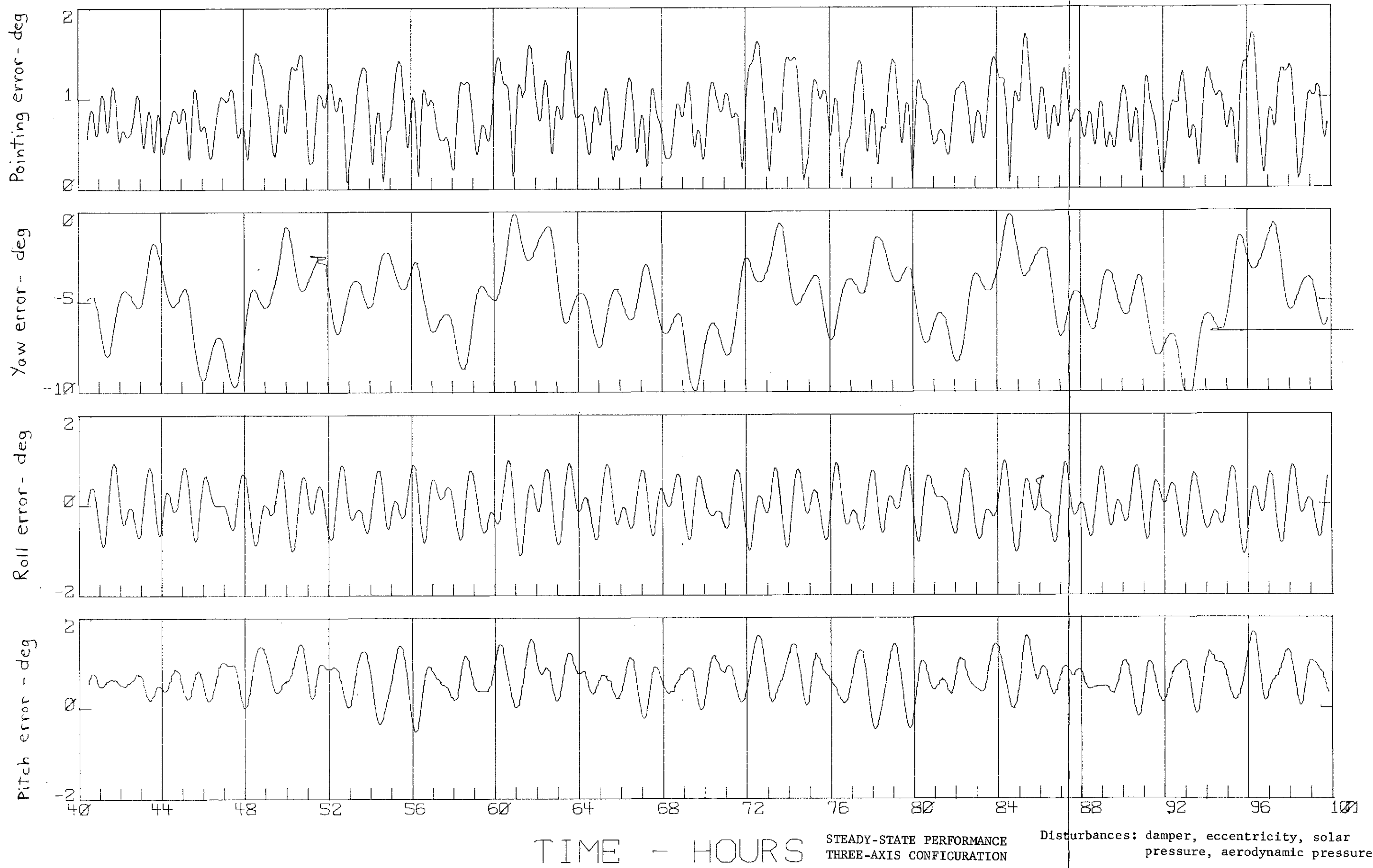


FIGURE 5.8



nounced than in Figure 5.7 and Figure 5.8.

5.2.2 TRANSIENT AND CAPTURE PERFORMANCE

The transient behavior of the spacecraft from initial rates of 0.04 deg/sec on all axes and fifteen degrees of attitude error is shown in Figure 5.10. The spacecraft captured rightside up, and damped with a time constant of 46.6 orbits; in good agreement with the two axis simulation (Figure 5.5). The natural period in yaw is approximately eight hours as shown on the Figure. This oscillation is not to be confused with the 12 hour period shown in Figure 5.7.

A second transient simulation was made without external disturbance torques to determine the effect of aerodynamics, solar torque, etc. on the damping. The spacecraft behavior shown in Figure 5.11, is different than that shown in Figure 5.10, but the time constant is basically the same.

A third transient simulation was made with a damping coefficient of 1.36 n.m.sec (1.0 lb-ft-sec), and the results are shown in Figure 5.12. As with the lighter damping, the spacecraft captured rightside up; but the time constant is 27.7 orbits.

A capture run was made with 0.25 deg/sec on all axes, the results of which are shown in Figure 5.13. The spacecraft tumbled in pitch for approximately 76 hours, after which it stabilized rightside up and began damping. The prolonged tumble observed in the two axis configuration is not in evidence. The natural frequency of the three axis configuration is 0.93 orbital at large amplitudes, and hence the configuration is not in resonance with orbital frequency disturbances. As indicated in the Figure, the spacecraft stabilized in the rightside-up position, but rightside up capture is problematical with

these initial conditions.

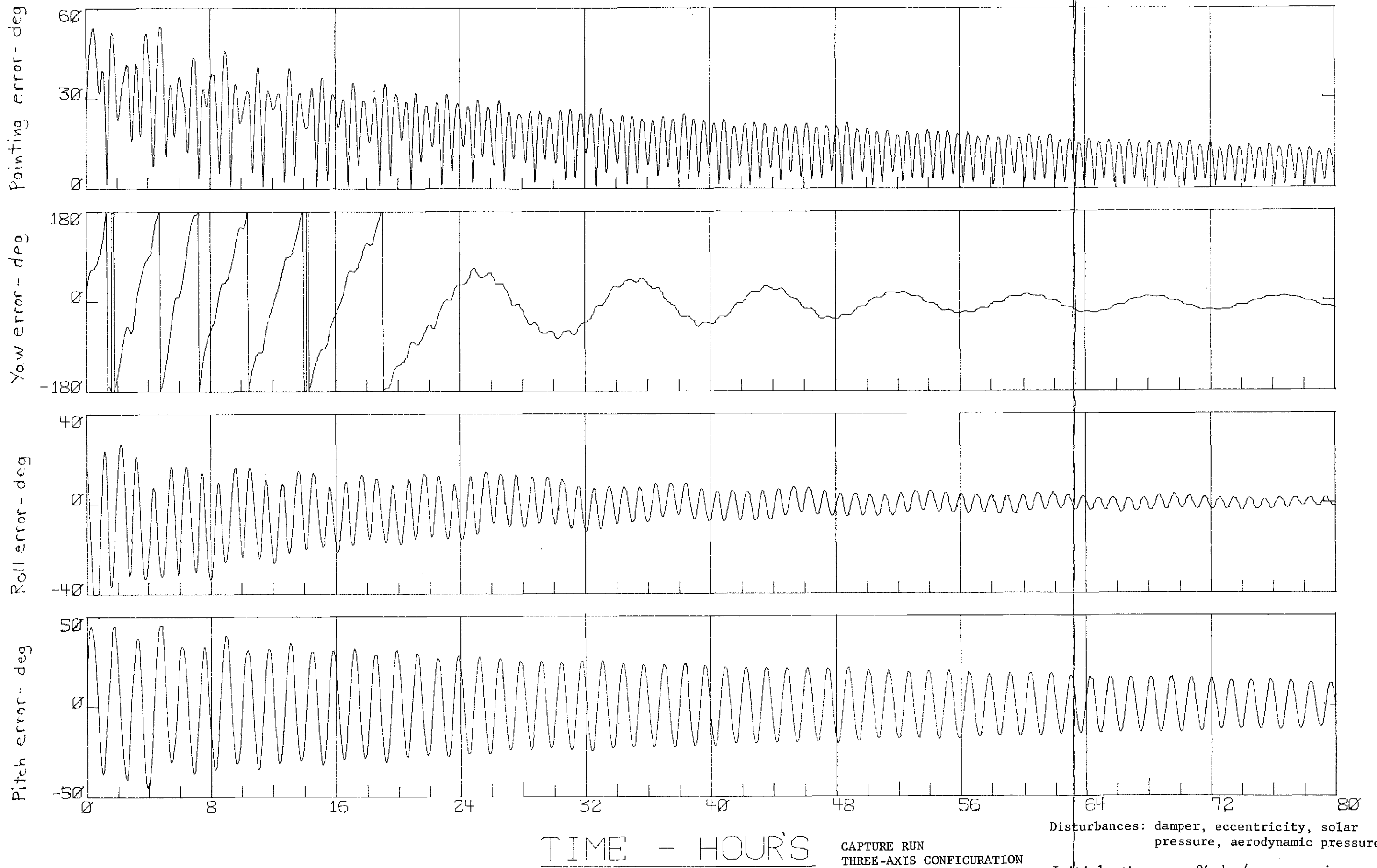
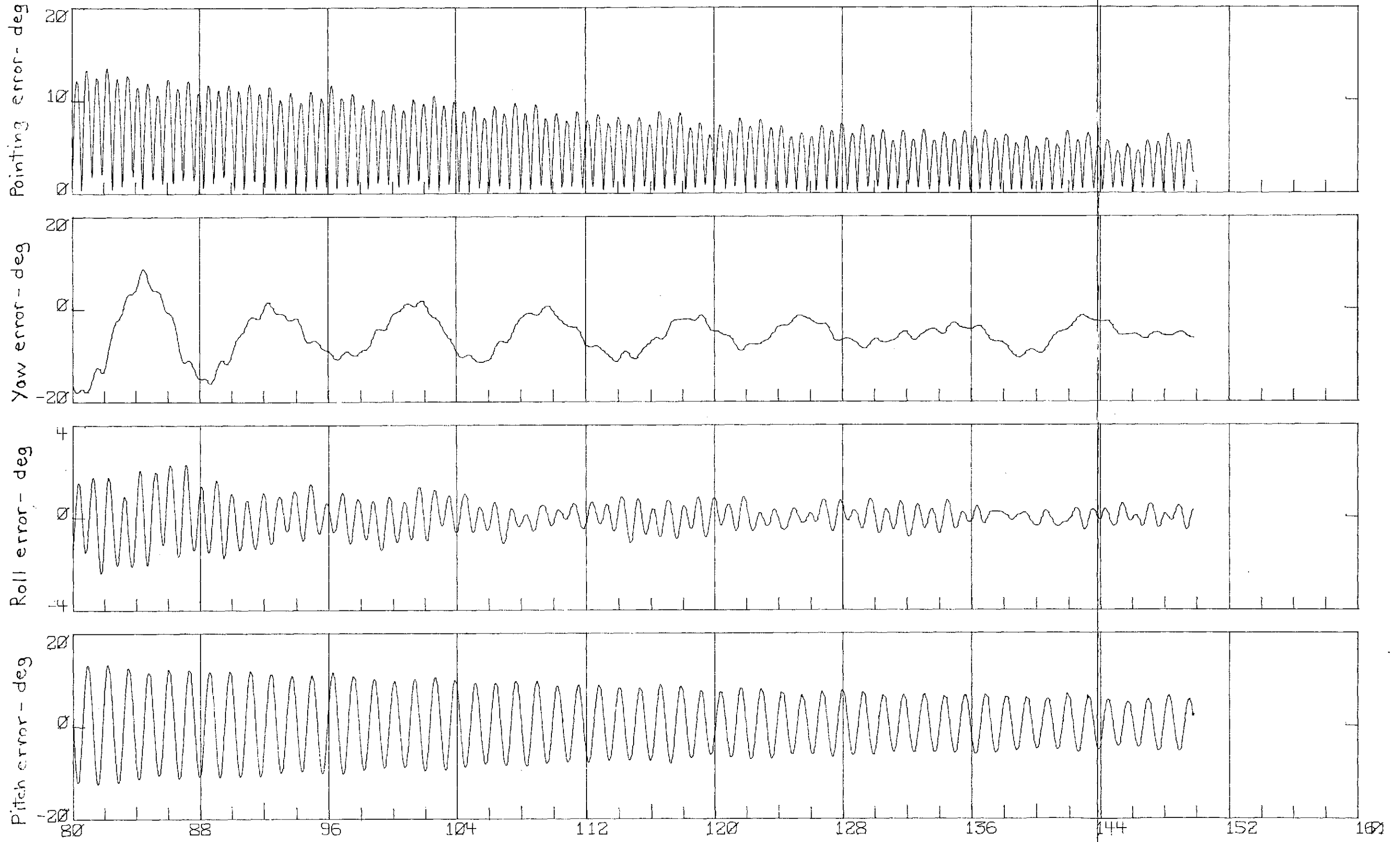


FIGURE 5.10

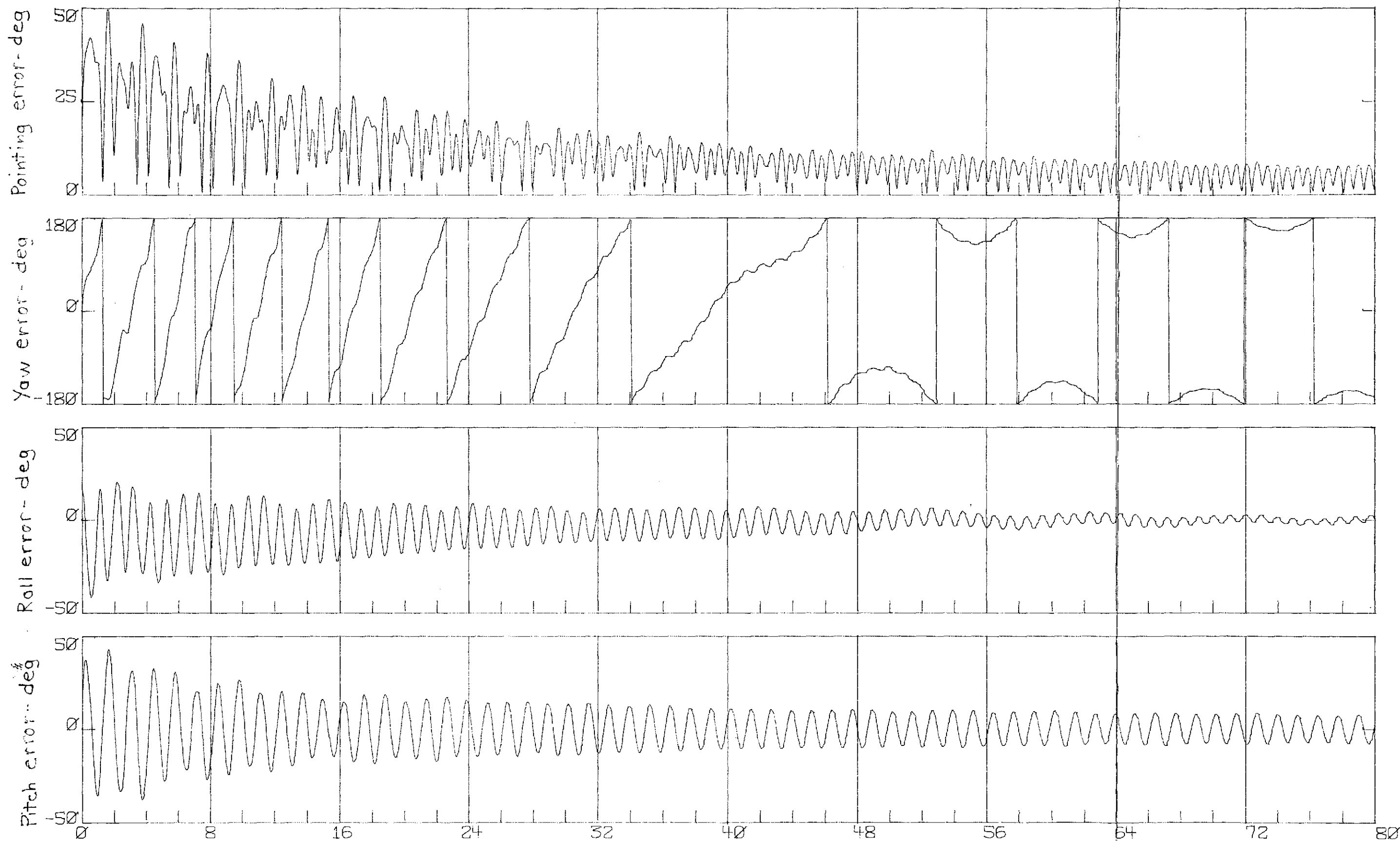


TIME - HOURS

CAPTURE RUN
THREE-AXIS CONFIGURATION

Disturbances: damper, eccentricity, solar pressure, aerodynamic pressure.
Initial rates = .04 deg/sec per axis.
Damping coefficient = 0.51 ft-lb-sec.

FIGURE 5.10 (cont'd)

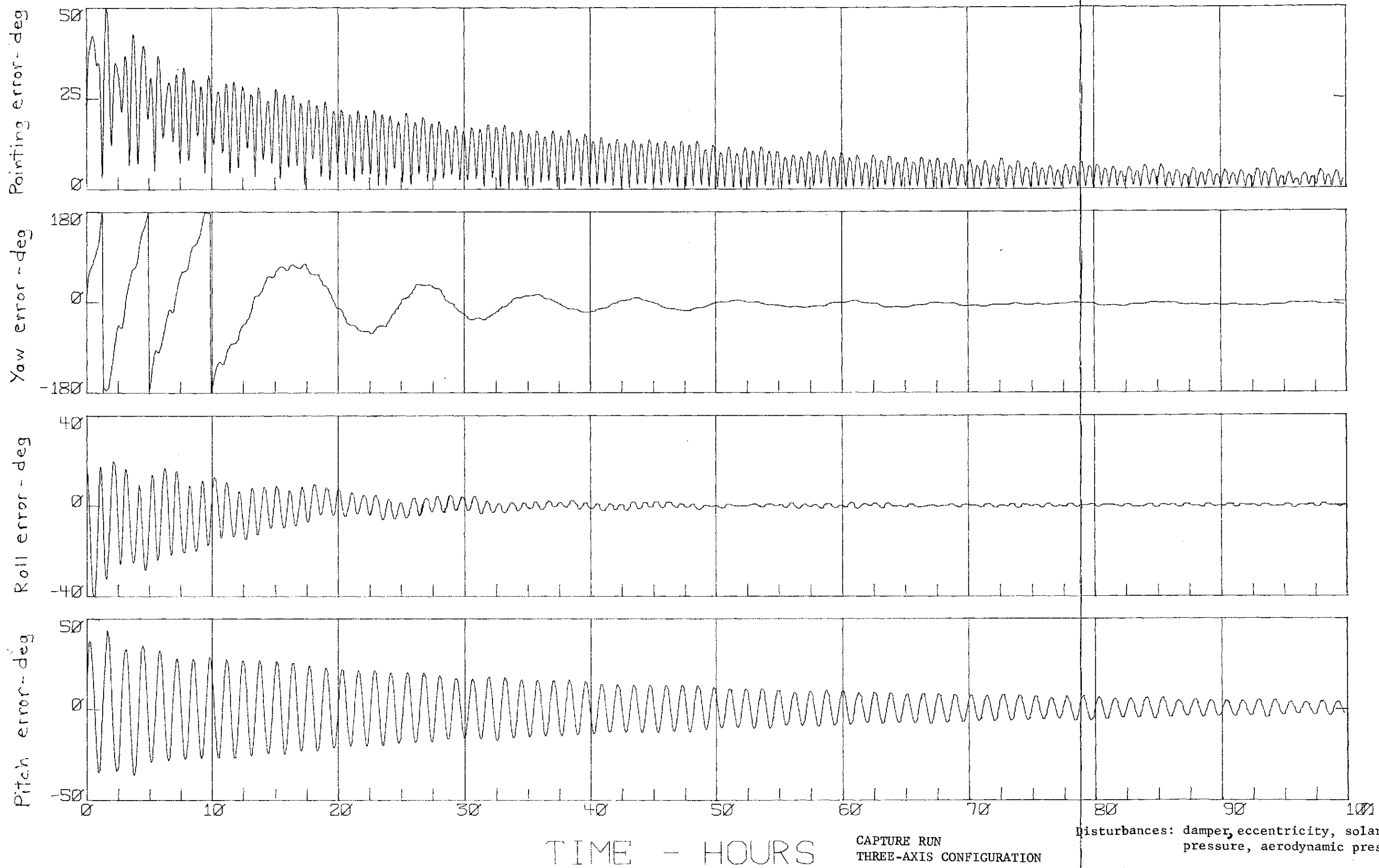


TIME - HOURS

CAPTURE RUN
THREE-AXIS CONFIGURATION

Disturbances: damper, eccentricity.
Initial rates = .04 deg/sec per axis.
Damping coefficient = 0.51 ft-lb-sec.

FIGURE 5.11



CAPTURE RUN
THREE-AXIS CONFIGURATION

Disturbances: damper, eccentricity, solar pressure, aerodynamic pressure.
Initial rates = .04 deg/sec per axis.
Damping coefficient = 1.0 ft-lb-sec.

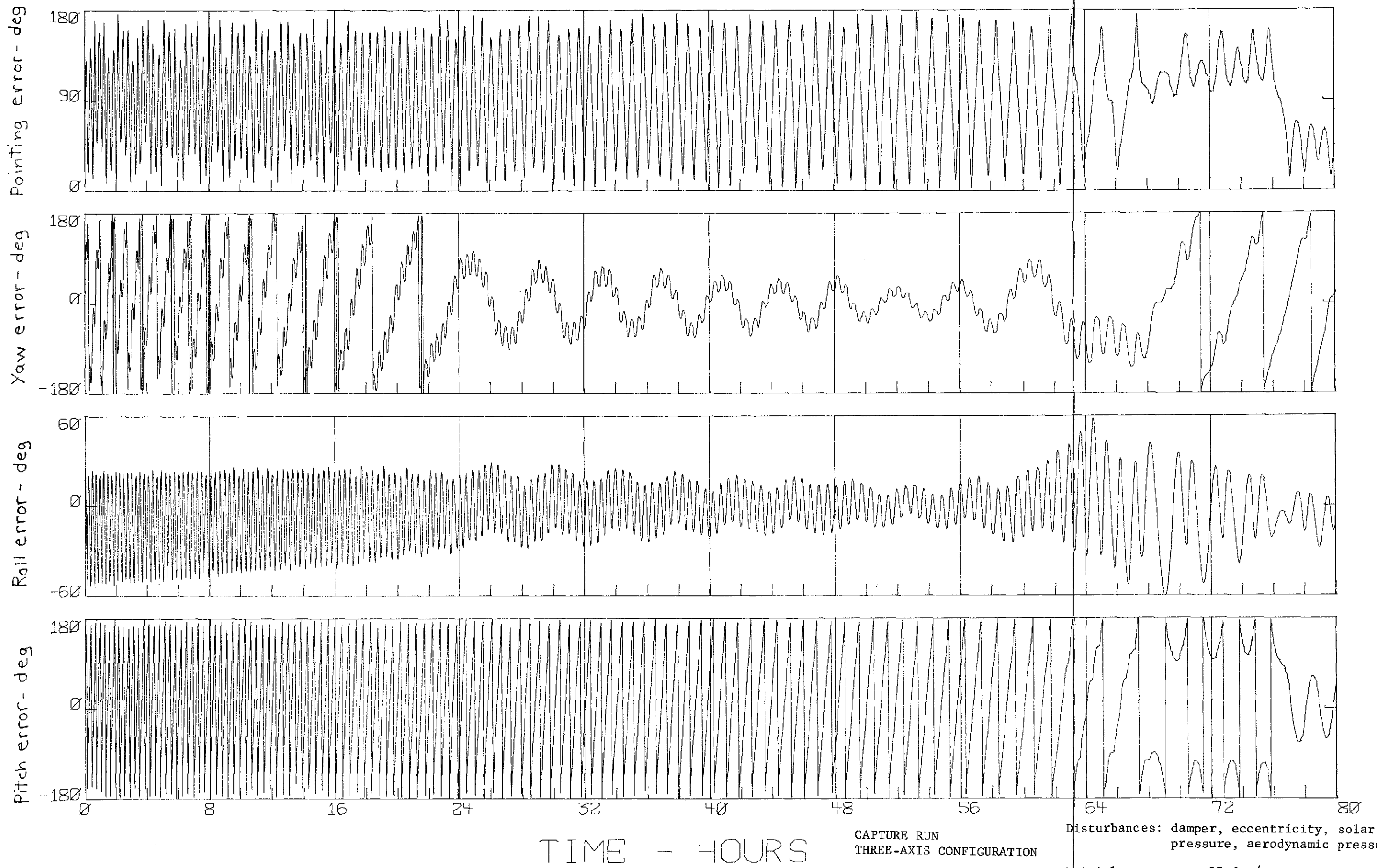
TIME - HOURS

FOLDOUT FRAME 1

ORIGINAL PAGE IS
OF POOR QUALITY

FIGURE 5.12

FOLDOUT FRAME 2



CAPTURE RUN
THREE-AXIS CONFIGURATION

Disturbances: damper, eccentricity, solar pressure, aerodynamic pressure

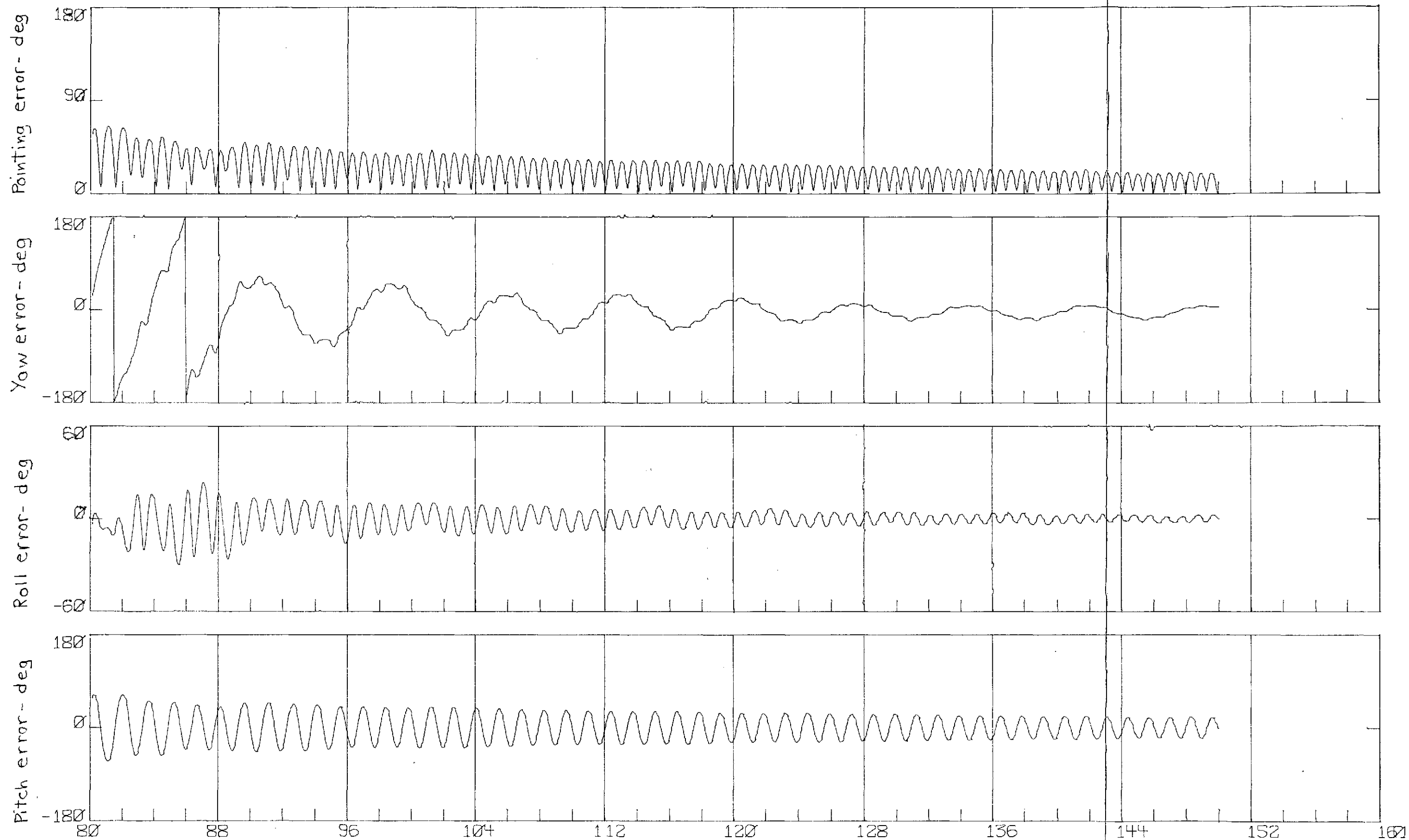
Initial rates = .25 deg/sec per axis

Damping coefficient = 0.51 ft-lb-sec.

FOLDOUT FRAME 2

TIME - HOURS

FIGURE 5.13



TIME - HOURS

CAPTURE RUN
THREE-AXIS CONFIGURATION

Disturbances: damper, eccentricity, solar pressure, aerodynamic pressure

Initial rates = .25 deg/sec per axis

Damping coefficient = 0.51 ft-lb-sec.

FOLDOUT FRAME 2

FIGURE 5.13 (cont'd)

References

- 1) A Variable Atmospheric Density Model from Satellite Accelerations, L. G. Jacchia, Journal of Geophysical Research, vol. 65 (1960, page 2775
- 2) Solar Activity Indices, NASA - Marshall Space Flight Center (10 May 1974)
- 3) Space Shuttle Level II Requirements, Payload Accomodations, JSC 07700, vol. 14, Johnson Spaceflight Center
- 4) Influence of Constant Disturbing Torques on the Motion of Gravity-Gradient Stabilized Spacecraft, T. B. Garber, AIAA Journal, vol. 1, No. 4, (April 1963)

APPENDIX - A

DAMPER MAGNET DYNAMICS

NOMENCLATURE

$[A], [B]$	State matrices; Eqs. (33), (34).
$[\hat{B}]$	Damping coefficient matrix; Eqs. (5), (6).
b	Scalar damping coefficient; Eq. (6).
$[C]$	State matrix; Eq. (35)
$[E]$	Coordinate transformation matrix; Eqs. (1), (8).
$e_{ij}; i, j = 1, 2, 3.$	Elements of $[E]$; Eq. (2).
I_x, I_y, I_z	Principal moments of inertia of the spacecraft in the xyz coordinates; Eq. (3).
I'_x, I'_y, I'_z	Principal moments of inertia of the magnet in the $x'y'z'$ coordinates.
$I_{ROLL}, I_{PITCH}, I_{YAW}$	Roll, pitch and yaw moments of inertia of the spacecraft in the three-axis configuration.
$[\bar{I}]$	Identity matrix.
K	Universal gravitational constant multiplied by the mass of the Earth.
M	Strength of the magnet in pole-cms.
$[O]$	Null matrix.
p, q, r	Orbital frame of coordinates; Eq. (1).
r_0	Geocentric distance of the spacecraft.

$[S_i]$; $i = 1-4$.

Coefficient matrices of the magnet equations of motion; Eqs. (28), (29).

$S_{i,jk}$; $j, k = 1, 2, 3$.

Elements of $[S_i]$; Eq. (29).

T

Maximum yaw stiffness of a magnet; Eqs. (25), (30).

T_{ds}

Damper torque on the spacecraft; Eq. (5).

T_g

Gravity gradient torque vector on the spacecraft; Eqs. (4), (7).

$T_{YAW}, T_{ROLL}, T_{PITCH}$

Magnet stiffnesses; Eq. (23).

T_m

Magnetic torque vector on the magnet; Eqs. (12), (15), (25).

$[T_i]$; $i = 1-4$.

Coefficient matrices of the spacecraft equations of motion; Eqs. (26), (27).

$T_{i,jk}$; $j, k = 1, 2, 3$.

Elements of $[T_i]$; Eq. (27)

t

Time from the ascending node.

\underline{u}

State vector; Eq. (31).

x, y, z

Body fixed coordinate system of the spacecraft; Eq. (1).

α

Local latitude.

δ

Orbit inclination.

$\dot{\eta}$

Orbital rate.

$\theta_p, \theta_r, \theta_y$

Pitch, roll and yaw angles of the spacecraft.

$\theta_{ps}, \theta_{rs}, \theta_{ys}$

Bias values of θ_p, θ_r and θ_y .

ϕ_p, ϕ_r, ϕ_y

Perturbed values of θ_p, θ_r and θ_y from the bias values.

$\underline{\phi}$

$[\phi_y, \phi_r, \phi_p]^T$.

$\underline{\omega}$

Spacecraft rate vector in xyz -coordinates.

$\underline{\omega}_{ds}$

Damper rate vector referred to the axes fixed on the spacecraft.

$\underline{\omega}'_{sd}$

Spacecraft rate vector referred to the axes fixed on the damper.

SUPERSCRIPTS

$(\cdot)'$

Denotes variables which relate to the damper magnet.

SUBSCRIPTS

x, y and z

Denotes the elements of a vector in the corresponding axes.

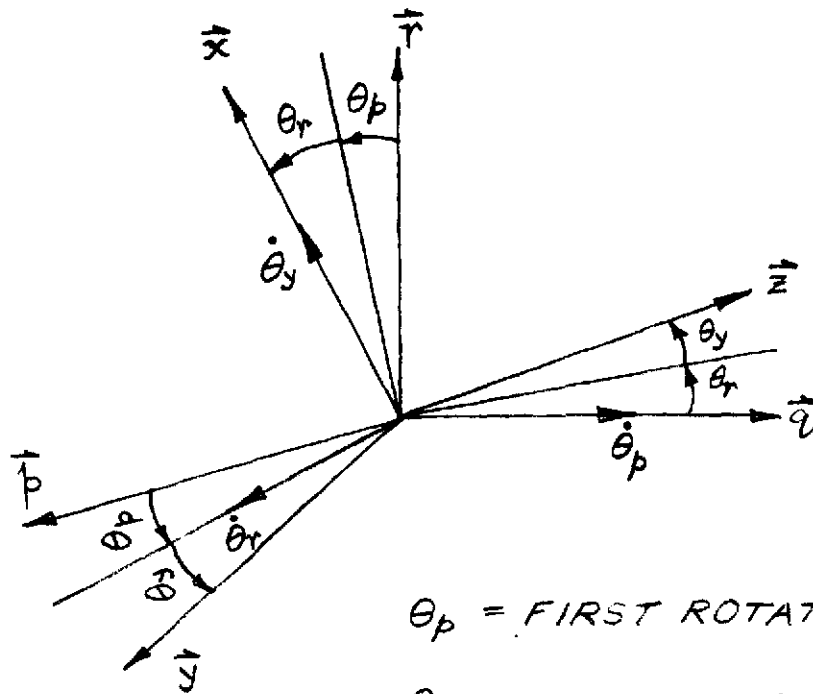
OPERATORS

$[\cdot]^T$

Transpose

$(\dot{\cdot})$

Derivative with respect to time.



$\theta_p = \text{FIRST ROTATION}$

$\theta_r = \text{SECOND ROTATION}$

$\theta_y = \text{THIRD ROTATION}$

*COORDINATE SYSTEM
RELATIONSHIP*

FIGURE A1.

ORIGINAL PAGE IS
OF POOR QUALITY

EULER'S EQUATIONS OF MOTION

A coordinate system xyz is assumed to be attached to the orbiting spacecraft. Let rpg be the orbital coordinate system rotating at the orbital rate of the spacecraft about the q -axis. The relationship between the coordinate systems is defined as

$$\begin{Bmatrix} x \\ y \\ z \end{Bmatrix} = [E(\theta_p, \theta_r, \theta_y)] \begin{Bmatrix} r \\ p \\ q \end{Bmatrix} \quad (1)$$

where the elements e_{ij} , $(i, j = 1, 2, 3)$, of the matrix $[E]$ are given by

$$\begin{aligned} e_{11} &= \cos \theta_p \cos \theta_r \\ e_{12} &= \sin \theta_p \cos \theta_r \\ e_{13} &= -\sin \theta_r \\ e_{21} &= \cos \theta_p \sin \theta_r \sin \theta_y - \sin \theta_p \cos \theta_y \\ e_{22} &= \cos \theta_p \cos \theta_y + \sin \theta_p \sin \theta_r \sin \theta_y \\ e_{23} &= \cos \theta_r \sin \theta_y \\ e_{31} &= \sin \theta_p \sin \theta_y + \cos \theta_p \sin \theta_r \cos \theta_y \\ e_{32} &= \sin \theta_p \sin \theta_r \cos \theta_y - \cos \theta_p \sin \theta_y \\ e_{33} &= \cos \theta_r \cos \theta_y \end{aligned} \quad (2)$$

The angles θ_p , θ_r and θ_y are the pitch, the roll and the yaw angular displacements, respectively, of the spacecraft and define the rotation of the xyz coordinates with respect to the rpg coordinates. This angular relationship between the coordinate systems is shown in Figure A1.

The x -axis is taken along the local vertical and the y -axis is parallel to the trajectory in the direction of motion of the center of mass of the spacecraft. The z -axis is normal to the orbit plane forming a right handed coordinate frame. With this convention, and assuming that the system is coincident with the axes of principal moment of inertia of the spacecraft, these moments of inertia are given by

$$I_x = I_{YAW} ; I_y = I_{ROLL} ; I_z = I_{PITCH} . \quad (3)$$

With the preceding assumptions, the gravity gradient torque vector, T_g , in the xyz coordinate system on the spacecraft is given by

$$\begin{aligned} T_{gx} &= \frac{3K}{r_0^3} [(I_z - I_y) e_{z1} e_{31}] \\ T_{gy} &= \frac{3K}{r_0^3} [(I_x - I_z) e_{11} e_{31}] \\ T_{gz} &= \frac{3K}{r_0^3} [(I_y - I_x) e_{11} e_{21}] \end{aligned} \quad (4)$$

where the subscripts x , y and z refer to the corresponding axes, and

K = universal gravitational constant multiplied by the mass of the Earth,

r_0 = geocentric distance of the satellite.

Let $\underline{\omega}_{ds}$ be the angular velocity vector of the damper magnet expressed in the xyz coordinate system fixed on the spacecraft. Then the damping torque vector \underline{T}_{ds} on the spacecraft created by its motion relative to that of the damper magnet is given by

$$\underline{T}_{ds} = [\hat{B}] \{ \underline{\omega}_{ds} - \underline{\omega} \} \quad (5)$$

where

$\underline{\omega}$ = the angular velocity vector of the spacecraft in the xyz coordinates, and

$[\hat{B}]$ = the damping coefficient matrix for the damper assembly.

Due to the isotropy and symmetry of the damper assembly, the matrix is a scalar matrix, and is of the form

$$[\hat{B}] = b [\bar{I}] \quad (6)$$

where b is the scalar damping coefficient and

$[\bar{I}]$ is the identity matrix.

Torques on the spacecraft from all other sources are neglected as the effects of only the damper are under investigation. Hence, the equations of motion of the spacecraft are given by

$$\begin{aligned} I_x \dot{\omega}_x + (I_z - I_y) \omega_y \omega_z + b(\omega_x - \omega_{dsx}) &= T_{gx} \\ I_y \dot{\omega}_y + (I_x - I_z) \omega_x \omega_z + b(\omega_y - \omega_{dSY}) &= T_{gy} \\ I_z \dot{\omega}_z + (I_y - I_x) \omega_x \omega_y + b(\omega_z - \omega_{dsz}) &= T_{gz} \end{aligned} \quad (7)$$

where

$\underline{\dot{\omega}}$ = the angular acceleration vector of the spacecraft in the $x y z$ coordinates.

Let the principal moments of inertia of the magnet of the damper be along the axes of the $x'y'z'$ coordinate system. Let θ'_p, θ'_r and θ'_y be the pitch, the roll and the yaw angular displacements of the $x'y'z'$ system with respect to the r, p, q coordinate axes. The relative orientations of the $x'y'z'$ coordinates from the $r p q$ coordinates are similar to those of the $x y z$ coordinates from the $r p q$ coordinates. Hence, the $r p q$ coordinates can be transformed to the $x'y'z'$ coordinates in a manner analogous to that given by Eq. (1). Therefore,

$$\begin{Bmatrix} x' \\ y' \\ z' \end{Bmatrix} = [E(\theta'_p, \theta'_r, \theta'_y)] \begin{Bmatrix} r \\ p \\ q \end{Bmatrix} \quad (8)$$

Let $\underline{\omega}'$ be the angular velocity vector of the magnet in the $x'y'z'$ coordinates. Then $\underline{\omega}'$ and $\underline{\omega}_{ds}$ are related by the transformation

$$\underline{\omega}_{ds} = [E(\theta_p, \theta_r, \theta_y)] [E(\theta'_p, \theta'_r, \theta'_y)]^{-1} \underline{\omega}' \quad (9)$$

For small angular displacements, Eq. (9) can be approximated by

$$\underline{\omega}_{ds} = [E(\theta_p, \theta_r, \theta_y)] [\dot{\theta}'_y, \dot{\theta}'_r, (\dot{\eta} + \dot{\theta}'_p)]^T \quad (10)$$

Hence, Eq. (8) becomes

$$\left\{ \begin{array}{l} I_x \ddot{\omega}_x + (I_z - I_y) \left(\omega_y \omega_z - \frac{3K}{r_0^3} e_{21} e_{31} \right) \\ I_y \ddot{\omega}_y + (I_x - I_z) \left(\omega_x \omega_z - \frac{3K}{r_0^3} e_{11} e_{31} \right) \\ I_z \ddot{\omega}_z + (I_y - I_x) \left(\omega_x \omega_y - \frac{3K}{r_0^3} e_{11} e_{21} \right) \end{array} \right\} + b [E(\theta_p, \theta_r, \theta_y)] \left\{ \begin{array}{l} (\dot{\theta}_y - \dot{\theta}'_y) \\ (\dot{\theta}_r - \dot{\theta}'_r) \\ (\dot{\theta}_p - \dot{\theta}'_p) \end{array} \right\} = \left\{ \begin{array}{l} 0 \\ 0 \\ 0 \end{array} \right\} \quad (11)$$

Let I'_x , I'_y and I'_z be the principal moments of inertia along the $x'y'z'$ coordinate axes. Also, let $\underline{\omega}'_{sd}$ the angular velocity vector of the spacecraft expressed in the $x'y'z'$ coordinates. Then the equations of motion of the damper magnet are given by

$$\begin{aligned} I'_x \ddot{\omega}'_x + (I'_z - I'_y) \omega'_y \omega'_z + b(\omega'_x - \omega'_{sdx}) &= T_{mx} \\ I'_y \ddot{\omega}'_y + (I'_x - I'_z) \omega'_x \omega'_z + b(\omega'_y - \omega'_{sdy}) &= T_{my} \\ I'_z \ddot{\omega}'_z + (I'_y - I'_x) \omega'_x \omega'_y + b(\omega'_z - \omega'_{sdz}) &= T_{mz} \end{aligned} \quad (12)$$

where $\underline{\dot{\omega}}'$ is the angular acceleration vector of the magnet in the $x'y'z'$ coordinates and I_m is the Earth's magnetic torque vector on the damper magnet.

It is evident that $\underline{\omega}$ and $\underline{\omega}'_{sd}$ are related by the relation

$$\underline{\omega}'_{sd} = [E(\theta'_p, \theta'_r, \theta'_y)] [E(\theta_p, \theta_r, \theta_y)]^{-1} \underline{\omega} \quad (13)$$

Approximating Eq. (13) by the relation

$$\underline{\omega}'_{sd} = [E(\theta'_p, \theta'_r, \theta'_y)] [\dot{\theta}_y, \dot{\theta}_r, (\dot{\eta} + \dot{\theta}_p)]^T \quad (14)$$

Equation (12) can be rewritten as

$$\left\{ \begin{array}{l} I'_x \dot{\omega}'_x + (I'_z - I'_y) \omega'_y \omega'_z \\ I'_y \dot{\omega}'_y + (I'_x - I'_z) \omega'_x \omega'_z \\ I'_z \dot{\omega}'_z + (I'_y - I'_x) \omega'_x \omega'_y \end{array} \right\} + b[E(\theta'_p, \theta'_r, \theta'_y)] \left\{ \begin{array}{l} (\dot{\theta}'_y - \dot{\theta}_y) \\ (\dot{\theta}'_r - \dot{\theta}_r) \\ (\dot{\theta}'_p - \dot{\theta}_p) \end{array} \right\} = \left\{ \begin{array}{l} T_{mx} \\ T_{my} \\ T_{mz} \end{array} \right\} \quad (15)$$

Equations (11) and (15) constitute the approximate coupled set of Euler's equations for the spacecraft and the damper magnet.

LINEARIZED EQUATIONS

Let a circular orbit be assumed such that

$$\begin{aligned} \dot{\eta} &= \text{the orbital rate} = \text{the rate about the } \eta\text{-axis} \\ &= \text{a constant} = \sqrt{\frac{K}{r_0^3}} \end{aligned} \quad (16)$$

In terms of the Euler angle rates, the angular velocities of the spacecraft are then given by

$$\begin{aligned} \omega_x &= \dot{\theta}_y - (\dot{\theta}_p + \dot{\eta}) \sin \theta_r \\ \omega_y &= \dot{\theta}_r \cos \theta_y + (\dot{\theta}_p + \dot{\eta}) \sin \theta_y \cos \theta_r \\ \omega_z &= -\dot{\theta}_r \sin \theta_y + (\dot{\theta}_p + \dot{\eta}) \cos \theta_y \cos \theta_r \end{aligned} \quad (17)$$

Let it be assumed that the angles θ_p , θ_r and θ_y have a non-zero bias such that

$$\begin{aligned} \theta_p &= \theta_{ps} + \phi_p \\ \theta_r &= \theta_{rs} + \phi_r \\ \theta_y &= \theta_{ys} + \phi_y \end{aligned} \quad (18)$$

where

$\theta_{ps}, \theta_{rs}, \theta_{ys}$ = the bias angles

ϕ_p, ϕ_r, ϕ_y = small changes of the attitude angles from their bias values.

Let it also be assumed that θ_{ps} and θ_{ys} are constants but θ_{rs} is a variable.

The expressions for the angular velocities as given by Eq. (17) are linearized about the bias positions to become

$$\begin{aligned}
 \omega_x &= \dot{\phi}_y - \dot{\phi}_p \sin \theta_{rs} - \dot{\eta} \phi_r \cos \theta_{ys} - \dot{\eta} \sin \theta_{rs} \\
 \omega_y &= \dot{\phi}_r \cos \theta_{ys} + \dot{\phi}_p \sin \theta_{ys} \cos \theta_{rs} - \dot{\eta} \phi_r \sin \theta_{ys} \sin \theta_{rs} \\
 &\quad + \dot{\eta} \phi_y \cos \theta_{rs} \cos \theta_{ys} + \dot{\eta} \sin \theta_{ys} \cos \theta_{ys} \\
 \omega_z &= -\dot{\phi}_r \sin \theta_{ys} + \dot{\phi}_p \cos \theta_{ys} \cos \theta_{rs} - \dot{\eta} \phi_y \sin \theta_{ys} \cos \theta_{rs} \\
 &\quad - \dot{\eta} \phi_r \cos \theta_{ys} \sin \theta_{rs} + \dot{\eta} \cos \theta_{ys} \cos \theta_{rs}
 \end{aligned} \tag{19}$$

Similarly, the linearized forms of the angular accelerations are given by

$$\begin{aligned}
 \dot{\omega}_x &= \ddot{\phi}_y - \ddot{\phi}_p \sin \theta_{rs} - \dot{\eta} \dot{\phi}_r \cos \theta_{rs} \\
 &\quad + \dot{\theta}_{rs} (\dot{\eta} \phi_r \sin \theta_{rs} - \dot{\phi}_p \cos \theta_{rs} - \dot{\eta} \cos \theta_{rs}) \\
 \dot{\omega}_y &= \ddot{\phi}_r \cos \theta_{ys} + \ddot{\phi}_p \sin \theta_{ys} \cos \theta_{rs} - \dot{\eta} \dot{\phi}_r \sin \theta_{ys} \sin \theta_{rs} \\
 &\quad + \dot{\eta} \dot{\phi}_y \cos \theta_{rs} \cos \theta_{ys} - \dot{\theta}_{rs} (\dot{\phi}_p \sin \theta_{ys} \sin \theta_{rs} \\
 &\quad + \dot{\eta} \phi_r \sin \theta_{ys} \cos \theta_{rs} + \dot{\eta} \phi_y \sin \theta_{rs} \cos \theta_{ys} + \dot{\eta} \sin \theta_{ys} \sin \theta_{rs})
 \end{aligned}$$

$$\begin{aligned}
\dot{\omega}_z = & -\ddot{\phi}_r \sin \theta_{ys} + \ddot{\phi}_p \cos \theta_{ys} \cos \theta_{rs} - \dot{\eta} \dot{\phi}_r \cos \theta_{ys} \sin \theta_{rs} \\
& - \dot{\eta} \dot{\phi}_y \cos \theta_{rs} \sin \theta_{ys} - \dot{\theta}_{rs} (\dot{\phi}_p \cos \theta_{ys} \sin \theta_{rs} \\
& + \dot{\eta} \dot{\phi}_r \cos \theta_{ys} \cos \theta_{rs} - \dot{\eta} \dot{\phi}_y \sin \theta_{rs} \sin \theta_{ys} + \dot{\eta} \cos \theta_{ys} \sin \theta_{rs})
\end{aligned} \tag{20}$$

Similarly, writing

$$\theta'_p = \theta'_{ps} + \phi'_p \tag{21}$$

and

$$\theta'_r = \theta'_{rs} + \phi'_r$$

$$\theta'_y = \theta'_{ys} + \phi'_y$$

equations for the damper magnet rates and accelerations analogous to Eqs. (19) and (20) are obtained.

It should be noted that though $\dot{\theta}_{rs}$ can be set equal to zero without too much error; $\dot{\theta}'_{rs}$ cannot be. This is because the magnet continuously follows the Earth's magnetic field. In a polar or in an equatorial orbit, the magnet stays parallel to the field at all times and does not roll. But if the orbit inclination ψ lies between zero and ninety degrees, the magnet roll angle oscillates between 0 and ψ degrees with twice the orbital frequency. This is because the Earth's resultant magnetic field makes an angle of approximately 2α degrees with the polar axis at a place with a latitude of α degrees. Thus, θ'_{rs} can be expressed as

$$\theta'_{rs} = \psi (1 - \cos 2\eta t) \tag{21}$$

and hence,

$$\dot{\theta}'_{rs} = 2\psi \eta \sin 2\eta t \tag{22}$$

where t is the time from the ascending node and ψ is the inclination of the orbit.

Let T be the maximum yaw stiffness for an orbiting magnet. Thus, T must necessarily be the yaw stiffness for a magnet in a polar orbit at the equator.

Hence, at any arbitrary orbit inclination,

$$\begin{aligned}
 T_{YAW} &= \text{Yaw stiffness} = T \cos \alpha \\
 T_{ROLL} &= \text{Roll stiffness} = T \cos \psi \\
 T_{PITCH} &= \text{Pitch stiffness} = T \sin \psi
 \end{aligned}
 \tag{23}$$

where α is the local latitude.

The variation of the absolute value of α over a full orbit can be approximately written as

$$|\alpha| = \psi (1 - \cos 2\eta t) = \theta'_{rs} \tag{24}$$

From these relations, the magnetic torques on the dampers can be expressed as

$$\begin{aligned}
 T_{mx} &= - [T \cos \theta'_{rs}] \phi'_y \\
 T_{my} &= - [T \cos \psi] \phi'_r \\
 T_{mz} &= - [T \sin \psi] \phi'_p
 \end{aligned}
 \tag{25}$$

Substituting the expressions for $\underline{\omega}$ and $\underline{\dot{\omega}}$ from Eqns. (19) and (20) together with the similar expressions for $\underline{\omega}'$ and $\underline{\dot{\omega}}'$ into Eq. (11), the linearized homogeneous form of Eq. (11) can be expressed as

$$[T_1]\ddot{\underline{\phi}} + [T_2]\dot{\underline{\phi}} + [T_3]\underline{\phi} + [T_4]\dot{\underline{\phi}}' = \underline{0} \quad (26)$$

where $\dot{\theta}_{ys}$ has been set equal to zero.

The elements of the 3x3 matrices $[T_i]$, $i = 1-4$, are as follows:

$$T_{1,11} = I_x$$

$$T_{1,12} = 0$$

$$T_{1,13} = -I_x \sin \theta_{rs}$$

$$T_{1,21} = 0$$

$$T_{1,22} = I_y \cos \theta_{ys}$$

$$T_{1,23} = I_y \sin \theta_{ys} \cos \theta_{rs}$$

$$T_{1,31} = 0$$

$$T_{1,32} = -I_z \sin \theta_{rs}$$

$$T_{1,33} = I_z \cos \theta_{ys} \cos \theta_{rs}$$

$$T_{2,11} = b$$

$$T_{2,12} = [(I_z - I_y) \cos 2\theta_{ys} - I_x] \dot{\eta} \cos \theta_{rs}$$

$$T_{2,13} = \dot{\eta} (I_z - I_y) \sin 2\theta_{ys} \cos^2 \theta_{rs} - b \sin \theta_{rs}$$

ORIGINAL PAGE IS
OF POOR QUALITY

$$\begin{aligned}
T_{2,21} &= (I_x + I_y - I_z) \dot{\eta} \cos \theta_{ys} \cos \theta_{rs} \\
T_{2,22} &= (I_x - I_y - I_z) \dot{\eta} \sin \theta_{ys} \sin \theta_{rs} + b \cos \theta_{ys} \\
T_{2,23} &= (I_z - I_x) \dot{\eta} \cos \theta_{ys} \sin 2\theta_{rs} + b \sin \theta_{ys} \cos \theta_{rs} \\
T_{2,31} &= (I_y - I_x - I_z) \dot{\eta} \sin \theta_{ys} \cos \theta_{rs} \\
T_{2,32} &= (I_x - I_y - I_z) \dot{\eta} \cos \theta_{ys} \sin \theta_{rs} - b \sin \theta_{ys} \\
T_{2,33} &= (I_x - I_y) \dot{\eta} \sin \theta_{ys} \sin 2\theta_{rs} + b \cos \theta_{ys} \cos \theta_{rs} \quad (27b)
\end{aligned}$$

$$\begin{aligned}
T_{3,11} &= (\dot{\eta})^2 (I_z - I_y) \left[\cos^2 \theta_{rs} \cos 2\theta_{ys} - 3(\sin \theta_{rs} \cos \theta_{ys} \right. \\
&\quad \left. - \sin \theta_{ys} \cos \theta_{ps} \sin \theta_{rs}) (\sin \theta_{ys} \cos \theta_{ps} \sin \theta_{rs} - \sin \theta_{ps} \cos \theta_{ys}) \right. \\
&\quad \left. - 3(\cos \theta_{ys} \cos \theta_{ps} \sin \theta_{rs} + \sin \theta_{ys} \sin \theta_{rs}) (\sin \theta_{ps} \sin \theta_{ys} \right. \\
&\quad \left. + \cos \theta_{ys} \cos \theta_{ps} \sin \theta_{rs}) \right]
\end{aligned}$$

$$\begin{aligned}
T_{3,12} &= (\dot{\eta})^2 (I_y - I_z) \left[\frac{1}{2} \sin 2\theta_{rs} \sin 2\theta_{ys} \right. \\
&\quad \left. + 3 \cos \theta_{ys} \cos \theta_{rs} \cos \theta_{ps} (\sin \theta_{ys} \cos \theta_{ps} \sin \theta_{rs} \right. \\
&\quad \left. - \sin \theta_{ps} \cos \theta_{ys}) + 3 \sin \theta_{ys} \cos \theta_{rs} \cos \theta_{ps} (\sin \theta_{ps} \sin \theta_{ys} \right. \\
&\quad \left. + \cos \theta_{ps} \sin \theta_{rs} \cos \theta_{ys}) \right]
\end{aligned}$$

$$\begin{aligned}
T_{3,13} &= (\dot{\eta})^2 (I_z - I_y) \left[\cos^2 \theta_{rs} \sin 2\theta_{ys} - 3(\cos \theta_{ps} \sin \theta_{ys} \right. \\
&\quad \left. - \cos \theta_{ys} \sin \theta_{ps} \sin \theta_{rs}) (\sin \theta_{ys} \cos \theta_{ps} \sin \theta_{rs} \right. \\
&\quad \left. - \sin \theta_{ps} \cos \theta_{ys}) + 3(\sin \theta_{ps} \sin \theta_{rs} \sin \theta_{ys} \right.
\end{aligned}$$

$$+ \cos \theta_{ps} \cos \theta_{ys}) (\sin \theta_{ps} \sin \theta_{ys} + \cos \theta_{ys} \cos \theta_{ps} \sin \theta_{rs})]$$

$$T_{3,21} = (\dot{\eta})^2 (I_x - I_z) \left[\frac{1}{2} \cos \theta_{ys} \sin 2\theta_{rs} \right. \\ \left. + 3 \cos \theta_{ps} \cos \theta_{rs} (\sin \theta_{ps} \cos \theta_{ys} - \sin \theta_{ys} \cos \theta_{ps} \sin \theta_{rs}) \right]$$

$$T_{3,22} = (\dot{\eta})^2 (I_z - I_x) \left[\cos \theta_{ys} \cos 2\theta_{rs} + 3 \cos \theta_{ys} \cos^2 \theta_{ps} \cos^2 \theta_{rs} \right. \\ \left. - 3 \cos \theta_{ps} \sin \theta_{rs} (\sin \theta_{ps} \sin \theta_{ys} + \cos \theta_{ys} \cos \theta_{ps} \sin \theta_{rs}) \right]$$

$$T_{3,23} = 3(\dot{\eta})^2 (I_z - I_x) \left[\cos \theta_{ps} \cos \theta_{rs} (\cos \theta_{ps} \sin \theta_{ys} \right. \\ \left. - \cos \theta_{ys} \sin \theta_{ps} \sin \theta_{rs}) - \sin \theta_{ps} \cos \theta_{rs} (\sin \theta_{ps} \sin \theta_{ys} \right. \\ \left. + \cos \theta_{ys} \cos \theta_{ps} \sin \theta_{rs}) \right]$$

$$T_{3,31} = (\dot{\eta})^2 (I_x - I_y) \left[\frac{1}{2} \cos \theta_{ys} \sin 2\theta_{rs} \right. \quad (27c) \\ \left. - 3 \cos \theta_{ps} \cos \theta_{rs} (\sin \theta_{ys} \sin \theta_{ps} + \cos \theta_{ys} \cos \theta_{ps} \sin \theta_{rs}) \right]$$

$$T_{3,32} = (\dot{\eta})^2 (I_x - I_y) \left[\sin \theta_{ys} \cos 2\theta_{rs} + 3 \sin \theta_{ys} \cos^2 \theta_{ps} \cos^2 \theta_{rs} \right. \\ \left. - 3 \sin \theta_{rs} \cos \theta_{ps} (\sin \theta_{ys} \cos \theta_{ps} \sin \theta_{rs} \right. \\ \left. - \sin \theta_{ps} \cos \theta_{ys}) \right]$$

$$T_{3,33} = 3(\dot{\eta})^2 (I_y - I_x) \left[\sin \theta_{ps} \cos \theta_{rs} (\sin \theta_{ys} \cos \theta_{ps} \sin \theta_{rs} \right. \\ \left. - \sin \theta_{ps} \cos \theta_{ys}) + \cos \theta_{ps} \cos \theta_{rs} (\sin \theta_{rs} \sin \theta_{ps} \sin \theta_{ys} \right. \\ \left. + \cos \theta_{ps} \cos \theta_{ys}) \right]$$

$$T_{4,11} = -b$$

$$T_{4,12} = 0$$

$$T_{4,13} = b \sin \theta_{r,s}$$

$$T_{4,21} = 0$$

$$T_{4,22} = -b \cos \theta_{ys}$$

(27d)

$$T_{4,23} = -b \sin \theta_{ys} \cos \theta_{rs}$$

$$T_{4,31} = 0$$

$$T_{4,32} = b \sin \theta_{ys}$$

$$T_{4,33} = -b \cos \theta_{ys} \cos \theta_{rs}.$$

ORIGINAL PAGE IS
OF POOR QUALITY

Proceeding similarly, the linearized homogeneous form of Eq. (15) can be expressed as

$$[S_1] \ddot{\underline{\phi}}' + [S_2] \dot{\underline{\phi}}' + [S_3] \underline{\phi}' + [S_4] \underline{\phi} = \underline{0} \quad (28)$$

The elements of the 3x3 matrices $[S_i]$, $i = 1-4$, can be obtained as follows:

$$\begin{aligned} S_{1,11} &= I_x' \\ S_{1,12} &= 0 \\ S_{1,13} &= -I_x' \sin \theta'_{rs} \\ S_{1,21} &= 0 \\ S_{1,22} &= I_y' \cos \theta'_{ys} \\ S_{1,23} &= I_y' \sin \theta'_{ys} \cos \theta'_{rs} \\ S_{1,32} &= -I_z' \sin \theta'_{ys} \\ S_{1,33} &= I_z' \cos \theta'_{ys} \cos \theta'_{rs} \\ S_{1,31} &= 0 \\ \\ S_{2,11} &= b \\ S_{2,12} &= \dot{\eta} [(I_z' - I_y') \cos 2\theta'_{ys} - I_x' \cos \theta'_{rs}] \\ S_{2,13} &= \dot{\eta} (I_z' - I_y') \cos^2 \theta'_{rs} \sin 2\theta'_{ys} - b \sin \theta'_{rs} - \dot{\theta}'_{rs} I_x' \cos \theta'_{rs} \end{aligned} \quad (29a)$$

$$\begin{aligned}
S_{2,21} &= \dot{\eta} (I_y' + I_x' - I_z') \cos \theta_{rs}' \cos \theta_{ys}' \\
S_{2,22} &= \dot{\eta} (I_x' - I_z' - I_y') \\
S_{2,23} &= \dot{\eta} (I_z' - I_x') \cos \theta_{ys}' \sin 2\theta_{rs}' + b \sin \theta_{ys}' \cos \theta_{rs}' \\
&\quad - \dot{\theta}_{rs}' I_y' \sin \theta_{ys}' \sin \theta_{rs}' \\
S_{2,31} &= \dot{\eta} (I_y' - I_x' - I_z') \sin \theta_{ys}' \cos \theta_{rs}' \\
S_{2,32} &= \dot{\eta} (I_x' - I_y' - I_z') \cos \theta_{ys}' \sin \theta_{rs}' - b \sin \theta_{ys}' \\
S_{2,33} &= \dot{\eta} (I_x' - I_y') \sin 2\theta_{rs}' \sin \theta_{ys}' + b \cos \theta_{ys}' \cos \theta_{rs}' \quad (29b) \\
&\quad - \dot{\theta}_{rs}' I_z' \cos \theta_{ys}' \sin \theta_{rs}'
\end{aligned}$$

$$\begin{aligned}
S_{3,11} &= (\dot{\eta})^2 (I_z' - I_y') \cos^2 \theta_{rs}' \cos 2\theta_{ys}' + T \cos \theta_{rs}' \\
S_{3,12} &= \frac{1}{2} (\dot{\eta})^2 (I_y' - I_z') \sin 2\theta_{ys}' \sin 2\theta_{rs}' \\
&\quad + \dot{\theta}_{rs}' I_x' \dot{\eta} \sin \theta_{rs}' \\
S_{3,13} &= 0 \\
S_{3,21} &= \frac{1}{2} (\dot{\eta})^2 (I_x' - I_z') \sin \theta_{ys}' \sin 2\theta_{rs}' \\
S_{3,22} &= (\dot{\eta})^2 (I_z' - I_x') \cos \theta_{ys}' \cos 2\theta_{rs}' + T \cos \theta_{rs}' \\
&\quad - \dot{\theta}_{rs}' I_y' \dot{\eta} \sin \theta_{ys}' \cos 2\theta_{rs}' \\
S_{3,23} &= 0
\end{aligned} \quad (29c)$$

$$S_{3,31} = \frac{1}{2} (\dot{\eta})^2 (I_x' - I_y') \cos \theta'_{y_s} \sin 2\theta'_{r_s} \\ + \dot{\theta}'_{r_s} I_z' \dot{\eta} \sin \theta'_{r_s} \sin \theta'_{y_s}$$

$$S_{3,32} = (\dot{\eta})^2 (I_x' - I_y') \sin \theta'_{y_s} \cos 2\theta'_{r_s} \\ - \dot{\theta}'_{r_s} I_z' \dot{\eta} \cos \theta'_{y_s} \cos \theta'_{r_s}$$

$$S_{3,33} = T \sin \psi$$

$$S_{4,11} = -b$$

$$S_{4,12} = 0$$

$$S_{4,13} = b \sin \theta'_{r_s}$$

$$S_{4,21} = 0$$

$$S_{4,22} = -b \cos \theta'_{y_s}$$

$$S_{4,23} = -b \sin \theta'_{y_s} \cos \theta'_{r_s}$$

$$S_{4,31} = 0$$

$$S_{4,32} = b \sin \theta'_{y_s}$$

$$S_{4,33} = -b \cos \theta'_{y_s} \cos \theta'_{r_s}$$

(29d)

ORIGINAL PAGE IS
OF POOR QUALITY

It can easily be verified that assuming a simple dipole model for the Earth's magnetic field, the value of \mathcal{T} is given by

$$\mathcal{T} = 0.0149 (\dot{\eta})^2 M \text{ lb. ft./rad.} \quad (30)$$

where

M = the strength of the magnet in pole-cms.,

$\dot{\eta}$ = the orbital rate in radians/sec.

In view of Eqs. (21) and (25), it is evident that the coefficient matrices

$[T_i]$ and $[S_i]$, $i = 1-4$, of Eqs. (26) and (28) contain time-dependent terms. Since these terms are small, and since the time constants of the dependent variables are usually of the order of twenty or more orbital periods, these time-dependent terms in Eqs. (26) and (28) are replaced by their average values over one orbit period. This procedure converts the Eqs. (26) and (28) into equations with constant coefficients.

Let the state vector $\underline{u}(t)$ be defined as follows:

$$\underline{u} = [\underline{\phi}, \underline{\phi}', \underline{\dot{\phi}}, \underline{\dot{\phi}'}]^T \quad (31)$$

Then Eqs. (26) and (28) can be combined to become

$$[A] \dot{\underline{u}} + [B] \underline{u} = \underline{0} \quad (32)$$

The 12x12 matrices $[A]$ and $[B]$ are defined as

$$[A] = \begin{bmatrix} [\bar{I}] & [O] & [O] & [O] \\ [O] & [\bar{I}] & [O] & [O] \\ [O] & [O] & [T_1] & [O] \\ [O] & [O] & [O] & [S_1] \end{bmatrix} \quad (33)$$

$$[B] = \begin{bmatrix} [O] & [O] & -[\bar{I}] & [O] \\ [O] & [O] & [O] & -[\bar{I}] \\ [T_3] & [O] & [T_2] & [T_4] \\ [O] & [S_3] & [S_4] & [S_2] \end{bmatrix} \quad (34)$$

where

$[O]$ = the null matrix, and

$[\bar{I}]$ = the identity matrix.

Let $[C]$ be the (12x12) matrix defined by

$$[C] = -[A]^{-1}[B]. \quad (35)$$

The time constants and the Garber stability boundaries of the spacecraft-magnet system are obtained by computing the eigenvalues of the matrix $[C]$.

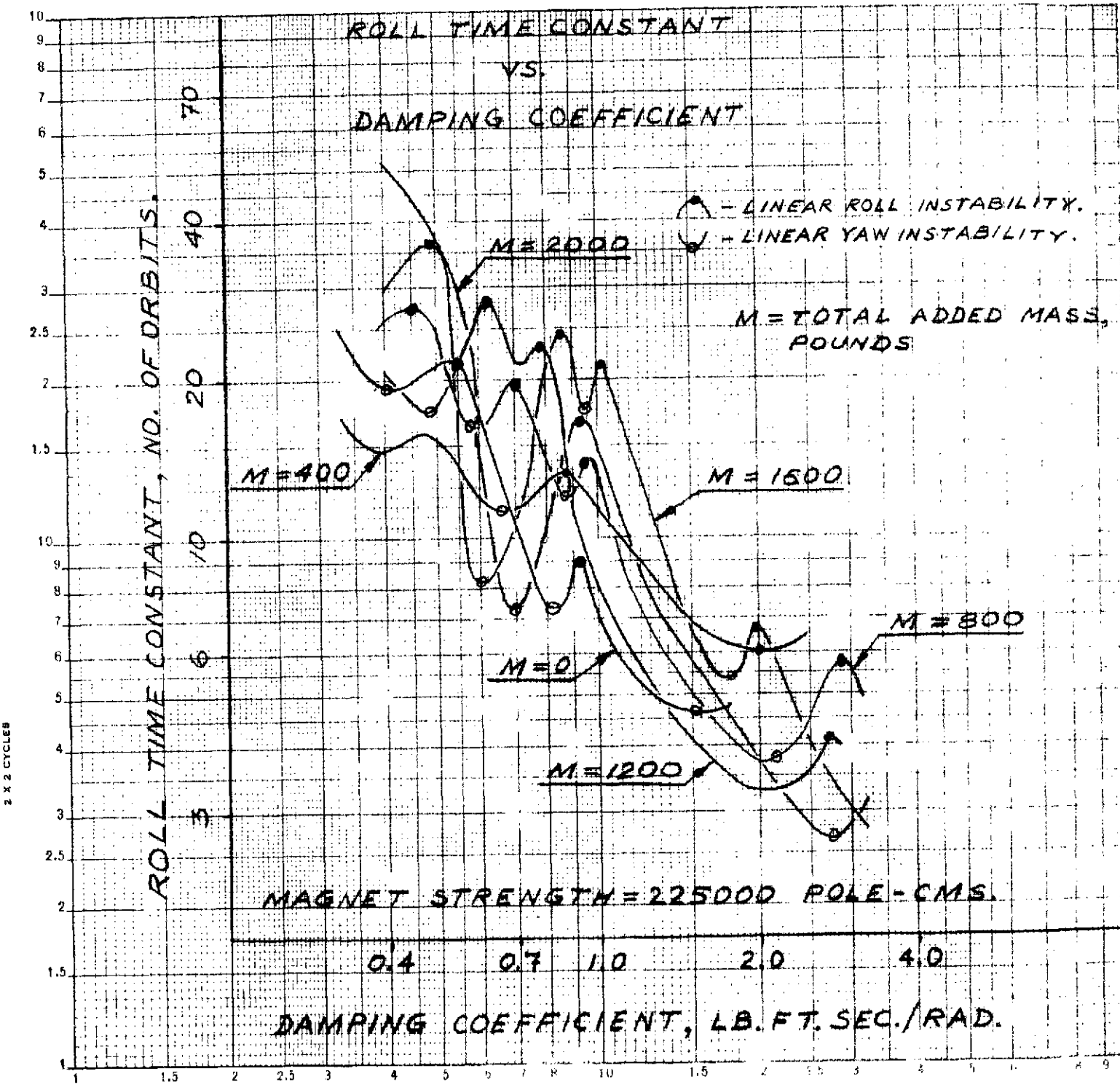


FIGURE A2.

ORIGINAL PAGE IS
OF POOR QUALITY

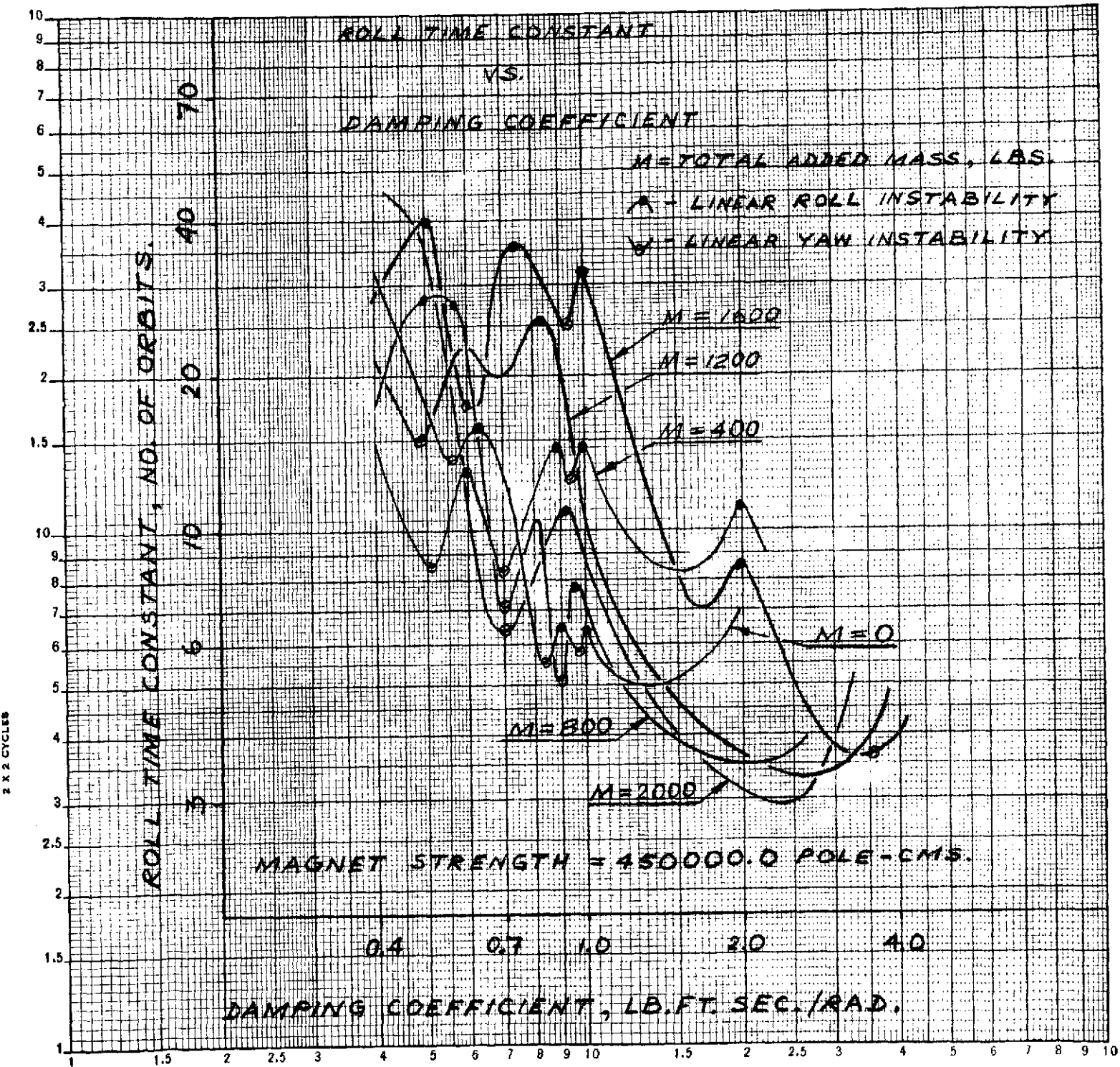


FIGURE A3.

ORIGINAL PAGE IS
OF POOR QUALITY

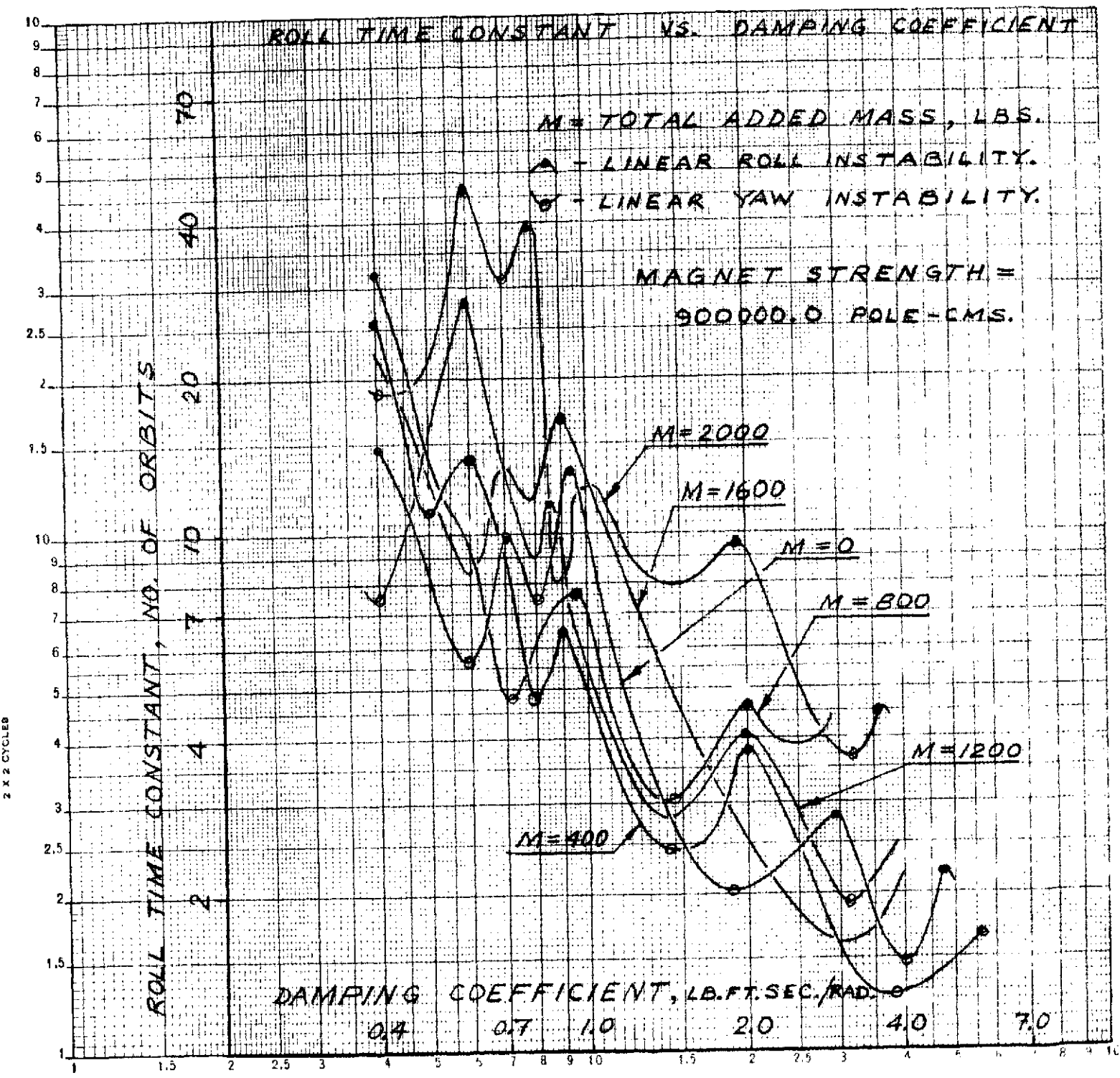


FIGURE A4.

RESULTS

The results of the linear eigenvalue analysis have been plotted in Figs. A2, A3 and A4 and in Figures 4.11, 4.12 and 4.13 which are included in the main body of this report. These figures show the effects of the damping coefficient, b , and those of the extra mass added to the satellite in its pitch plane to create a difference in the pitch and roll moments of inertia of the satellite.

Figures 4.11, 4.12 and 4.13 show the variation of the pitch damping time constant for three different magnet strengths. For a given magnet strength, M , a given set of the moments of inertia of the satellite and for low damping levels, the pitch time constant, as expected, shows a linear variation with the damping coefficient when plotted on a log-log scale. For large values of the damping coefficient, the magnet is pulled away from the Earth's magnetic field and the time constant rises.

Figures A2, A3 and A4 show the corresponding effects of the damping coefficient, added mass and the magnet strength on the roll time constant. Though the roll time constants are less than the pitch time constants, the effects of the roll-yaw coupling between the spacecraft and the magnet is predominant here. The linear analysis with zero bias positions shows alternating points at which roll and yaw instability occurs. But at these unstable points, the spacecraft rolls or yaws to a new non-zero bias position which is stable. Thus, the spacecraft will show a small but constant deviation from the zero bias positions when the spacecraft is operated at these unstable points.

abstract

SECTION 1.0

INTRODUCTION

This report, entitled "Passive Stabilization of the Long Duration Exposure Facility" has been prepared for Langley Research Center under contract number NAS 1-13440. It presents the results of a seventeen week study on the application of the Magnetically Anchored Rate Damper to gravity gradient stabilization of the Long Duration Exposure Facility (LDEF). The study objectives were to perform the analyses and simulations required to investigate the use of an existing viscous magnetic rate damper for rate stabilizing the LDEF spacecraft. The study itself was broken into three main tasks; Linear Performance Estimates, Capture and Damper Requirements, and Performance Prediction. Each of these tasks was performed for two gravity gradient stabilization configurations; an axisymmetric configuration for two-axis (pitch and roll) stability; and a non-axisymmetric configuration for three-axis stability. The report presents the results by stabilization configuration.

SECTION 2.0

SUMMARY AND CONCLUSIONS

2.1 SUMMARY

The nominal LDEF configuration and the anticipated orbit parameters are shown in Table 2.1. Using these parameters, two linear steady state analyses were performed; one for two axis (pitch and roll) stabilization, and one for three axis (pitch, roll and yaw) stabilization. In each of these analyses, the effects of orbit eccentricity, solar pressure, aerodynamic pressure, magnetic dipole, and the magnetically anchored rate damper were evaluated to determine the configuration sensitivity to variations in these parameters. The worst case conditions for steady state were identified, and the performance capability calculated.

Garber instability bounds (a linear instability associated with gravity gradient stabilized spacecraft) were evaluated for the range of configurations and damping coefficients under consideration.

The transient damping capabilities of the damper were evaluated for both the two and three axis configurations, and the time constant as a function of damping coefficient, magnet strength, and spacecraft moment of inertia determined. The capture capabilities of the damper were calculated, and the results combined with the steady state, transient, and Garber instability analyses to select a damper design.

After completion of the linearized analyses, the selected configurations and damper design were simulated on a large three axis digital computer program.